**UNIVERSITY OF WEST BOHEMIA**

**FACULTY OF MECHANICAL ENGINEERING**

**Study programme: N0715A270011 – Machining, additive technology, and quality assurance**

**Study specialization: None**

# DIPLOMA THESIS

**Design of experiment on process parameters for a combination of SLM and LMD technology**

Author: Bc. Matěj ROTT

Supervisor: Ing. Ivana ZETKOVÁ, Ph.D.

Academic year 2021/2022

ZÁPADOČESKÁ UNIVERZITA V PLZNI
Fakulta strojní
Akademický rok: 2021/2022

# ZADÁNÍ DIPLOMOVÉ PRÁCE

(projektu, uměleckého díla, uměleckého výkonu)

| | |
|---|---|
| Jméno a příjmení: | **Bc. Matěj ROTT** |
| Osobní číslo: | **S19N0106P** |
| Studijní program: | **N0715A270011 Obrábění, aditivní technologie a zabezpečování kvality** |
| Téma práce: | **Design of experiment on process parameters for a combination of SLM and LMD technology** |
| Zadávající katedra: | **Katedra technologie obrábění** |

## Zásady pro vypracování

1. Introduction
2. State of the art
3. Design of experiment
4. Results
5. Conclusion

| | |
|---|---|
| Rozsah diplomové práce: | **50 – 70 stran** |
| Rozsah grafických prací: | **dle potřeby** |
| Forma zpracování diplomové práce: | **tištěná/elektronická** |
| Jazyk zpracování: | **Angličtina** |

Seznam doporučené literatury:


- R. Nogueira a C. Costa, „Sinterability of High-Speed Steels M2, M3/2 and T15“, *Mater. Sci. Forum – MATER SCI FORUM*, roč. 498–499, s. 238–243, lis. 2005, doi: 10.4028/www.scientific.net/MSF.498-499.238.
- Q. Hu, J. Fuh, Y. Wong, L. Lu, C. Choy, a Z. Chen, „Powder Metallurgy of M2 High-Speed Steel for Rapid Tooling Applications“, 2002. doi: 10.26153/TSW/3428.
- Y. Uematsu, R. Sasaki, T. Kakiuchi, S. Yamamoto, A. Zensho, a R. Sano, „Fatigue Design Curves for Laser-Metal-Deposited Type 420 Stainless Steel and Effect of an Interval during Deposition Process“. lis. 08, 2021. doi: 10.21203/rs.3.rs-386020/v1.
- W. Yi, H. Chen, Y. Wu, Y. Chen, a H. Li, „Effect of Deposition Strategy on Fatigue Behavior of Laser Melting Deposition 12CrNi2 Alloy Steel“, in *2019 IEEE 4th Optoelectronics Global Conference (OGC)*, zář. 2019, s. 5–8. doi: 10.1109/OGC.2019.8925011.
- Y. rye Choi, S. Sun, Q. Liu, M. Brandt, a M. Qian, „Influence of deposition strategy on the microstructure and fatigue properties of Laser Metal Deposited Ti-6Al-4V powder on Ti-6Al-4V substrate“, *Int. J. Fatigue*, roč. 130, s. 105236, srp. 2019, doi: 10.1016/j.ijfatigue.2019.105236.
- R. Mesquita a C. Barbosa, „Evaluation of As-Hipped PM High Speed Steel for Production of Large-Diameter Cutting Tools“, *Mater. Sci. Forum – MATER SCI FORUM*, roč. 416–418, s. 235–240, úno. 2003, doi: 10.4028/www.scientific.net/MSF.416-418.235.


| | |
|---|---|
| Vedoucí diplomové práce: | **Ing. Ivana Zetková, Ph.D.**<br>Katedra technologie obrábění |
| Konzultant diplomové práce: | **Daniel Braga, Ph.D.**<br>Institute of Science and Innovation in Mechanical and Industrial Engineering, University of Porto |
| Datum zadání diplomové práce: | **15. října 2021** |
| Termín odevzdání diplomové práce: | **27. května 2022** |

L.S.

| | |
|---|---|
| **Doc. Ing. Milan Edl, Ph.D.**<br>děkan | **Doc. Ing. Jan Řehoř, Ph.D.**<br>vedoucí katedry |

# Prohlášení o autorství

Předkládám tímto k posouzení a obhajobě diplomovou práci zpracovanou na závěr studia na Fakultě strojní Západočeské univerzity v Plzni.

Prohlašuji, že jsem tuto diplomovou práci vypracoval samostatně, s použitím odborné literatury a pramenů uvedených v seznamu, který je součástí této diplomové práce.

V Plzni dne: ……. …….

podpis autora

# Acknowledgments

I would like to express my gratitude towards the crew of the Laboratory of Experimental Mechanics at the Inegi research institute in Porto for all of their help and support, namely to Paulo Tavares Ph.D. for making my work internship possible and for the warm welcome, and Daniel Braga, Ph.D. for his patient guidance on my road to the thesis completion. I would also like to thank the crew of the Additive manufacturing department at the company Quantal S.A., specifically Carlos Furtado, Lucas Azavedo and Miguel Costa for arranging my stay at the company, and helping me with the sample preparation and caring approach during my training.

My thanks further go to Ivana Zetková Ph.D. for supervising my thesis, and to the head of the Laboratory of Metal Additive Manufacturing doc. Miroslav Zetek Ph.D. for helping me arrange my work internship in Portugal. Special thanks to my colleagues Martin and Yusuf for both professional and emotional support during my time abroad.

I acknowledge the project POCI- 01-0247-FEDER-072260 / LTE220006, financed by European Funds, through program COMPETE2020 / Inter-Excellence, INTER-EUREKA, under the Eureka smart label S0318-*STREAM -Surface TREatment for Additive Manufacturing*.

The funding provided by project *AditivPeen – Reparação e fabrico aditivo com equipamento híbrido para otimização de propriedades mecânicas*, POCI-01-0247-FEDER-038401, is also acknowledged.

# ANOTAČNÍ LIST DIPLOMOVÉ PRÁCE

| | | |
|---|---|---|
| **AUTOR** | **Příjmení**<br>Rott | **Jméno**<br>Matěj |
| **STUDIJNÍ PROGRAM** | N0715A270011 Obrábění, aditivní technologie a zabezpečování kvality | |
| **VEDOUCÍ PRÁCE** | **Příjmení (včetně titulů)**<br>Ing. Zetková, Ph.D. | **Jméno**<br>Ivana |
| **PRACOVIŠTĚ** | ZČU - FST - KTO | |
| **DRUH PRÁCE** | **DIPLOMOVÁ** | ~~**BAKALÁŘSKÁ**~~ |
| **NÁZEV PRÁCE** | Design of experiment on process parameters for the combination of SLM and LMD technology | |

| | | | | | |
|---|---|---|---|---|---|
| **FAKULTA** | strojní | **KATEDRA** | KTO | **ROK ODEVZD.** | 2022 |

**POČET STRAN (A4 a ekvivalentů A4)**

| | | | | | |
|---|---|---|---|---|---|
| **CELKEM** | 113 | **TEXTOVÁ ČÁST** | 74 | **GRAFICKÁ ČÁST** | 25 |

| | |
|---|---|
| **STRUČNÝ POPIS (MAX 10 ŘÁDEK)**<br><br>**ZAMĚŘENÍ, TÉMA, CÍL POZNATKY A PŘÍNOSY** | Práce se zabývá problematikou způsobů efektivního využití kombinace dvou technologií Aditivní výroby, Selective Laser Melting a Laser Metal Deposition. Součástí práce je podrobná rešerše zmíněných technologií a jejich porovnání. Jsou vysvětleny výhody využití Digital Image Correlation při zkoušce tahem a metody DoE při plánování experimentů. Byly vyrobeny a následně testovány na tah díly z různých materiálů oběma technologiemi za využití metod DoE. Výsledky ukázaly na významné rozdíly mezi oběma technologiemi, a take na děje specifické pro Aditivní výrobu. Tyto byly rozebrány a byly navrženy možnosti jejich vysvětlení. Je představen popis a porovnání testovaných materiálů a jejich vlastností. |
| **KLÍČOVÁ SLOVA**<br><br>**ZPRAVIDLA JEDNOSLOVNÉ POJMY, KTERÉ VYSTIHUJÍ PODSTATU PRÁCE** | Aditivní výroba, Selective Laser Melting, Laser Metal Deposition, Design of Experiment, Central Composite Design, Digital Image Correlation, 316L, Maraging 300, C300, TS700, nástroj k tváření za tepla |

# SUMMARY OF DIPLOMA SHEET

| | | |
|---|---|---|
| **AUTHOR** | **Surname**<br>Rott | **Name**<br>Matěj |
| **STUDY PROGRAMME** | N0715A270011 Machining, Additive Technology and Quality Assurance | |
| **SUPERVISOR** | **Surname (Inclusive of Degrees)**<br>Ing. Zetková, Ph.D. | **Name**<br>Ivana |
| **INSTITUTION** | ZČU - FST - KTO | |
| **TYPE OF WORK** | **DIPLOMA** | ~~**BACHELOR**~~ |
| **TITLE OF THE WORK** | Design of experiment on process parameters for the combination of SLM and LMD technology | |

| | | | | | |
|---|---|---|---|---|---|
| **FACULTY** | Mechanical Engineering | **DEPARTMENT** | KTO | **SUBMITTED IN** | 2022 |

**NUMBER OF PAGES (A4 and eq. A4)**

| | | | | | |
|---|---|---|---|---|---|
| **TOTALLY** | 113 | **TEXT PART** | 74 | **GRAPHICAL PART** | 25 |

| | |
|---|---|
| **BRIEF DESCRIPTION**<br><br>**TOPIC, GOAL, RESULTS, AND CONTRIBUTIONS** | Present work deals with the problematics of combining two different technologies of Additive Manufacturing, Selective Laser Melting and Laser Metal Deposition, with an added benefit. Thorough research including description and comparison of said technologies is presented. The benefits of using Digital Image Correlation for tensile testing and DoE methods for planning of experiment are explained. Parts were manufactured from different materials using both technologies, utilizing methods of DoE, and subsequently tested. The results showed specific differences between the technologies, as well as phenomena specific for AM, which were discussed and several possible explanations were suggested. Characterization and comparison of processed materials and their properties is presented. |
| **KEYWORDS** | Additive Manufacturing, Selective Laser Melting, Laser Metal Deposition, Design of Experiment, Central Composite Design, Digital Image Correlation, 316L, Maraging 300, C300, TS700, Hot-forming tool |

# Table of contents

# List of acronyms and symbols

| | |
|---|---|
| 3D | Three-dimensional |
| CAD | Computer aided design |
| SLM | Selective Laser Melting |
| LMD | Laser Metal Deposition |
| AM | Additive manufacturing |
| DoE | Design of Experiment |
| ISO | International Organization for Standardization |
| ASTM | American Society for Testing and Materials |
| DED | Direct Energy Deposition |
| PBF | Powder-bed fusion |
| LBW | Laser beam welding |
| 2D | Two-dimensional |
| Fe | Iron |
| Ti | Titanium |
| Ni | Nickel |
| Al | Aluminium |
| Co | Cobalt |
| Cu | Copper |
| Ar | Argon |
| N | Nitrogen |
| He | Helium |
| DLMS | Direct Laser Metall Schmeltzen |
| .stl | Standard Triangle Language - file format |
| .stp | Standard for the Exchange of Product model data – file format |
| EBM | Electron Beam Melting |
| LOF | Lack of fusion |
| LENS | Laser Engineered Net Shaping |
| CNC | Computer numerical control |
| LMD-w | Laser Metal Deposition using wire as stock material |
| OM | Optical Microscopy |
| SEM | Scanning Electron Microscopy |
| CT | X-ray tomography |
| FSW | Friction Stir Welding |
| OFAT | One factor at a time |

| | |
|---|---|
| COST | Change one separate factor at a time |
| CCD | Central Composite Design |
| ANOVA | Analysis of variance |
| PVD | Physical Vapour Deposition |
| AISI | American Iron and Steel Institute |
| UNS | Unified Numbering System for Metals and Alloys |
| DIN | Deutsche Industrial Norms |
| EDM | Electrical Discharge Machining |
| .csv | Comma Separated Value – file format |
| DIC | Digital Image Correlation |
| SS | Stress-strain |
| HAZ | Heat affected zone |

# List of quantities and units

| | | |
|---|---|---|
| Laser power | P | [W] |
| Scanning speed | $v_s$ | [$mms^{-1}$] |
| Layer thickness | w | [mm] |
| Hatch distance | h | [mm] |
| Volumetric Energy Density | VED | [$Jmm^{-3}$] |
| Linear Energy Density | LED | [$Jmm^{-1}$] |
| Laser spot diameter | d | [mm] |
| Cooling rate | | [$Ks^{-1}$] |
| Bead height | h | [mm] |
| Bead width | w | [mm] |
| Deposition speed | v | [$mms^{-1}$] |
| Powder feed rate | | [$gmin^{-1}$] |
| Shielding gas flow rate | | [$lmin^{-1}$] |
| Carrier gas flow rate | | [$lmin^{-1}$] |
| Track overlap | | [%] |
| Temperature | T | [°C] |
| Pressure | p | [Pa] |

| | | |
|---|---|---|
| Hardness Rockwell B | HRB | [-] |
| Hardness Rockwell C | HRC | [-] |
| Ultimate tensile stress | UTS | [MPa] |
| Strain at failure/Ultimate strain | | [%] |

# List of figures

# List of tables

# 1 Introduction

As industrial progress advances, new methods of manufacturing and material processing are being introduced every year. Additive manufacturing has also found its place among modern technologies and is being integrated into various phases of industrial production. Ranging from designing and prototyping all the way to the serial manufacturing process, it is hard these days to find an industrial branch, that could not benefit from implementing the additive technologies. Especially in the last decade, additive manufacturing has drawn a lot of attention as a next-generation manufacturing technology and matured in the meantime. While the initial concerns for most technologies were issues such as printability, stability, or the appearance of the resulting part, demands have moved deeper into the problematics over the years and showed that there is a lot yet to be discovered about each 3D printing technology that is introduced.

In terms of material, the research has gone as far as printing concrete, food, or organic cells. However, the usual materials used for 3D printing are still plastics and metals, which are the two most significant materials in the industrial world. Despite its higher difficulty, metal 3D printing has always remained at the top of the interest. The demand for having a machine capable of creating complex-shaped metal parts from a CAD model simply at the press of a button has driven development forward and resulted in research into many new different technologies. The two technologies discussed in this work, Laser Metal Deposition and Selective Laser melting, might be considered more traditional, since they have been among the metal 3D printing technologies for the longest time. Despite having a lot in common, the principles, as well as their applications, differ significantly. Each of them has its own drawbacks, but maybe more importantly its own benefits, which help to keep them among the most progressive manufacturing methods of today. And as with all technologies, their convenient combination might bring even more benefits.

Due to its relative youth, 3D printing brings a lot of new aspects to consider during the production process in comparison to conventional manufacturing methods. Terms such as the choice of material, final material properties, or the working conditions and environment often need to be approached in a completely new way. This brings many new challenges, but more importantly, it opens up new possibilities. Among them, besides innovative design or a shorter production loop, is the possibility to combine materials effectively and with added benefit, utilizing multiple material values at once. Not just discovering, but mainly mastering all the new techniques, that 3D printing offers, is fundamental for its full inclusion into everyday life as well as into large-scale industrial manufacturing.

## 1.1 Aim of the work

This thesis consists of two parts – research (theoretical) part, and experimental (practical) part.

The research part of the work focuses on powder based additive manufacturing technologies, specifically on Selective Laser Melting (SLM) and Laser Metal Deposition (LMD). Its purpose is to clarify their main principles in order to give a knowledge base for the experimental part. Their benefits and drawbacks are presented and compared. Finally, the research part should provide sufficient information to understand the idea behind combining these two technologies for added benefits.

The experimental part consists of two phases. As these phases are closely related, it is possible and beneficial to conduct them simultaneously and gather the information in one work.

The first phase is be conducted under the project AdditivePeen, which deals with the investigation of the surface treatment of AM parts using Laser Shock Peening. For the purposes of the project, the mechanical properties of two different materials manufactured by two different AM technologies will be characterized, based on tensile testing. The main goal is to compare the properties of as-built parts made by different technologies.

The second phase will be conducted within the project STREAM, which deals with surface treatment of AM parts using Laser Shock Peening, Mechanical treatment and Thermo-chemical treatment. In the framework of this project, several use cases should be produced, including a conformally cooled hot-forming tool manufactured by combining LMD and SLM technology. As a part of preliminary testing before manufacturing the actual component, the material and technology combination have to be tested. Within this work, a DoE on the process parameters of the LMD part of the manufacturing process is be prepared. The combined parts are investigated again using tensile testing and the resulting characteristics are presented.

# 2 State of the art

## 2.1 3D metal printing

### 2.1.1 Industrial role of 3D metal printing

The additive manufacturing process (AM), also referred to as 3D printing, is generally speaking a process for creating a part by joining individual layers of material together, usually according to a previously created CAD model. The name "additive" comes from the contrast with conventional manufacturing methods, such as machining, during which the material is subtracted from the bulk instead of added. Since the 1980s, when the first patent for a 3D printing machine was introduced, many new methods of 3D printing have been introduced and constantly improved, creating a wide scope of terminology and approaches. Even the variety of materials, that are being printed has increased. Besides metals and polymers, research has also focused on the printing of ceramics, concrete, cells, or even food.

An ISO/ASTM Committee F42 was formed in 2009 with the purpose of "promotion of knowledge, stimulation of research and implementation of technology through the development of standards for additive manufacturing technologies." According to the F42 committee, there are seven types of 3D printing processes [1]:

- Binder jetting
- Direct energy deposition (DED)
- Material extrusion
- Material jetting
- Powder bed fusion (PBF)
- Sheet lamination
- Vat photopolymerization

From a broader perspective, however, the processes can be further divided. A good overview including the division by the form of the entry material is shown in the figure below.

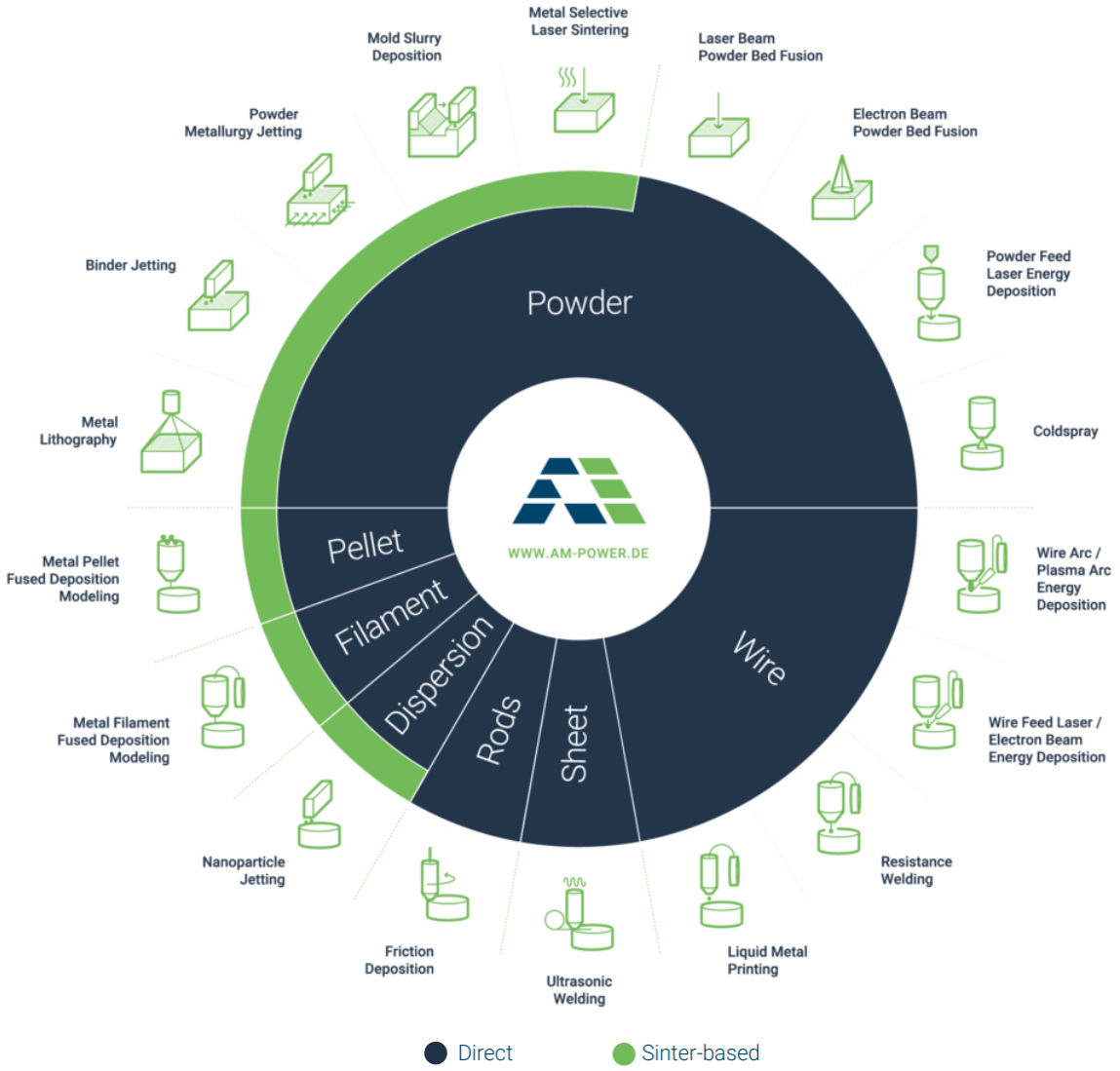


**Fig. 1 Overview of 3D printing technologies [2]**

Although 3D printing of polymers (plastic) is in the public eye the most, the materials much more significant for industry are metals. Given the differences in the level of complexity and costs of the equipment, it is only understandable that resin and plastic filament printers are widespread even among casual end users. However, using them at different stages of industrial parts development is very common as well. From hobby-printing of action figures to complex parts in moving 3D printed assemblies, polymer printing finds its place everywhere. But when it comes to prototyping of high-demand industrial parts, metal printing has the upper hand. And not only there. With the rise of part quality in recent years, the reliability of 3D metal printed parts allows them to be produced even for end-use applications, often in a whole series.

Introducing additive technologies as a way of producing functional metal parts offers benefits and new approaches, that would otherwise be hard to achieve. In terms of design, not only can additive manufacturing save a significant amount of time and resources, but it also allows the manufacturing of non-machinable shapes and geometries. Generally speaking, many restrictions that limit traditional manufacturing, such as undercuts or tool access, do not apply here [3]. This gives 3D printing technologies a large advantage over traditional machining in many specific applications. A good example would be components designed with the use of

topology optimization – a technique that helps create designs based on prescribed requirements and constraints. It uses mathematical models to either alter an existing design or create a completely new one. Whereas conventionally optimized designs (sizing and shape optimization) can usually easily follow the rules of manufacturability, topology optimization often results in complex geometries that are not always suitable for conventional manufacturing methods. Additive manufacturing, on the other hand, is a technology well suited to manufacturing complex structures with ease. This makes the combination of topology optimization and AM a very strong tool, which allows the engineer to get rid of many standard manufacturing limitations and focus on the part performance [4].

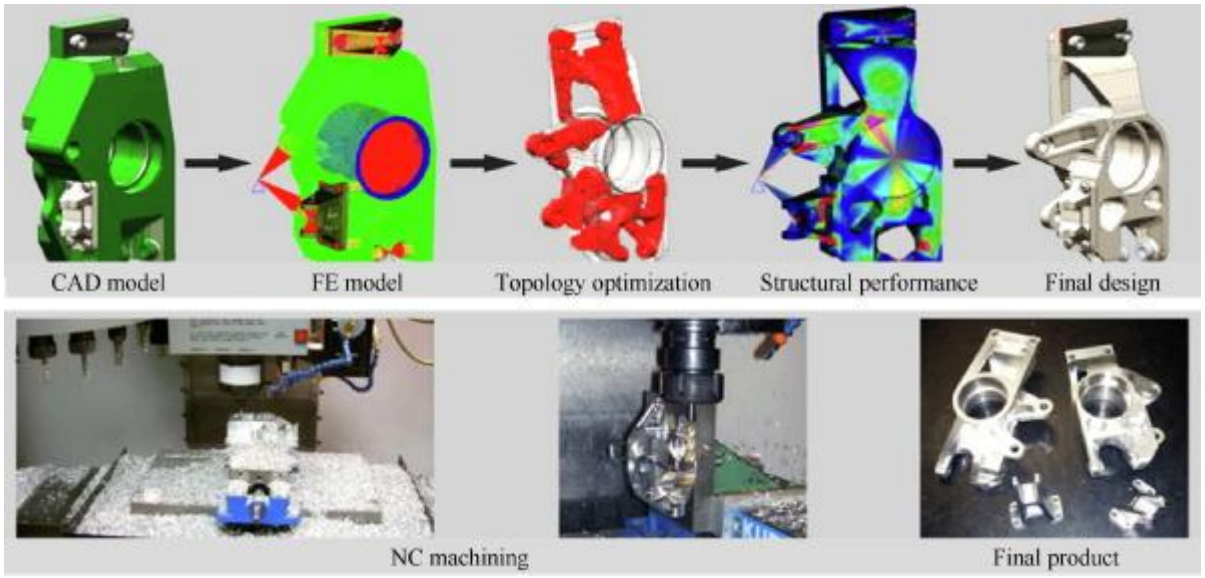


**Fig. 2 Process of topology optimization [4]**

Conformal cooling is another great example of how the 3D printing principle allows the manufacturing of complex integrated shapes. It is a design of cooling channels, usually in manufacturing tools, that are placed close under the contact surface and allow a flow of coolant dissipate the heat from the process. Conventionally, these are limited to straight holes, as they need to be drilled. AM on the other hand allows the channels to copy the geometry of the surface, ensuring more effective and even heat dissipation [5].

SLM and LMD will be discussed in further depth as these two AM technologies are related to the work developed in the context of this thesis. These technologies are among the most widely used methods of metal 3D printing today [6] and share many similarities. Before describing each of the technologies in detail, shared and general principles will be described, to create a knowledge base for better understanding and easier comparison of the individual technologies discussed in the following chapters.

### 2.1.2 Process principles

Both selected metal AM technologies share similarities with Laser Beam Welding (LBW). The laser beam is focused on a small area (laser spot) on the substrate material, causing it to melt locally creating a melt pool. The laser spot is moved across the surface of the substrate, causing the melt pool to move by melting more material in front of it while allowing solidification of the melted material in its wake. During this, additional material in form of fine metallic powder is being introduced into the melt pool, to increase the mass of the resulting solidified weld.

These weld tracks can be stacked next to each other, as well as on top of each other, allowing the method to build three-dimensional objects in a layerwise manner [7], [8].

Similar to laser welding, the nature of the interaction between the laser and the material is of importance, as well as the process parameters and conditions. Depending on the energy delivered by the laser, speed of the laser spot movement, and other factors, the welding process can usually be carried out in between two regimes – conduction welding (lower power density) and keyhole (penetration) welding (higher energy density).

Conduction welding represents the stable side of the scope. It is performed by heating the material at a slower rate until it reaches its melting point. The heat is tranfered solely by conduction, which means that the maximum weld depth is limited by the heat conductivity of the material. This results in a melt pool, that is usually wider than it is deep. Such a welding regime may be feasible in applications, where process stability, as well as the resulting appearance of the weld, play an important role. However, due to its low penetration, it is not suitable for heavy-duty applications, as it may lead to an insufficient connection of the materials. In the case of 3D printing, this welding mode increases the risk of poor inter-layer cohesion and delamination, as well as porosity and other defects in the final structure [9]–[14].

When the heat cannot dissipate fast enough (i.e. high energy input), the melt pool starts overheating and the liquid metal starts evapourating. The metal vapor expansion above the melt pool causes a steep rise of recoil pressure, which pushes down on the liquid, changing the shape of the melt pool and allowing the laser to penetrate deeper into the substrate. By further increasing the energy, a deep narrow cavity (keyhole) is created, filled mostly with the emerging metal vapour. This keyhole welding regime is much less stable for multiple reasons. First, the steep temperature gradients cause a strong flow of the melt due to changing surface tension, also called the Marangoni effect. The flow is further increased by the pressure from the expanding vapour. Moreover, the keyhole may start collapsing periodically depending on the laser scanning speed, which results in undesirable oscillation [11]. All these factors may add to an uncontrollable process of continuous keyhole creation and collapse, resulting in a highly unpredictable outcome. During the collapse of such a keyhole-shaped melt pool, gas cavities can be entrapped inside the material, making the keyhole regime prone to undesired porosity. At the same time, the increased liquid flow and vapour pressure on the melt pool surface usually cause spattering – ejecting of melt or other particles from the melt pool. Finally, plasma may appear in the process depending on the energy input parameters and surrounding atmosphere. This combined with other by-products of the process (vapour, ejected particles) creates a plume, that forms above the melt pool, where it may interact with the incident laser radiation, lowering its efficiency and altering the whole welding process. The trade-off for the overall instability is good penetration depth, which can ensure a much better connection between the materials (layers) if carried out properly. Stabilizing the keyhole is therefore of the highest importance during laser welding, as well as during 3D metal printing. Since both process stability and sufficient penetration depth are desirable, it is believed that the best results are achieved by optimizing the process parameters, so that the process is carried out in a quasi-stable transition regime between conduction and keyhole welding [11]–[14].

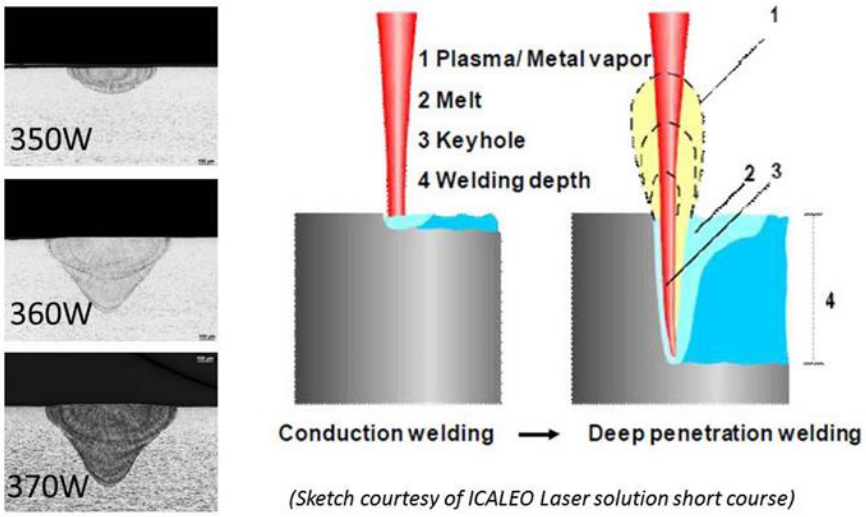


**Fig. 3 Welding regimes example [15]**

Concerning geometry, both SLM and LMD obey similar rules that apply to polymer extrusion technologies. Since the structure of the final part is made out of many single weld tracks, the resolution corresponds to the size of those welds. Although the shape of the track is often simplified as cylindrical, the actual cross-section of the weld is very different and asymmetrical.

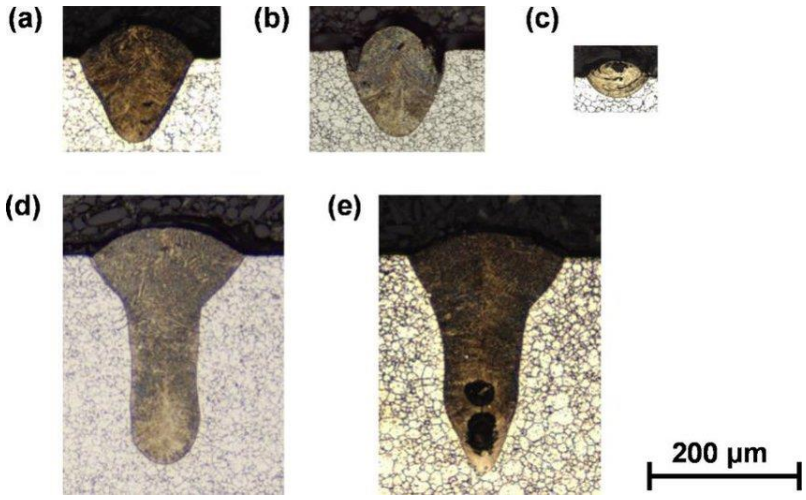


**Fig. 4 Examples of different melt pool modes; a) desirable, b) undercut/balling c) conduction mode d) keyhole mode e) keyhole porosity**

Due to this, the resolution may change depending on the process orientation. Moreover, while extrusion methods usually keep the printed bead the same, the shape and dimensions of the laser weld may vary throughout the process in relation to the changes in heat dissipation (e.g. thin structures or edges). However, the simplified model can be used to understand the resolution limitations. The cross-sectional 2D resolution is limited by the top-view dimensions of the weld track, similar to how milling resolution is limited by the milling cutter diameter. Therefore, sharp edges are not obtainable, but smooth geometries and contours are otherwise achievable. On the other hand, the side view resolution corresponds to the deposited layer thickness, as successive layers need to be shifted in respect of each other to create shapes and curves. Due to this, the printed parts will always have a stepped surface, often referred to as the staircase effect [16]. The following figure shows, how the staircase effect can be theoretically mitigated by changing the layer thickness.

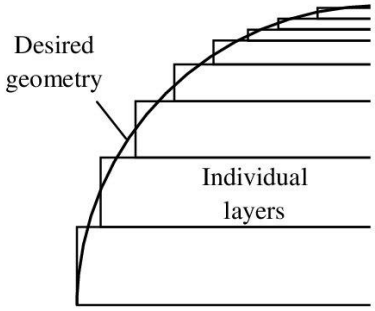


**Fig. 5 Staircase effect [16]**

### 2.1.3 Metal powders

Metal powders are an important part of the manufacturing world these days since they offer many advantages in areas, where wrought materials fall short. Tungsten carbide, which is widely used mainly in tooling, is a good example. Besides extrusion, sintering, injection moulding, and so on, additive technologies also use metallic powders as the starting material. Not only the chemical composition but also other properties of the powder particles affect the manufacturing process and resulting properties of the printed parts. A lot of these properties are determined by the type of powder preparation technology, which is called atomization.

The main properties of metallic powders are grain size distribution and grain morphology. These affect other properties, such as apparent density, tap density, angle of repose, flow rate (flowability), compressibility, and so on [17]. Sources define the usual particle size to be roughly between 2 – 200 μm, but the mean particle sizes are usually between 20 – 80 μm [18], [19]. The suitable size of the particles can differ for different technologies. For SLM, particles smaller than 5 μm would be considered as small, as they tend to form clusters which can be undesirable in the deposited powder bed. On the other hand, only particles up to the size of the deposited layer thickness can be used. For the best powder bed packing density, an optimal distribution is a combination of larger and smaller particles, as they fill the voids in between each other [19].

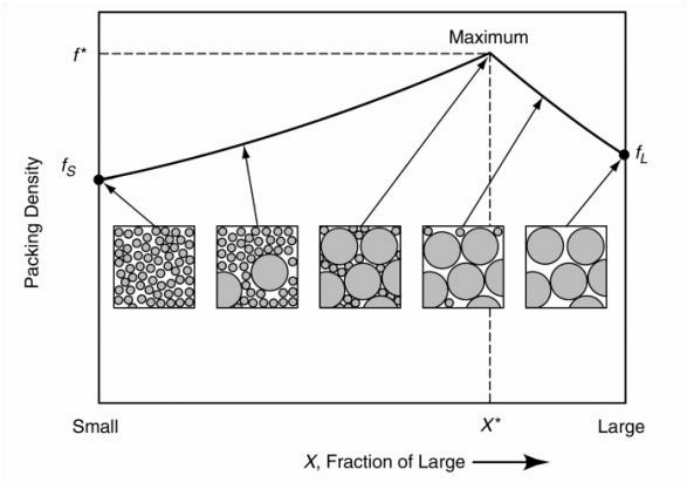


**Fig. 6 Influence of the particle size distribution on the packing density [19]**

For LMD, an important attribute is the flowability of the powder, as the stability of the process is conditioned by constant powder mass flow [20]. This can be affected by humidity or material composition (adhesion), but mostly by the grain morphology. This is usually determined by the type of powder atomization technology.

### 2.1.4 Materials used in powder AM

SLM can fabricate using a wide variety of materials. Among the most frequently used are Fe, Ti, Ni, Al, Co, and Cu-based alloys [21]–[23], but also pure metals such as Au, Cu, Nb, Ta, and Ti [24], all with their specific benefits and demands.

The printability of a certain material usually depends mainly on the ability to develop process parameters, which can ensure a stable process of the material melting and consolidating. Although the parameter combinations are usually very specific for every single material, they can vary significantly for different machines, powder properties, or quality requirements.

Similar to SLM, the ability of LMD to process a material depends mainly on its ability to create suitable powder particles and the capacity to develop reliable process parameters, which can be used to achieve sufficient results. This makes the range of materials used in powder AM very broad. Some of the most commonly used materials are listed below [25]–[27].

| Material group | Examples | Applications |
|---|---|---|
| Fe-based alloys, steels | 18Ni300 (Maraging steels)<br><br>316L, PH (Stainless steels)<br><br>H13, H20 (Tool steels) | Tooling, mechanical engineering parts<br><br>Medical<br><br>Hot-working, extrusion tools |
| Ti-based alloys | Ti6Al4V<br>CP – Ti (commercially pure)<br>Ti6Al7Nb | Aerospace/automotive lightweight components, Medical instruments/implants |
| Ni-based alloys | Inconel 625, 718. 939<br>Chromel<br>HX<br>Nimonic 263 | Aircraft engines, combustion chambers, High temperature + corrosion resistance |
| Al-based alloys | AlSi10Mg<br>AlSi7Mg0.6 | Heat exchangers, lightweight components |

**Tab. 1 Selection of materials processed by powder AM technology [21]–[23]**

## 2.2 SLM

### 2.2.1 Description of SLM

SLM stands for "Selective Laser Melting" and belongs to the Powder Bed Fusion (PBF) family of AM. Several closely related inventions and patents have been filed for liquid and non-metal materials before, but the first to acquire the rights for this specific method of fabrication was the company EOS GmbH from Krailling, Germany, under the label DMLS®[1] in 1997. At roughly the same time, it was also being developed by the Frauenhofer Institute for Laser Technology in Aachen, which later introduced the name SLM [27].

The method works by creating thin layers (usually 10 – 100 μm thick [30], [31]) of fine metallic powder using a recoating element, which are subsequently scanned by a laser, melting the powder material and connecting it with the previous layers. After scanning the desired area in one layer, the part is lowered by the height equal to the powder layer thickness, after which the recoater spreads a new layer of powder across the building plate, and the process repeats.

At first, a digital 3D model needs to be prepared using CAD software, usually in the format ".stl" or ".stp". The model is further digitally sliced, uniaxially with steps equal to the intended powder layer thickness, converting the model into a set of tightly packed 2D geometries. These represent the individual areas to be scanned by the laser in each step, layer by layer [1], [32].

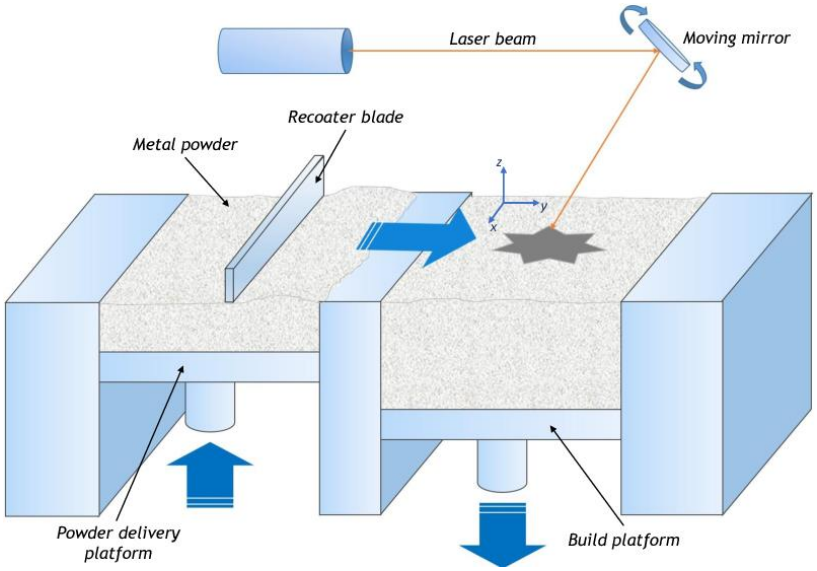


**Fig. 7 SLM process schematic [33]**

The process usually takes place in an enclosed chamber for multiple reasons, one of which is to ensure a nonreactive environment. Before the start of the process, the chamber is filled with protective gas to avoid oxidation due to the high temperatures. The most commonly used gases are nitrogen or argon, depending on the reactivity of the processed material. Nitrogen is usually the cheaper option since it can be obtained from the atmosphere using an integrated (or external) generator [34]. However, materials that have an affinity to Nitrogen require the use of argon as

[1] The abbreviation DMLS stands for German "Direkt Metall Laser Schmelzen" which translates to English as "Direct Metal Laser Melting" [28]. The incorrect translation "Direct Metal Laser Sintering" often leads to a misleading interpretation, and an incorrect claim is often found in scientific publications, that, unlike SLM, this technology does not fully melt the material [1], [29].

the shielding atmosphere. Besides preventing oxidation, the gas plays another important role in the process, and that is carrying away the by-products that condense above the melt pool as the laser scans the powder bed. This vapour plume (a mix of plasma, metal condensate, and smoke) would interfere with the incident laser beam, causing disruption and instability of the melting process. Therefore, a continuous flow of shielding gas across the powder bed is desired. The quality and effects of the gas flow are usually specific to different machine architectures and have been extensively studied, as they have a strong influence on the resulting quality of the process [35]–[38].

A build platform is used as a base for the printing process and all the parts are firmly connected to it from the beginning. This connection serves two main purposes – heat dissipation and prevention of part deformation. The laser irradiation heats the part significantly over time and the accumulation of heat in the part may lead to its overheating. Therefore good conduction to the platform needs to be ensured, which can be achieved by including additional removable support structures [39]. However, due to high-temperature gradients, the evolution of residual stresses in the material is unavoidable, which can lead to deformation of the parts during the print, thus the second important role of sufficient connection to the build platform [40]. After the printing process, the platform is extracted together with the parts and support structures, which is followed by postprocessing including additional heat treatment and the removal of the platform and support structures.

The theoretical resolution of the print is defined by the layer thickness (which also affects the severity of the staircase effect) as well as by the size of the melt pool created at the focal point of the laser. This is proportional to the laser beam spot diameter and can be also slightly adjusted by altering the laser power output. For SLM, the spot diameter is usually 40-100 μm (for EBM it is usually larger) but can reach up to 500 μm in the biggest machines [41], [42]. Experimental measurements have shown the maximum melt pool dimensions to be around 250 μm for a laser beam spot diameter of 50 μm [43]. However, as mentioned above, the accuracy may vary depending on the specific face orientation, process parameters, etc. Lasers used in SLM technology can vary, but most used are continuous fibre lasers with power between 200 W and 1000 W [34], [44], [45].

Maximum part dimensions are limited by the dimensions of the process chamber. These may vary for different manufacturers and machine types. For example, the “EOS M100” can print parts Ø100 x 95 mm [41], while the “Concept Laser XLine 2000R” is referred to by Concept Laser as the world’s largest SLM with 800 x 400 x 500 mm build volume [46].

### 2.2.2 Benefits and applications of SLM

The benefits of applying this technology come to the fore in various fields such as the aerospace, automotive, and healthcare industries [47]–[49].

An important role in the medical field is the effective manufacturability of prosthetics and implants, such as joint or teeth replacements. Typically, the implants need to be tailored for each patient, meaning that only single numbers of each part are made. This fact combined with the often irregular and complicated geometry of the implants makes the conventional manufacturing methods economically unsuitable for such applications. Also, organic-like porous structures on the implant surfaces are often desired, so that the body tissues can connect with them properly. This is also easily achievable with SLM compared to conventional manufacturing [50]. Typically near-net-shape geometries are obtained using this technology, which can significantly reduce preparation and lead times in other similar cases of patient-specific applications, such as dental implants [51].

In the aerospace and automotive industries, the focus is on creating lightweight structures, reducing the prices of complex parts with low production volume, and integrating large assemblies into a smaller number of parts. In this manner, complex monolithic thrust chambers or landing gear fittings have been made [52], as well as optimized parts for space satellites [53]. The automotive industry also uses the design freedom of the technology to optimize parts for functionalities such as safety properties while maintaining their weight [54].

The ability to create functional internal geometries, that are hard to achieve by other means, is advantageous in the tooling industry when designing dies and moulds. Conformal cooling can be made by printing cooling channels during the build of the parts, rather than drilling them afterward. The freedom of internal design allows the channels to be at a constant distance from the tool surface, regardless of the complexity of its shape. This means more uniform cooling of the tool is achievable, increasing the resulting part properties and reliability of the moulding process [55], [56].

### 2.2.3 SLM parameters

There are many parameters and factors affecting the final part during the process. Since the scale of the process phenomena is arguably small (melt pool size ~ 100 μm), it can be quite sensitive to changes in ambient temperature and pressure [57], as well as the characteristics of the atmosphere and gas flow in the process chamber [35]. Even factors such as choice of recoating element, recoating speed, or the delay between scanning successive layers should be considered. Depending on the depth of understanding of the process, the number of factors can go up to 100 [8]. The parameters mostly discussed, however, are those directly affecting the melting process and quality of single welds:

- **Laser power - P [W]:** Laser power is one of the most important parameters in SLM. It is closely related to the laser spot size and the overall energy input. It is also the main determinant of the welding regime. Higher laser power usually leads to deeper melt pool and therefore better density of the material, but also to stronger forces of the flow and vapor pressure above the melt pool. The power of the lasers used in SLM can range from 100 W to 1 kW [8], [58]–[60].
- **Scanning speed - $v_s$ [$mms^{-1}$]:** Also referred to as laser speed or scanning velocity determines the rate, by which the laser spot moves across the powder bed. Together with laser spot size and laser power, they define the incident energy density on the powder bed surface. The scanning speed plays a major role in setting the process productivity, but is highly limited, mainly because higher scanning speed causes instabilities in the weld track formation. The drawbacks of saving process time by increasing the scanning speed are usually worse surface properties and lower process stability. The usual scanning speed varies between 500 $mms^{-1}$ and 1000 $mms^{-1}$ [13], [61]–[64].
- **Layer thickness - w [μm]:** The thickness of the deposited powder bed affects mainly productivity and geometry resolution in the vertical print direction. The optimal layer thickness depends on the material absorptivity, particle morphology, and other powder characteristics. The usual layer thicknesses are 20 μm, 40 μm, 60 μ,m or 80 μm, but even a thickness of 200 μm has been experimentally proved to be able to handle a stable process [31]. Usually, the process parameters are developed for specific layer thickness, which does not vary throughout a single build job. Higher layer thickness is usually associated with higher productivity but also a higher risk of insufficient melting and defect formation [65], [66].

- **Hatch distance – h [mm]:** The distance between adjacent laser paths. It affects the overlapping ratio of the tracks which is important for ensuring maximum material density. Therefore it should be around the size of the melt pool diameter [8].
- **Scanning strategy:** The order and distribution of individual laser paths (hatch lines) across individual layers. Optimizing the scanning strategy can save production time, but more importantly, it affects the resulting properties of the part, such as residual stresses or subsurface porosity [8], [67].

Complex factors, such as Energy Density or Volumetric Energy Density (VED) are often used in publications to describe process windows with the intention of finding a correlation between these factors and the resulting properties. This is based on the theoretical calculation of energy needed to melt a defined amount of the material.

$$VED = \frac{P}{V_s \cdot d \cdot w} \; [Jmm^{-3}] \quad (1)$$

This equation is often further simplified to Linear Energy Density (Linear Energy Input, LED)

$$LED = \frac{P}{V_s} \; [Jmm^{-1}] \quad (2)$$

*P – laser power, Vs – scanning speed, d – laser spot diameter, w – layer thickness*

It has been experimentally disproved that the process window can be well defined just by a range of a single factor such as VED. It is not able to capture the complex physics such as Marangoni flow, hydrodynamic instabilities, recoil pressure, and other factors, that in the end define the morphology of the weld tracks [58]. It is, however, able to effectively capture certain process characteristics and can be useful for getting an approximate idea about the energy input in the process from a thermodynamic point of view [58], [67], [68].

### 2.2.4 Defects and challenges in SLM

The most common challenge to overcome with the SLM technology is the **porosity** or part density. There are many mechanisms for how pores and cavities of different sizes and shapes can be formed in the fabricated part, most of which can be mitigated by optimizing the process parameters.

**Gas porosity**

One type of porosity is **gas entrapment**, when a gas bubble becomes stuck in the solid material, often due to the collapse of a keyhole [69]. Another cause can be the insufficient packing density of the powder bed, which raises the amount of free space between the particles and therefore the risk of entrapping the gas in the material. Gases can also be present in the powder grains prior to the build [70]. Gas porosity can be identified in the metallographic analysis due to their typically round shape of the pores.

**Cavities and Lack of fusion**

Irregular cavities are also often present in the material but are usually of different origins. As has been said before, cavities can occur when the spacing between individual weld tracks is too big or when the melt pool penetration is not deep enough. They can also be caused by improper track formation, as it may also lead to poor overlapping of the tracks [13], [70]. A specific type of defect is called **Lack of fusion** which are areas of insufficient material bonding (LOF) [70].

These usually occur in the interface between layers, as the melted layer reaches the previous one, but does not create a metallurgical connection. This can be caused by insufficient energy input or insufficient wettability caused by oxidation of the solid surface [70], [71]. LOF defects are typically thin cavities with sharp edges that may contain non-melted particles.

**Balling, spatter, and inclusions**

Another defect typical for powder-based additive technologies is different types of inclusions. These are usually non-melted particles of the original powder or particles created during the melting process that were redeposited on the powder bed. With proper choice of processing parameters, non-melted original particles mostly coexist only with other types of defects, like LOF [70]. However, two mechanisms of creating new particles that can be hard to melt are commonly present during the process. **Balling** is a phenomenon describing the forming of round particles that have a poor connection to the bulk material. Surface tension and insufficient wettability usually play a big role in their evolution. Balling usually refers to particles significantly larger than the original powder particles and can also be responsible for the introduction of other defects due to their problems with melting [67], [68], [72]. Another phenomenon called **spatter** refers to particles that are ejected from the melt pool or its surroundings due to the vapour pressure and strong flows inside the melt pool. These particles can be of various sizes, shapes, and origins, including ejected original powder particles and bigger products of balling. The redeposited particles can again be hard to melt, for example due to oxidation of their surface during their flight [67], [69], [73]. All of those particles can end up included in the material without proper metallurgical bonding.

**Residual stress and cracking**

Due to extremely local high heat input, the cooling rates of the melt pool during the process can reach up to $10^8 Ks^{-1}$ [69], [74]. This large temperature gradient causes a large residual stress in the material. This can, besides other problems like part deformation, cause crack initiation and propagation in the fabricated part. Materials with lower heat conductivity may be more vulnerable to this effect [40], [70].

Hot isostatic pressing and specific heat treatment have been successfully used in some cases to improve the part density post build [75], [76], by closing some of the cavities and pores, improving the mechanical properties. However, the main goal is to achieve a density as close to full as possible during the build.

All these defects decrease the mechanical performance of the material, as they often act as failure initiation points, especially during cyclic loading [75], [77]. Defects with sharp edges like LOF cavities present a higher risk of crack initiation, especially in combination with any residual stresses.

## 2.3 LMD

### 2.3.1 Description of LMD

LMD stands for Laser Metal Deposition, which is one of the DED technologies. Also referred to as Laser Engineered Net Shaping (LENS), Laser Power Deposition, Laser Material Deposition, or Laser-aided Direct Metal Deposition, it belongs to the family of Direct Energy Deposition technologies, together with other techniques such as Directed Light Fabrication or 3D Cladding. The early concept developed from welding techniques by implementing the idea of consolidating multiple welds on top of each other. With the earliest patents being submitted in the 1950s [78], this method evolved over the years as a tool for repairing metal parts as well as building whole three-dimensional parts and was given the name LENS for the first time by the laboratories of National Technology and Engineering Solutions of Sandia, LLC. in the USA [79].

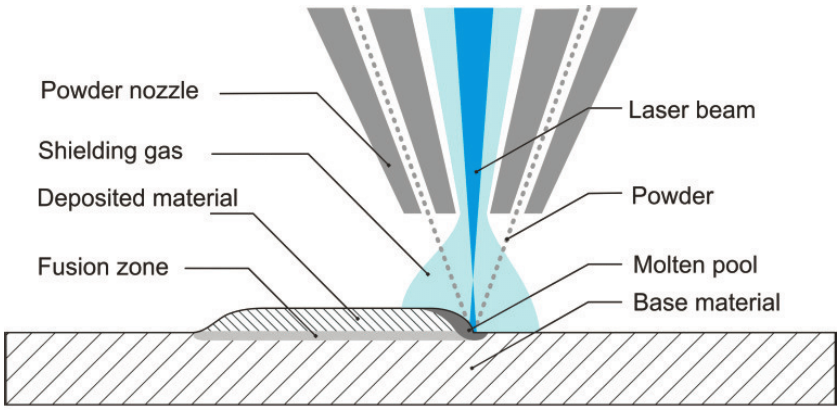


**Fig. 8 LMD process schematic [80]**

Similar to SLM, this method also uses a laser to create a melt pool and fine metallic powder as a building material. However, the principle of delivering the material to the substrate differs fundamentally. The laser, in this case, is mounted on a printing head. The laser optics inside the head are fixed, which means that for moving and targeting the laser spot, the whole laser head needs to be moved relative to the printed part. The positioning of the head is usually don in a similar way to CNC machines, by moving both the part and the printing head in multiple axes. The additional powder is simultaneously delivered directly into the melt pool via channels mounted on the printing head. This assembly together with the shielding gas delivery system creates the work nozzle [81]–[83].

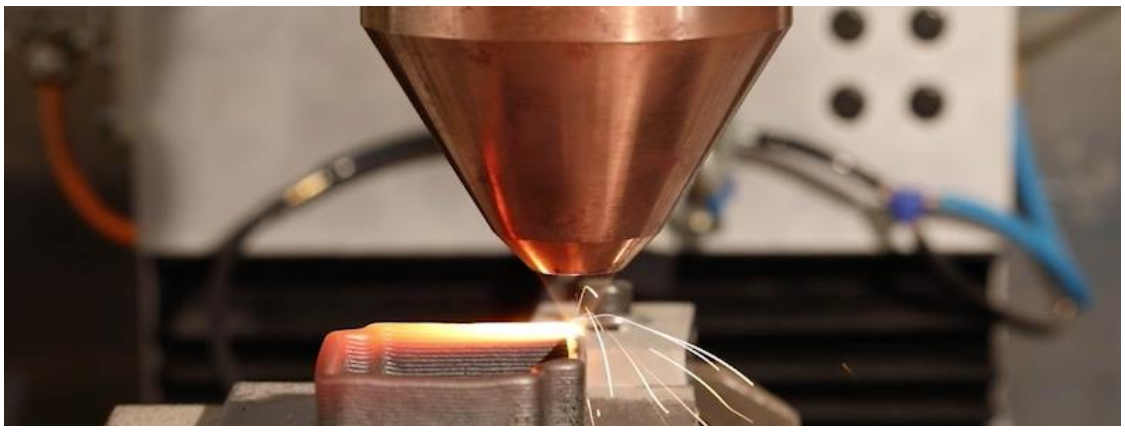

**Fig. 9 LMD process [84]**

Originally developed for coating, this technology is very close to numerically controlled welding, with the biggest difference being the deposition strategy and amount of material deposited. Before powder was used, wire-fed systems (LMD-w) were commonly used and still have the upper hand over the powder-based process in many respects. Based on the material and the form of the feedstock, the material costs can be up to twice as high for powder than for wire [85]. Also, the efficiency of the wire process is near to 100%, whereas during the powder-based process the effective use of the material may vary between 35 % - 97 % [86]. Last but not least, the homogeneity of the resulting part is easier to achieve using the wire, as the laser-wire interaction is much more stable than the laser-powder interaction. The powder-fed process on the other hand is much more flexible, as the range of the work-nozzle movement is larger, and better resolution is achievable, as the melt pool size is adjustable and usually smaller [85], [87]. In general, the wire-fed system is considered more robust, as well as faster in terms of deposition rate. However, direct comparison of deposition rates is difficult, as it may vary significantly for different parameters and materials [88], [89].

Three types of nozzles are commonly used for powder-based LMD. They differ in their construction, properties, and also applications for which they are meant to be used [90].

The off-axis setting derives from the wire-fed process, which is fundamentally the same as laser welding with metal wire filler material. This construction delivers the powder to the melt pool via a single channel from one side. Such nozzles can be overall smaller overall, offering better access to the printing location. It is also an economical option. On the other hand, the productivity is rather low and the process is limited to being unidirectional since the movement of the work head should be always performed in the same relative position of the powder channel to the deposition direction. It is commonly used for depositing layers on rotational parts, where the direction of deposition does not change.

In order to allow the work head to move freely, coaxial nozzles were developed. The coaxial-discrete setup feeds the powder into the melt pool via multiple channels (usually 3 or 4), which focus the streams of powder to the melt pool. These channels are placed radially around the nozzle outlet, allowing sufficient quality of deposition in all directions. These nozzles ensure high productivity while maintaining a wide range of movement.

The coaxial-continuous nozzle setup delivers the powder to the melt pool via a thin space between two conical surfaces. This nozzle delivers powder uniformly among the whole circumference of the outlet, ensuring great stability of the process in all directions. They are widely used for their high efficiency. They have also the strong advantage of a small area of powder focus, which allows more precise deposition. However, this design comes with the drawback of higher cost resulting from the more complex geometry. Also, continuous nozzles are the most sensitive to working angles, since the inclination of the nozzle changes the

direction of the gravity vector and therefore influences the distribution of the powder across the nozzle outlet. [90]–[92]


**Fig. 10 Powder feeding nozzles [87]**

The resolution of the print, similarly to SLM, is mostly affected by the laser spot diameter, which can vary from around 0,5 mm – 1,5 mm [93], [94]. The maximum part size varies for different process environments. For enclosed machines, the workspace is usually well defined and goes up to 1200 mm x 800 mm x 800 mm in the Magic 800 machine from AddUp Inc. (BeAM) [95]. However, external systems are commonly used, where the work nozzle is mounted on an industrial robot arm which allows more movement freedom. This is especially beneficial for processing large parts such as turbine blades or long shafts.

Multiple gases are usually present in the process. Just like other welding processes, a shielding atmosphere needs to be deployed to prevent oxidation and other undesirable reactions during the melting. While some processes take place in enclosed chambers filled with inert gas (or vacuum in case of electron beam melting), a more common, and cost-effective method is to deliver the shielding gas locally to the area of melting, using channels inside the printing nozzle. Optimizing the amount of shielding gas used has a strong impact on the quality of the deposited material. Secondly, a carrier gas is used to drag the powder through the delivery system to the nozzle. It is responsible for accelerating and injecting the powder into the melt pool. The interaction of both gases with the powder directly influences the powder distribution in the melt pool [91], [96].

The gases used are in most cases argon and helium as the shielding and carrier gas respectively. The use of nitrogen as shielding gas is often feasible for its lower cost, however, its reactivity with the processed elements needs to be considered. Especially alloys containing Titanium, Niobium, or Vanadium are prone to undesirable reactions with nitrogen. Alloys like Inconel 718 or Ti6Al4V are therefore incompatible with nitrogen shielding. Helium is a good alternative, considering its inert properties. However, since the amount of shielding gas needed during the process can be rather high (7-15 l/min [91]), cheaper argon is usually a more favourable option. However, helium has, in comparison to argon, lower density and therefore overall better dynamical properties. This ensures smoother fluid flow, which is why it is usually preferred over argon as the carrier gas in the powder delivery system [96], [97].

### 2.3.2 Benefits and applications of LMD

Besides building whole functional parts, LMD is known for its ability to repair damaged parts. This is usually performed by building up several layers at the desired location, which adds enough material, from which the final geometry can be machined and finished. Conventional welding in such cases is often not feasible, because of the high energy input which might cause part distortion and typically creates a large heat-affected zone around the weld beads. LMD overcomes these problems with its fast laser exposure, which usually leads to smaller melt-pools and lower impact of the heat input on the joint area [98], [99].

Another aspect that makes this technology advantageous for repairs is its flexibility in terms of geometry. Unlike SLM (PBF), the layers do not need to be deposited in a plane, since the nozzle (welding head) can move in multiple axes relatively to the workpiece. Non-planar layers are therefore manufacturable. All these benefits also come to the fore when creating coatings of different thicknesses on surfaces of various geometries. Typically this is used for simple parts such as drive shafts but is often used for parts with complex geometry like turbine blades [25], [98]–[101].

Besides altering the geometry, this ability of LMD is also used to create coatings with different properties. Layers of materials with different compositions are often deposited as protection from the work environment [25]. The deposition of porous coatings has also been investigated, and used to create biocompatible features on the surfaces of implants [102], [103].

Thanks to continuous powder delivery from the powder hoppers, LMD has the option to mix different materials in-situ and change the material composition during the run of the process. This allows creation of functionally graded materials for different purposes. However, different material compositions are usually sensitive to changes in the process parameters, and therefore require extensive parameter development and control, in order to be printed properly [104], [105], [105], [106].

A significant benefit of LMD is the ability to print material on parts, that have been previously processed. Together with good automatization, this allows the integration of the technology into existing manufacturing cycles. A good example of this is hybrid manufacturing solutions. These usually consist of a multi-axis machining machine with an integrated LMD work head. In such machines, the additive process can be included in the CNC program, either prior to or after machining, or even in between individual machining cycles [103]. But this attribute of LMD can be beneficial even without integration into hybrid systems. Besides repairing and renewing original geometries, LMD can add material to simple-shaped prefabricates to create more complicated geometries, that would otherwise require costly resources. An example of

this could be switching to cut-outs from sheet metal and adding features with LMD which saves the stamping tool wear and allows easy change of the knife contour [107].

**Fig. 11 Kitchen knives that used to be stamped [107]**

Compared to other metal 3D printing techniques, DED techniques usually have the fastest build rates, making them attractive in terms of integrating into the large-scale manufacturing of products like car or plane parts [108].

### 2.3.3 LMD parameters

One of the main process characteristics are the properties of deposited beads. These can vary based on the type of nozzle, material, laser power, deposition speed, and many other variables. Generally speaking, larger beads are associated with higher productivity, while smaller beads with higher accuracy. However, research papers have been presented, which show, that efficiency and accuracy can go hand in hand [88]. Other properties, such as resulting part density, porosity, microstructure, or residual stresses are also of high interest.

Similar to the SLM process, depending on the depth of understanding, the number of parameters influencing the process can get very high. Although the process is overall more robust than SLM, there are other variables that need to be considered. Factors such as powder flowability and nozzle working angle can strongly influence the results even though they are usually considered secondary control variables [20], [92]. There are, however, several parameters that are believed to influence the process significantly more than others:

- **Bead dimensions – h, w:** The cross-section shape and dimensions (height and width) are complex parameters that directly depend on other process variables. Nevertheless they are sometimes used to characterize the process as they directly affect other process characteristics, such as deposition rate and deposition strategy, as the bead height defines the **layer thickness**. They also determine the maximum resolution of the print [80], [109].
- **Laser power - P [W]:** Laser power is one of the most important parameters in LMD process. The amount of energy delivered by the laser is responsible for the welding regime and dimensions of the weld bead. Conduction regime is often sufficient, since it

provides enough penetration thanks to overall larger melt pool [110]. The size of the melt pool for a constant laser spot diameter is also affected by the laser power, especially in cases of low power processes [111]. The laser power of LMD machines can go up to 8kW [112].

- **Laser spot diameter - d [µm]:** The laser spot size together with laser power defines the overall energy density. It is the most influential factor affecting the melt pool size, and therefore print resolution. The challenge in maintaining constant spot size is control of the distance between the nozzle and the bulk surface [90]. The range of laser spot diameters is usually from 0.5 mm to 3.5 mm [111], [113].
- **Deposition speed - v [mms$^{-1}$]:** Besides laser power, the speed of the nozzle movement across the build surface is considered one of the main process parameters. It directly affects the deposition rate, but also the melt pool behavior and therefore the overall weld bead quality. High deposition speed ensures short exposure times, resulting in higher cooling rates and small heat affected zones. Slower deposition rates on the other hand, are sometimes related to larger melt pools and weld beads, resulting in high productivity. Works have been presented studying the influence of deposition speed on properties such as microhardness [114] or surface finish [115]. However, the resulting quality comes down to the stability of the melt pool and solidification characteristics [79], [116], [117].
- **Powder feed rate [g/min]:** The amount of material delivered into the process needs to be controlled with respect to the other process factors and conditions. For specific conditions, the range of feed rates is usually rather small. Too high feed rates can lead to insufficient melting of the powder resulting in bad connection to the bulk material or inclusions in the resulting part. It may also be uneconomical as the ratio of delivered material to effectively used material rises. On the other hand, too low feed rates can lead to excessive unused energy, which makes the melt pools bigger and less stable, with the possibility of evaporation or undesirable keyhole effects [79], [102].
- **Shielding gas flow rate [l/min]:** The purpose of shielding gas is to protect the process from undesired reacting with the process environment (mainly oxidation). In cases of closed process, the whole process chamber can be filled with the protective atmosphere. However, the shielding gas is more commonly employed locally from the work nozzle directly into the welding spot. Besides protection, the volume and velocity of the gas can also affect the weld bead properties, such as its shape or porosity. The amount of gas used is usually higher than the amount of carrier gas. Effect of shielding gas flow rate ranging from 0 lmin$^{-1}$ to 90 lmin$^{-1}$ have been investigated [118], however more common values vary between 5 lmin$^{-1}$ and 12 lmin$^{-1}$ [91], [96], [97].
- **Carrier gas flow rate [l/min]:** The carrier gas is responsible for delivering the powder material through the channels into the melt pool at desired speed and rate, whilst protecting it from oxidation on the way. Depending on the delivery system design, the carrier gas flow rate determines the impact velocity of the powder, as well as its distribution and therefore efficiency of the process [96]. The rate of the carrier gas flow usually varies from 2 lmin$^{-1}$ to 6 lmin$^{-1}$ [116], [118].
- **Track overlap [%]:** The overlapping ratio of the neighboring weld tracks is of importance not only because of sufficient metallurgical bonding, but affects also the resulting structure and porosity [119]. Overlap too small might lead to insufficient remelting and porosities at the weld bead boundaries, whereas overlap too high might result in overheating and instability of the process [79].

- **Deposition strategy [-]:** Deposition strategy is a complex factor that determines the arrangement of the weld beads as well as the order and direction of their deposition. With the geometrical complexity of the part rises the importance of choosing the right strategy, as it is often a decisive factor for buildability of the part. Although general rules can be followed, such as changing the bead direction in every layer in order to eliminate anisotropy and residual stresses of the material, a proper choice of deposition strategy requires significant amount of experience [60], [77], [120], [121].

Complex parameters similar SLM (equations (1) and (2)) are sometimes also used for LMD to estimate the power input to the process [110].

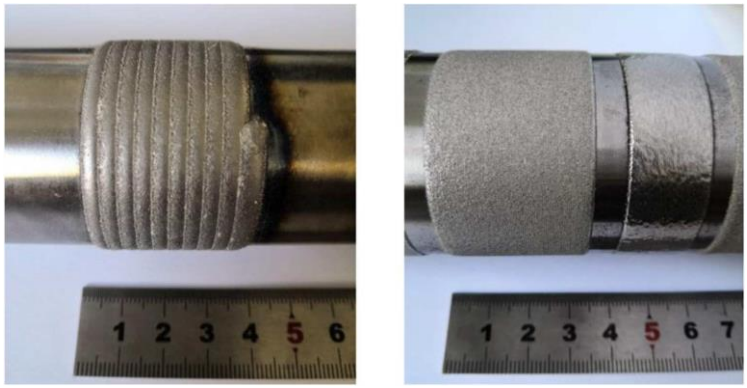

**Fig. 12 Surface of the deposited material for two different parameter sets [88]**

### 2.3.4 Defects and challenges in LMD

Defects and anomalies typical for LMD bring a more complex group of challenges than SLM or conventional welding, while sharing a lot of similarities with them. In case of density and porosity, the challenge is the same as with SLM but on slightly bigger scale. Introducing gas porosity in the bulk is even more likely to happen, as the gases are being blown directly into the melt pool area. The Lack of fusion defects on the other hand are less likely to happen, as the penetration is usually significantly deeper than in SLM. Inclusions and non-melted particles may also end up in the bulk material during deposition, causing similar threat to those occurring during the SLM process. Challenges shared with laser welding are mainly residual stresses, shrinkage and development of heat affected zones [102], [122].

Very significant area of problems are geometrical issues. Depending on the process characteristics, the deviation from the nominal geometry can vary a lot and usually stands as a reason for necessary postprocessing machining operations. Besides the tolerance issues, other specific geometric deviation can occur:

**Non-uniform layer thickness**

Although an optimized the process is usually suited for a constant layer thickness, the real layer thickness for one set of parameters may vary throughout the print job. This is caused mainly by the change of heat transfer, as the base plate usually serves as a heat sink. This causes the earlier layers to be cooled more effectively, creating higher beads. In the latter layers, the heat transfer rate decreases, the part heats up and the solidification rate drops, causing the welds to be broader but thinner in height. Proper process monitoring, as well as implementing support structures to create heat flow routes are possible ways of mitigation [122], [123].

**Edge effects**

Edge effects mean mostly material overlay or underlay (lifting or falling) which occur at the beginning and end of the weld track, or at a point of abrupt process direction change. Their cause may be in local parameter change, as well as in local change in thermal conductivity (edges in general). If stacked over multiple layers, this anomaly may have significant effect on the resulting geometry accuracy and can lead to process failure. Therefore it is important to choose proper scanning strategies and prevent part overheating [122], [123].

**Residual stresses and distortion**

The thermomechanical nature of the manufacturing process induces fast cooling rates, non-equilibrium solidification and therefore inevitably also residual stresses. During the building process, the heat-induced distortion is partially mitigated by strong connection to the base platform, maintaining correct dimensions. However, depending on the part geometry and orientation, the whole part or its features may deform, or even induce cracking and delamination of layers. This typically occurs at the part – base plate interface, or in the region of separate layer boundaries. The thermal history of the part manufacturing often dictates the means of heat treatment in the postprocessing. Besides heat expansion itself, depending on the material the part may undergo additional volume changes due to crytalographic changes during phase transformation. This often results in shrinkage [121], [122].

A popular approach to reducing of residual stresses is preheating of the substrate or process chamber in order to reduce the cooling rates. Different scanning strategies may also result in different distribution of residual stresses, possibly mitigating their impact by alternating the orientation of stress fields [77]. However, in most cases an additional heat treatment is employed either way, as a common step of the postprocessing.

**Porosity, cavities and inclusions**

The mechanisms of introducing cavities and inclusions of different types into the substrate during the manufacturing are close to identical to the ones in SLM technology discussed above, as well as their effects on the resulting part [123]. Thanks to the powder-stream based nature of material delivery to the melt pool, an additional challenge pose the danger of particle clusters occurrence. Under specific conditions, these may remain not melted completely and act as a large stress-concentrating defect. Parameter optimization can usually lead to porosity reduction, possibly reaching bulk densities over 99,5% [122].

## 2.4 Defect control and examples

3D printed metal components are usually investigated by conventional means of destructive testing, using optical microscopy (OM) and scanning electron microscopy (SEM) of different sections of the part, as well as the fracture surface after destructive testing (fractography). Especially beneficial for 3D printed parts are non-destructive methods, such as X-ray computed tomography (CT), as they can effectively investigate and evaluate single parts. CT is especially useful for parts with internal geometry, that needs to be controlled. Other methods such as the acoustic emission method have also been used in experimental works to investigate internal geometry [124].

Examples of results for different defect control methods are shown in the following figures.

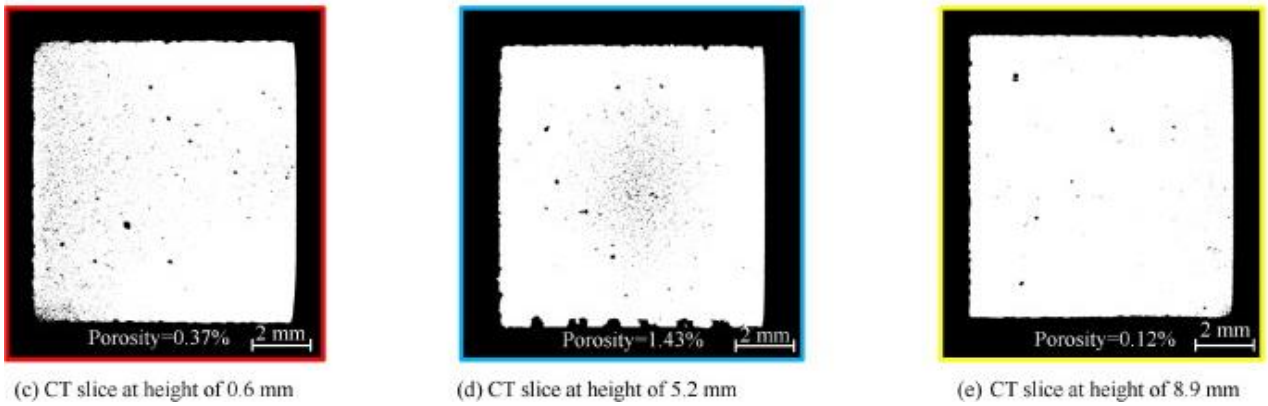


**Fig. 13 Porosity in cubic specimen AlSi10Mg by CT [125]**

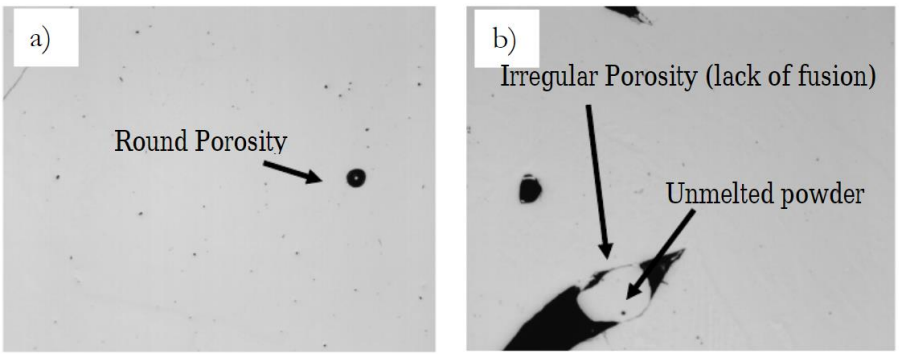


**Fig. 14 Optical microscopy of porosities in IN718 specimen [71]**

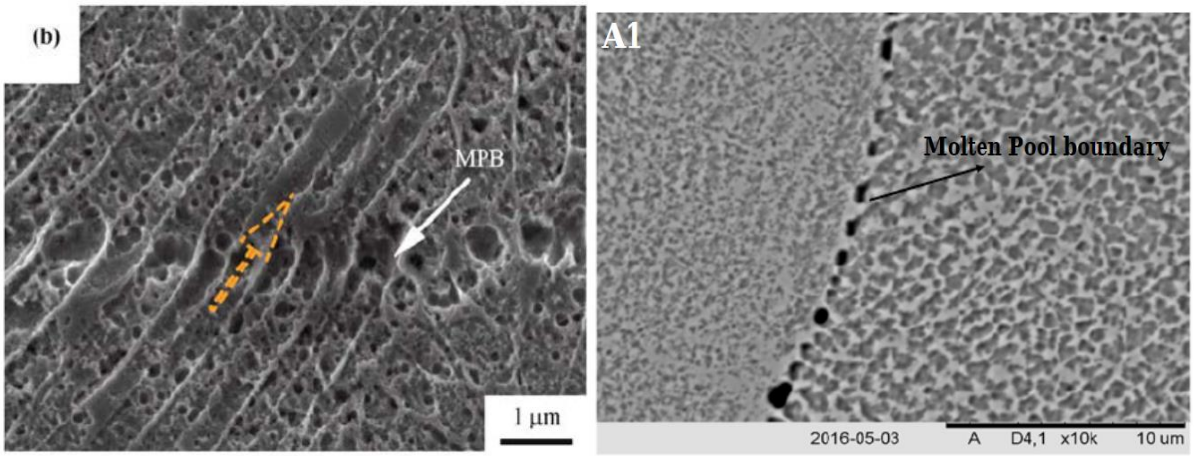


**Fig. 15 Examples of porosity at the melt pool boundaries in IN718 specimen, left: SEM, right: OM [71]**

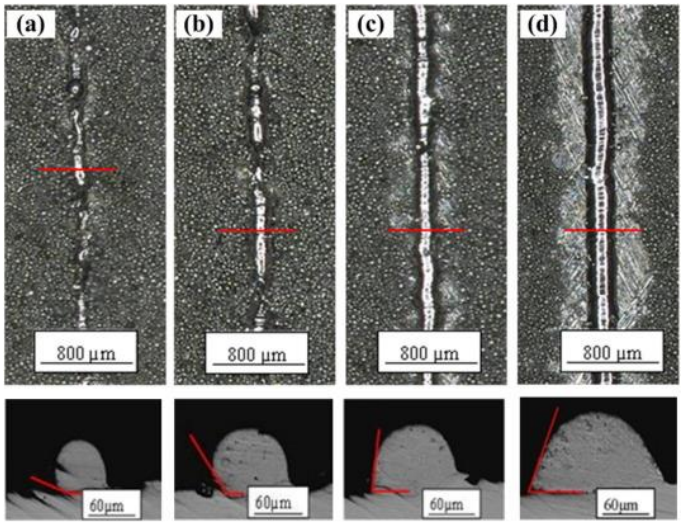


**Fig. 16 Single track formation for different parameters [126]**

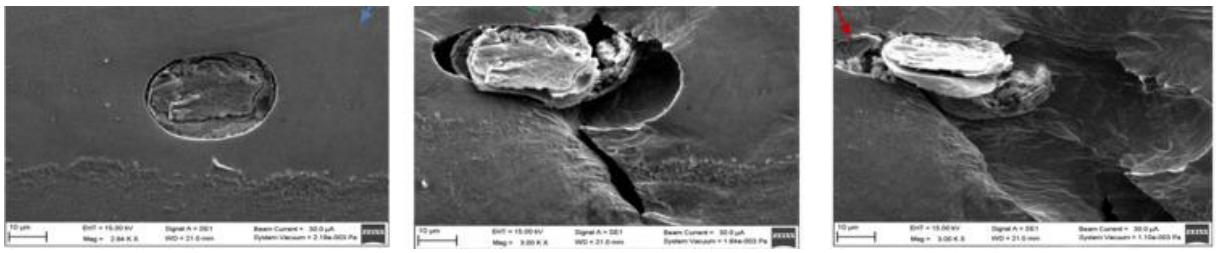

**Fig. 17 Fracture initiation and evolution at inclusion under SEM [127]**

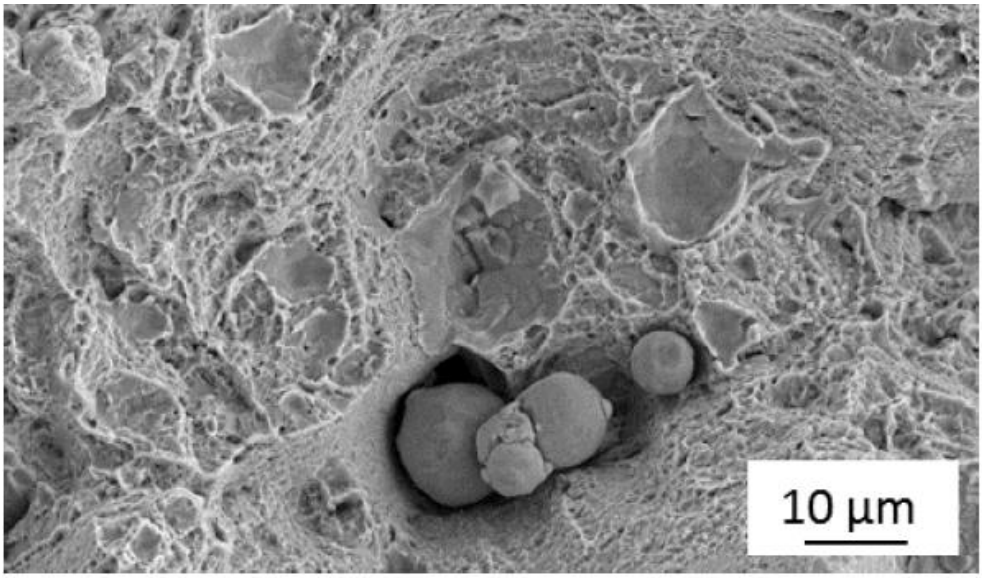


**Fig. 18 Inclusions in the fracture plane [128]**

## 2.5 Joining dissimilar materials

As mentioned earlier, both 3D printing techniques discussed in this work share a lot of similarities with the process of laser welding. Welding as a way of joining materials is of great importance in almost every industry. Its ability to join parts of different shapes and sizes is an essential prerequisite for the construction of large products, such as bridges or vehicles. Complex design these days, however, requires not only combining parts of different shapes but also of different materials. Welding together parts of different chemical compositions is called dissimilar welding. This technique can be very difficult, as the chemical difference between the materials often causes different behaviours under the welding conditions. These must be carefully adjusted to suit both of the weld materials, which can be extremely hard to achieve [129].

Traditionally both fusion welding (laser, electron, arc, etc.) and solid-state welding (friction, explosion, ultrasonic welding, etc.) are used to join dissimilar metals. Both of these groups suffer from specific disadvantages, with the common ones depicted in the figure below:

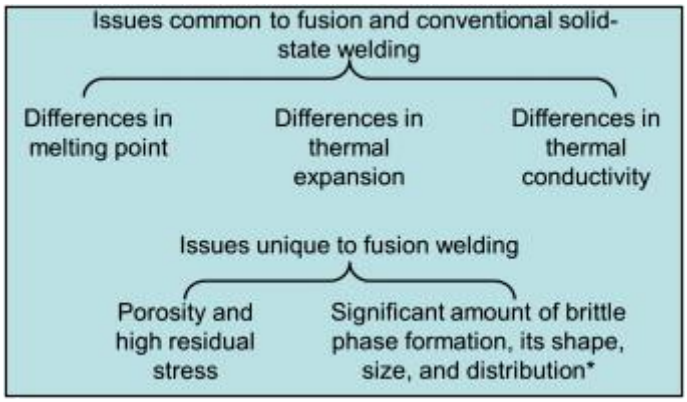


**Fig. 19 Disadvantages of conventional welding techniques for dissimilar materials [130, p. 1]**

Generally speaking, dissimilar welding is achievable with metals (alloys) that have good solubility in each other and a reasonably small difference in melting temperatures. It has also been shown, that solid state welding is a more feasible method since it usually does not require melting of the materials, which helps eliminate problems such as brittle phase formation [130].

Another problem comes with the difference in thermal expansion, and that is both during the welding process and under working conditions of the final part. This difference causes stress to be induced on the joint, which can lead to lower fatigue strength. To reduce this effect, a filler material is used, which has a the thermal expansion coefficient closer to the weaker material. This moves the line of thermal stresses to the side of the stronger material. Similarly, in the case of different melting points, the use of filler material shall be considered. The solidification and contraction of the materials affect the side with the lower melting point, which solidifies later and therefore inconsistently with the other material. This problem can often be eliminated by the application of the filler material on the strong material side prior to joining the sides together, which reduces the melting point differences during the actual welding [131].

Joining workpieces made by 3D printing differs for both technologies discussed. LMD is very close to actual laser beam welding with filler material, which allows it to create both simple welds as well as whole areas of complicated connecting areas. Another technique is building a whole new part on a previously manufactured surface. One of the advantages of such a method is the freedom of the shape of the interface, where solid-state welding methods (e.g. FSW) may be insufficient. Another advantage is the possibility to change the chemical composition of the

weld gradually along the connecting area [105]. In the case of the SLM technology, the idea remains the same, but without the advantages above - the material is usually fixed and the connecting area can be only planar. Another benefit, that both technologies share in this method, however, is the possibility of combining complex geometries suitable for 3D printing with high volume parts, that can be cost-effectively manufactured by other means of fabrication.

To reduce the stresses induced in the joint by the dissimilarity of materials, many works have been presented dealing with creating functionally graded joints using the LMD technology [104]–[106]. The usual approach is to gradually change the weight ratio of the two printed materials across several layers. While mostly successful, the observations show, that it is hard to completely eliminate problems such as brittle phase formation. On the other hand, it was shown that using the various advantages of graded materials is possible, such as controlling the hardness [105] or wear resistance [104] in specific areas of the part.

# 3 Design of Experiment

## 3.1 Methods of DoE

Design of experiments (DoE), also known as experimental design is a set of methods used to explain processes using mathematical statistics. It is often applied in technical, medical, and other fields in the early stages of the development of a new product or method. Applying DoE techniques helps describe the relations between the process inputs and their responses. It also allows the estimation of the best operating conditions. Its usual purpose is to intentionally change one or more process variables in order to observe how this change affects one or more response variables. The procedure helps planning experiments in such a way that they provide objective results of various complexity [132], [133].

The benefits of DoE can be expressed by comparing it with its alternatives. For problem-solving, where we try to investigate a specific (optimal) response of a process, the most fundamental method is the trial and error approach. Regardless of the number of factors affecting the process, this method consists of multiple trials with randomly chosen values of input variables. The goal is to run trials of different combinations of values until the experimenter gives up or succeeds. The optimal or the best result is usually picked from the separate responses. This approach is usually successful with simple problems and games and is also often used in situations, where the experimenter has little knowledge of the studied area. Its main problems are randomness and a high chance of completely missing the appropriate experimental region, as well as its inability to investigate multiple factors at once [134], [135].

A more structured approach to investigating the effect of a certain variable on the output is the "one factor at a time" (OFAT) or "change one separate factor at a time" (COST). This method changes one factor (independent variable) while keeping the other factors constant (control variables). The change is usually systematic so that the resulting response can be easily represented (e.g. in a graph). By running this method in the same way for a certain number of times for each of the factors, it is possible to get a fairly good idea of how each of the separate factors affects the process. It is a simple and intuitive problem-solving method that can lead to very useful results and in specific cases can even predict the process response outside of the experimental region. Its main drawback, however, is that it does not consider that the variables can affect each other. Therefore, the desired optimum of combinations can lie at a vast distance from the trialled setups, and no accurate prediction of the process outside the tested values can be made [133], [135].

These problems can be solved by using a set of statistically designed methods, which is DoE. The goal of using these methods is to perform a finite number of trials, and from their responses then extrapolate an acceptable prediction for a much wider range of combinations of factors, usually in the form of a regression model. The complexity of the model depends on the number of factors and their levels, as well as on the method used. The desired outcome is a statistical approximation of the results (a function of the factors) with acceptable variance, which can predict all possible responses inside the experimental region.

The complex process of designing an experiment usually starts with defining the problem and selecting the factors. As there may be multiple factors investigated at a time, there may also be multiple responses measured. The selection of the factors, for example by comparing their impact on the response, can be made using the DoE methods, but requires significant amount of professional insight into the problematics. After selecting the factors and their levels, the experimental region is roughly defined as the space in between the factorial points, i.e. points

of combinations of the separate levels of factors. This region can be further adjusted, if a curvature of the region is identified [132], [136].

For example, a graphical demonstration of the experimental region for two factor – two level design is shown in the figure below. In this case, the two factors are temperature and pressure, with levels 190 °C and 210 °C, and 50 MPa and 100 MPa. In this case, axial (star) points are also introduced to adjust the curvature of the experimental space.

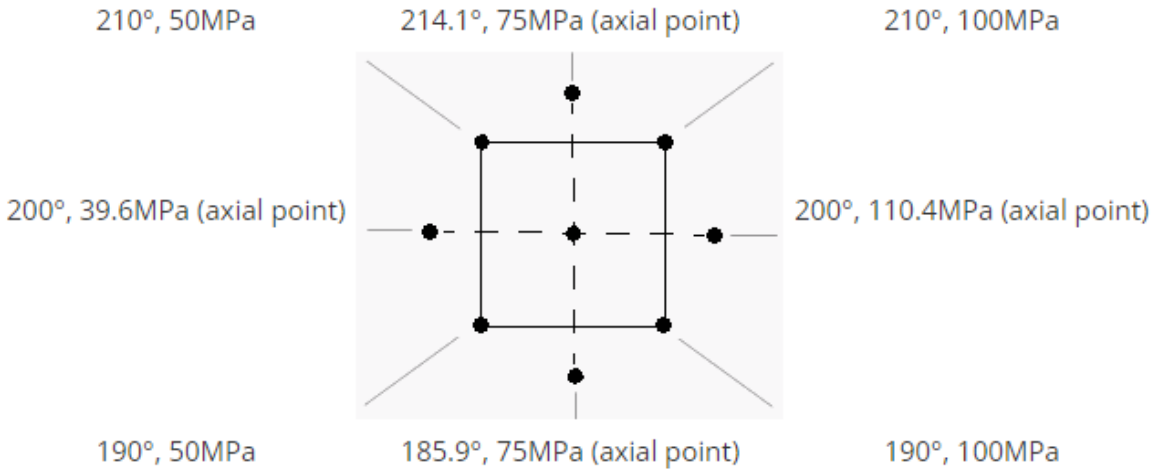


**Fig. 20 Example of the central composite design with two factors and two levels [137]**

For three factor – three level design the space would take the shape of a three-dimensional cube. The central points and factorial points define the experimental region for a full factorial or fractional factorial designs. By introducing the star points, a central composite design (CCD) is created [137].

Subsequently, the table of trials can be made, experiments performed, and a resulting regression model created. However, since the model is just an approximation, it is good practice to examine its quality. Usually, this is performed by analysing the residues – the differences between the model and the actual measured values. In an accurate model, these should normally be distributed around the theoretical value and their variance should be constant. This validation is usually performed by Graphical Residual Analysis, which illustrates well a broad range of aspects of the relationship between the data and the model. Numerical methods, such as ANOVA or Lack-Of-Fit Test also play an important role in validating the model, however, they tend to be narrowly focused on a specific aspect of the relationship between the model and the data [132], [136], [138].

## 3.2 Project use case

For the AdditivePeen project, surface quality of parts manufactured by additive manufacturing treated with Laser Shock Peening technology is meant to be investigated. Large part of the preliminary research consists of characterization of mechanical properties of the printed materials.

As one the drawbacks of AM technologies is poor fatigue, the project aims on improvement of the crack growth propagation. However, besides that, other properties such as strength and ductility need to be investigated as well. This entails testing and evaluation of samples manufactured by different technologies, and comparing their properties to identify the influence of each specific technology.

A specific component needs to be developed and produced in the framework of the STREAM project. This should be a hot-forming tool for automotive sheet metal parts. This tool's main attribute are conformal cooling channels, which are difficult to manufacture by other means than additive manufacturing methods. To utilize the potential of 3D printing the most, an approach of combining two materials and two technologies was suggested.

The base part of the tool was designed to be printed with SLM technology and the material C300. The fine and geometrically complex conformal cooling channels are created in this part, for which SLM technology is more suitable than other AM methods. On top of this base, a layer of the material TS700 will be deposited to create a contact, working surface. Since the starting surface for this deposition is not planar, LMD technology will be employed. The goal is to ensure proper metallurgical bonding between these two parts, creating a uniform part suitable for the hot-forming process.

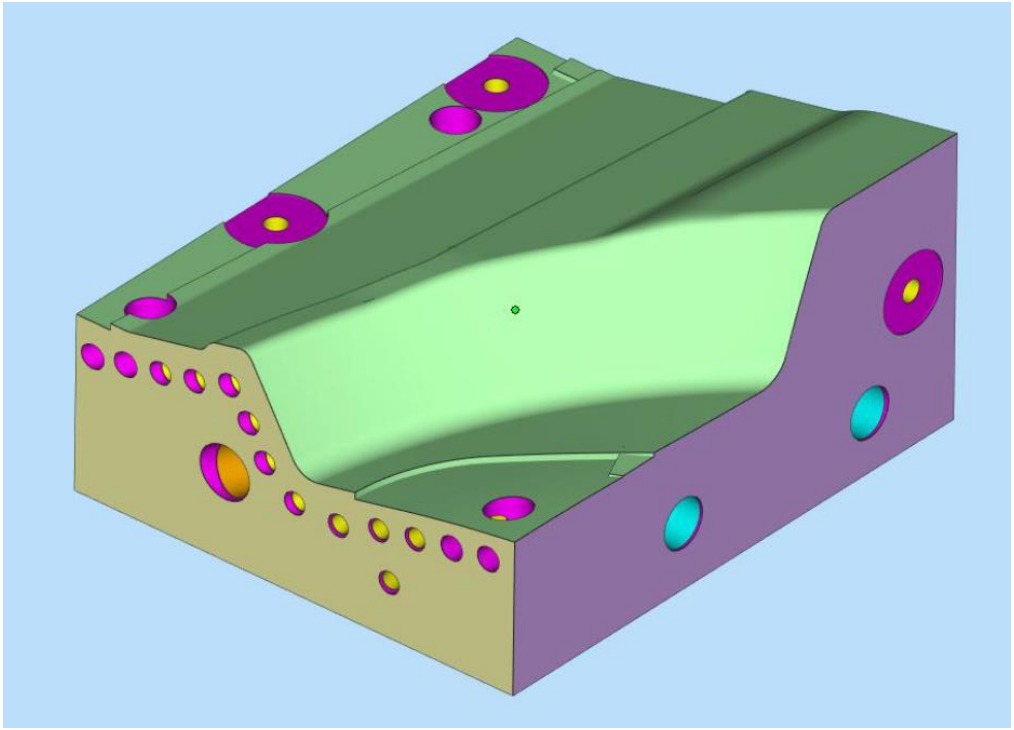

**Fig. 21 Illustration model of the tool with conformal cooling channels**

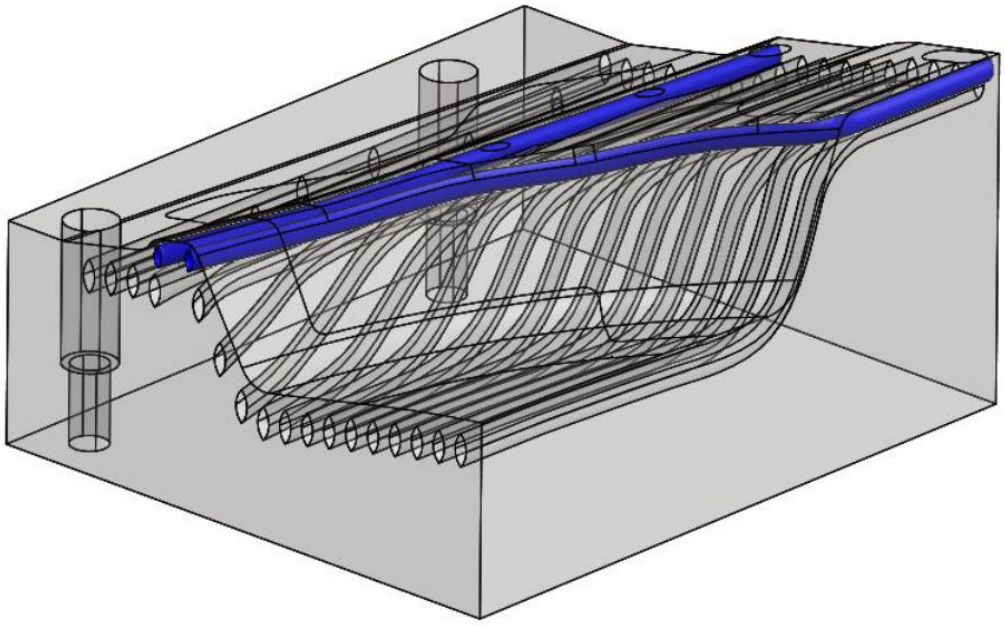

**Fig. 22 Wireframe model of the tool with conformal channels**

Before manufacturing, the materials need to be specified, and their process parameters have to be specified. The parametrization of each material and technology requires exhaustive testing and statistical evaluation, where a number of representative samples need to be manufactured and investigated. The results of this evaluation should be an optimized window of parameter sets, according to which a final reliable component with the desired properties can be manufactured.

### 3.2.1 Hot-forming tool requirements

During hot-forming, which is most commonly drawing, stamping, or punching, a blank part is heated above austenitization temperature, then transferred from the furnace to the tool, where it is pressed (shaped, formed) and cooled at the same time. Rapid cooling causes structural transformation in the material, improving material strength and hardness. Several factors affect the result of this process, including holder force and hardening time [139]. The process temperatures and cooling have the most significant effect on the result of this type of forming. While the lower forming temperature is usually limited by the solvus temperature of austenite, the upper forming temperature depends on the capabilities of the processing setup. A higher forming start temperature has been shown to increase the volumetric share of martensite, resulting in higher strength and hardness. It also hinders the risk of springback due to elastic deformation and distribution of residual stress [139]. On the other hand, high forming temperatures increase the thermal load on the dies, possibly increasing their wear and shortening their life. Therefore, choosing optimal forming temperatures and cooling is of utmost importance when designing hot-forming tools [139]–[141].

The desired properties of a hot forming tool are therefore thermal stability at high temperatures and good heat dissipation ability. A low coefficient of thermal expansion, crack propagation resistance, and notch sensitivity are also of high importance. Needless to say that none of these properties matter, unless the material can reach high hardness and wear resistance to withstand the harsh hot forming environment [139], [141].

## 3.3 Materials used

Virtually any material, that can be processed into powder of suitable properties, can be used in SLM technology, including materials that are conventionally hard to weld [24]. However, in common situations, the printability of material relates a lot to its weldability, as the principles of metallurgical bonding are similar. Carbon in steels plays an important role, as its higher content responds poorly to the steep temperature gradients. Brittle phase formation and cracking is a common issue, which is often partially mitigated by preheating the part, but since this is often complicated, users of 3D printing machines often prefer to avoid high carbon materials if possible [142], [143]. This narrows down the range of materials commonly used, especially the group of steels. A further selection of materials usually comes down to those, for which the machine suppliers offer optimized process parameters.

Materials for the project use case were chosen taking this fact into account, as well as other criteria, such as powder price and availability. Also, the compatibility of the materials had to be considered in terms of mutual solubility or structural similarity.

A tough and stable material was required for the forming tool base, so maraging steel C300 was chosen. However, it does not reach the hardness and tribological properties needed for the contact surface of the hot-forming tool. It is also a material commonly processed by various powder 3D printing techniques and therefore the literature about it is quite relevant.

Hard material with good thermal properties was required for the contact layer deposited with LMD. Originally, the advanced material ASP 2012 was suggested, but after further research, consultation with the powder distributor, and facing certain flowability issues with the powder, another material was chosen – TS700.

Another material was investigated in the part of the work related to the Additive Peen project, which was 316L stainless steel. This material is also popular among the users of 3D printers both for its versatility and good printability.

### 3.3.1 Maraging 300

Maraging 300 (also referred to as Maraging C300®, Vascomax® C300) corresponds with the composition of US 18% Ni Maraging 300 or DIN 1.2709, which are equivalent to X3NiCoMoTi 18-9-5, or Vaco 180 [144]–[148]. It is an iron-based high-alloy carbonless material. The main alloying element is Nickel (w%18.5), followed by Cobalt (w%9.0), Molybdenum (w%4.8), Titanium (w%0.6), and Aluminum (w%0.1). This material can produce yield strength over 1862 MPa while maintaining great toughness and ductility. Therefore, it is suitable for high tensile applications, like tooling. Good notch ductility is maintained down to minus 50°C, while the strength of the material is retained up to 450°C, making it suitable for thermal applications, e.g polymer, zinc, or silumin moulds. This is also associated with very good crack growth resistance, for which it is often used in highly demanding environments. (e.g. aerospace) [149].

As the name suggests, it is a grade of maraging steels, which have been around for over 50 years. The marking “C” stands for the main hardening element, which in this case is cobalt. The numbering 300 indicates the ultimate yield strength in ksi. The name “maraging” comes from the words “martensite” and “aging”, as they describe the main features of the material [150]. Fine lathe martensite is the stable phase of its microstructure and is responsible for the ductility and relative softness of the material (around 30 HRC in the annealed state). The final properties are then achieved by precipitation hardening, i.e. aging of the material. Due to theoretically zero carbon content, the material hardening cannot be performed by quenching, as with conventional steels, but rather by slow precipitation of the intermetallic phases, similar to Al-

Cu alloys. Usually, by heating and holding the material at 482 to 510°C for 1 to 6 hours [151], the phases start to precipitate inside the martensitic grains, creating obstacles for dislocations. [127], [152]

The main precipitates are Ni3Mo, Ni3Ti, Ni3Al, and Fe2Mo. The important role of cobalt is reducing the solubility of other alloys in iron, promoting more precipitates and their even distribution [153], [154]. Fine distribution of precipitates is desirable, as coarse precipitates don't have enough surface energy to effectively stop the dislocations and may act as a crack growth initiator instead. Coarse precipitates can form when the aging temperature is too high, therefore cooling the material to room temperature before the aging cycle is the usual approach. Finer precipitates are obtained by aging at lower temperatures for a longer time. However, aging the material for too long may cause overaging, which is also accompanied by undesirable growth of the precipitates. Aging the material at higher temperatures leads to an overall coarser structure with rising content of reverse austenite, which also decreases the material strength and hardness [154]. Restoring the smooth austenitic structure is possible by solution-annealing above 820°C. One of the advantages over other types of heat treatment is it avoiuds high-temperature gradients, as well as grain phase transformation, ensuring good resistance to distortion during this process [127], [149], [152], [153].

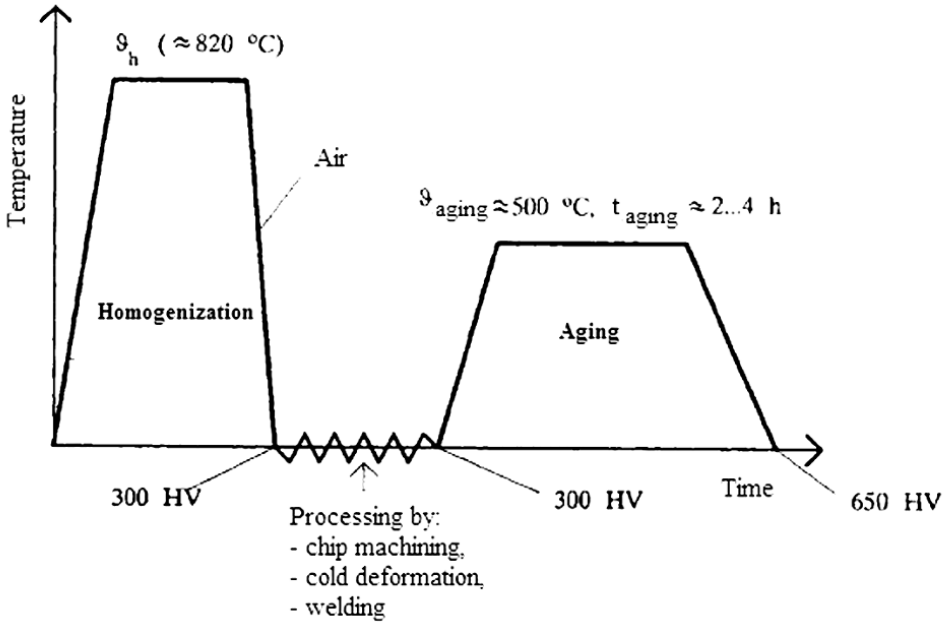


**Fig. 23 A flow diagram of the heat treatment process of MARAGING steels [155]**

Despite the aging process almost doubling the hardness of the material (up to 57 HRC), it is still considered a relatively soft material in comparison to other tool steels, making it unsuitable for applications such as cutting tools. Surface treatment methods have been investigated in pursuit of improving the wear resistance, which showed, that improving the surface properties with thermo-chemical treatment is in most cases a trade-off for losing the benefits of the original material. Carburizing does improve the wear resistance, but causes distortions to the material and worsens machinability, which are both significant benefits of this material. Boriding has a similar effect, which causes cracking on the surface layer as well. Nitrocarburizing on the other hand does not have any of these drawbacks, however, the usual process is carried out at high temperatures (550 to 600°C), which causes overaging of the core material, and therefore loss of the hardness and strength. Plasma nitriding is the only one which was successful in terms of

increasing the wear resistance while maintaining the beneficial properties of the material, although the increase was not as significant as with other methods. The TiN PVD coating have an additional value, which also showed a significant increase in wear resistance, suggesting the combination of the two latter processes may be favourable for applications demanding better abrasion resistance properties [155].

Thanks to properties mentioned together with good weldability, machinability, and dimension stability, this material is usually used in applications such as die-casting, landing gear components, transmission shafts or autosport components, ammunition or missile and rocket motor cases [144], [146], [151], [156].

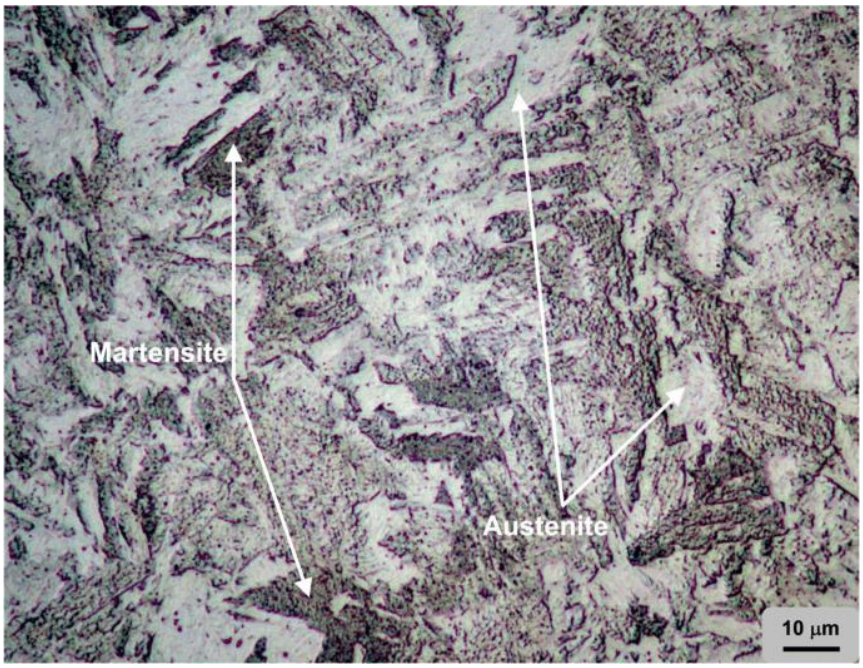


**Fig. 24 Optical microscope images of the 18Ni-300 MS substrate microstructure [157]**

This material has been extensively investigated in additive manufacturing. This is due to its properties, such as weldability and good dimension stability, which are beneficial in the additive manufacturing process [157]–[160]. The crack growth resistance is also of great importance since one of the biggest drawbacks of additive manufacturing technologies today are pores and inclusions in the material. These work as crack initiation points and are the usual cause of fatigue failure of the material.[127], [149], [152]

### 3.3.2 TS700

Tool steel Pearl® Micro TS700 is a powder material developed by the company Aubert & Duval© especially for additive manufacturing applications. It is a precipitation hardening steel intended for manufacturing of die casting tools and hot work tools. This iron-based alloy contains mainly Chromium (w%5.0), Nickel (w%2.0), Molybdenum (w%8.0), and Cobalt (w%11.0). It is considered a low-carbon steel (max w%0.05). The supplier emphasizes its good heat resistance as well as ductility, compared to the maraging 300 steel.

The yield strength of this material after hardening reaches 1430 MPa with maximum elongation up to 8%. The highest achievable hardness is around 51 HRC. The properties are maintained even at elevated temperatures, where while kept at 600°C for 100 hours, it does not lose its hardness. This combination makes the material suitable for hot working applications, while relatively high ductility hinders crack propagation and ensures higher durability.

As this material is not standardized and the literature concerning this particular material is scarce, most of the properties listed above are taken from the supplier's datasheet. This data also refers specifically to the 3D printed (and hardened) material.

To describe the material a little bit more thoroughly, a similar group of tool steels will be briefly described. The closest group composition-wise is the Chromium hot-work steels, known as H1-H19 according to AISI. Specifically, H11, H12, and H13 are the most commonly used hot-work steels, as their air-quenching ability ensures lower distortion during heat treatment than for example carbon-tool steels. The content of chromium helps deep quenching up to 150 mm. Their low carbon content hinders precipitation of carbides which would cause heat-induced cracking. They reach yield strengths up to 2070 MPa and hardness up to 55 HRC [161], [162].

TS700 shares a lot of properties with them, except for the high content of cobalt. It works as a main precipitation hardening element, similar to maraging steels, where it helps the precipitation by lowering the solubility of other elements in iron. This implies the main difference from other chromium hot-work steels, where the main hardening mechanism is quenching [161], [163]. As opposed to e.g. H13, this material reaches slightly lower strengths, with the exchange for thermal stability at higher temperatures.

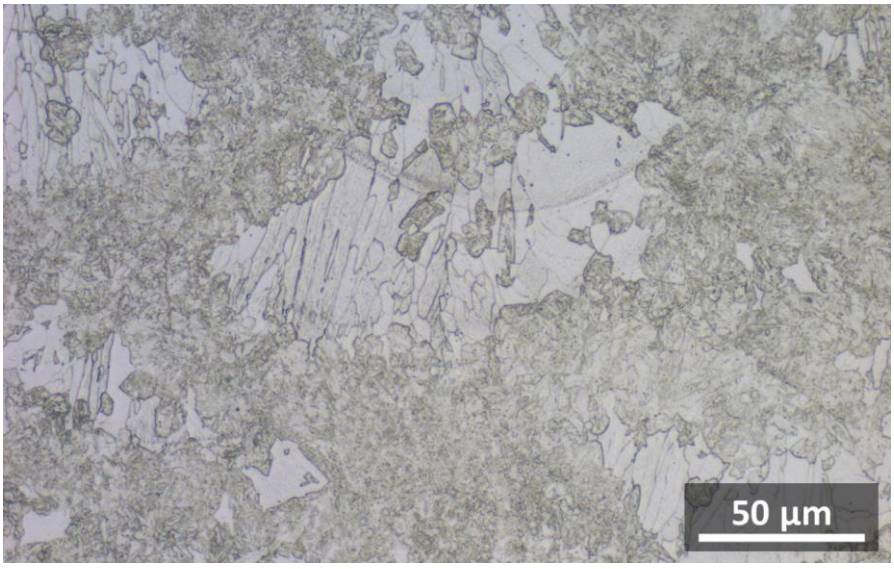


**Fig. 25 As-built microstructure of TS700**

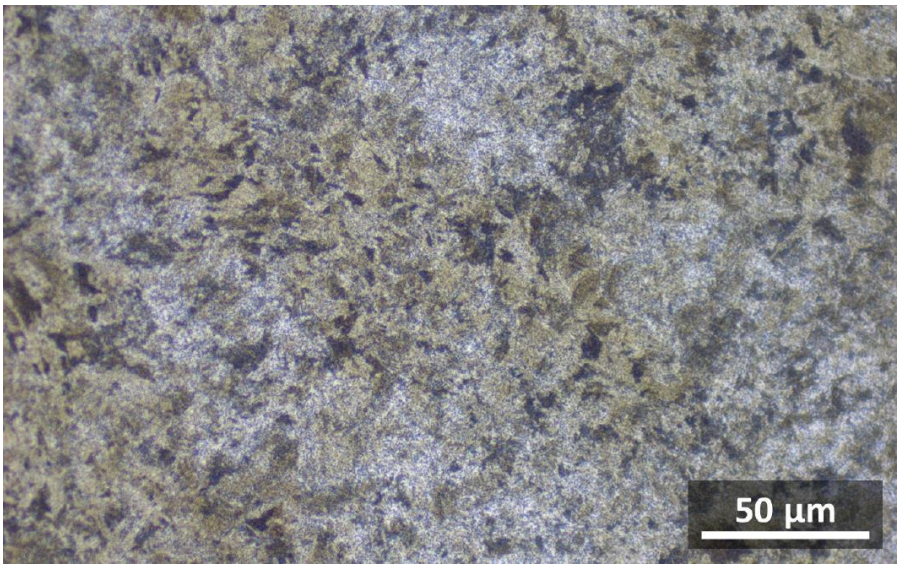


**Fig. 26 Microstructure of TS700 after age hardening**

TS700 was chosen based on a powder supplier's recommendation for the specific application (hot forming tools). It is a material that has good thermal conductivity, hardness properties and oxidation resistance, which makes it a good choice for manufacturing tools with cooling channels. In addition, it has mechanical properties suitable for tool steel. Its low carbon content promises good printability without undesirable precipitation and cracking [164], [165].

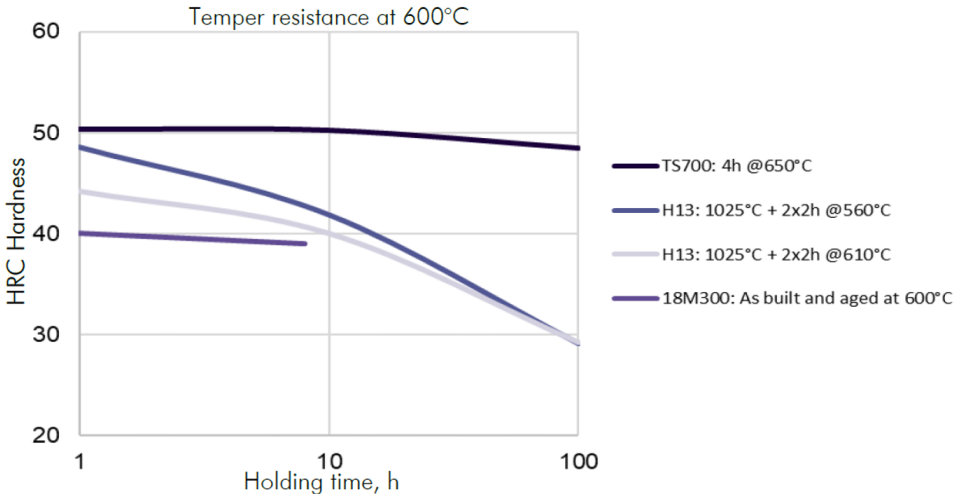


**Fig. 27 Temper resistance of TS700 compared to other tools steels [164]**

### 3.3.3 316L

AISI 316/316L (UNS S31600/ UNS S31603, DIN 1.4404) is one of the most commonly used stainless steels. It is a chromium-nickel-molybdenum austenitic stainless steel with excellent corrosion resistance properties. Its main alloying element is Chromium (w%17.0) followed by Nickel (w%12) and Molybdenum (w%2.5). The letter "L" in 316L stands for "Low carbon", which refers to lowered content of carbon down to a maximum of 0.03w%, whereas 316 contains a maximum of 0.08w% of carbon. This makes 316L less prone to precipitation cracking and therefore more suitable for welding, and other thermal applications, with little to no change in its other properties.

The material reaches yield tensile strengths of 205 MPa. In the annealed state it has relatively high ductility of about 60%, which makes it easy to process by most basic forming methods, such as shearing, stamping, or drawing. It is rather soft, with approximately 80 HRB in the annealed state. As for all austenitic steels, 316L is not hardenable by heat treatment, as it usually results in an austenitic structure, instead of hard bainite or martensite. It is however strain hardenable by cold-working [166]. Surface hardening is also a suitable option [167]. However, hardness is not the strong side of this material. Its main advantage is its corrosion resistance in almost all aggressive environments. It is labelled as marine steel, as it is suitable for long-time applications underwater or in other corrosive environments. Its good finish and abrasion resistance make it suitable for medical applications, such as medical tools or implants. It is also used in jewellery, for its durability and biocompatibility. The lower carbon in 316L ensures mitigation of carbide precipitation and intergranular corrosion, making it even safer for medical uses. 316 is commonly used for tubing, marine, and other underwater applications [168], [169].

This alloy is mostly paramagnetic, welding and cold working can induce slight ferromagnetism due to retained delta-ferrite and deformation-induced martensite.

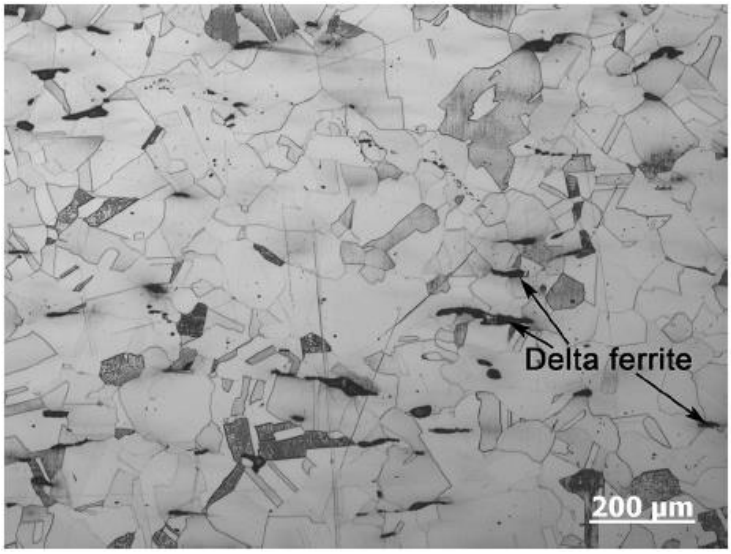


**Fig. 28 Austenitic structure of 316L with residues of delta-ferrite [170]**

The corrosion resistance, biocompatibility, and other things make 316L a popular material be processing by additive manufacturing due to its versatility and suitability for special applications. Its low carbon content and excellent ductility and fracture toughness make it relatively easy to print with most powder-based AM technologies [60], [166], [171], [172]. It is also one of the materials that in the as-built state reaches different mechanical properties than the conventionally wrought material, as datasheets of additively printed material advertise a yield strength of more than double [173].

## 3.4 Experimental

The first and main experimental part of the present work was the mechanical characterization of the materials C300 and 316L processed both by the SLM and LMD technology. For both materials, blocks were manufactured by both technologies using default parameter sets recommended by the supplier of the machines. Subsequently from these blocks, a number of tensile specimens were cut out using a conventional milling machine for the contour and an EDM wire cutter for high precision slicing. Due to the investigation of anisotropy of mechanical properties, the samples were cut out in three different orientations with respect to the build direction. Samples manufactured from conventionally wrought materials were also tested for validation and comparison.

Based on the knowledge gained from this testing, second part of the experiment was conducted. The goal of this was to create a Central Composite Design for testing of LMD process parameters. During this DoE a number of specimens manufactured with the combination of SLM and LMD technology was created, and will be subsequently investigated. The SLM part of the specimens was printed using the default parameter set recommended by the machine supplier. The result of this DoE will be an optimal set of parameters for such combined process, and these parameters will be later used for manufacturing of the specific component – hot-forming tool. For the part created by SLM the material C300 was used, while for the LMD part the material TS700 was used, with respect to the final component composition.

For all testing, materials were in the as-build state.

### 3.4.1 Methods and equipment

The SLM parts were manufactured using the TruPrint 3000 LMF/PBF/LPBF machine. This machine has a build volume of ⌀3000 mm x 4000 mm and uses a single 400 W fiber laser[2]. Laser beam diameter in the focus spot is ⌀80 μm. One-sided recoating is performed by a rubber lip, allowing powder layer thickness from 20 μm to 150 μm. The shielding gas used in the process was argon. The machine uses a system of internally exchangeable build and powder-supply cylinders, ensuring constant inert atmosphere in the building chamber and avoiding excessive powder and part oxidation. Additional peripheries of the machine were used, such as the powder sieving module and depowdering station, that increased the efficiency of the processes [112].

[2] A newer version of this machine model currently on the market already comes with multilaser solution with 2 overlapping 500 W fiber lasers [112].


**Fig. 29 TruPrint 3000 machine [112]**

The LMD parts were manufactured using the TruLaser Cell 3000 5-axis laser machine suitable for LMD, laser welding and two and three-dimensional laser cutting. The travel range of the axes defining the workspace is 800 mm x 600 mm x 400 mm, with the a work-head rotational B-axis range of ±135°. It uses an 8 kW disc laser, which is much more powerful than the needs of common LMD processes as the machine options for cutting and welding as well. For the LMD processes a three-beam (3-channel coaxial) nozzle SO12 was used, with a powder focus diameter of 2.5 mm and working distance of approximately 12 mm. The nozzle is water cooled and therefore needs to be connected to a water supply. The shielding gas used was argon [107].

The powder supply was via a the Flowmotion powder feeder made by Medicoat. This delivery system consists of two sets of powder hoppers, oscillating conveyors and delivery tubing which are connected to the work-nozzle module in the machine. The hoppers store the powdered material and provide a stable flow of the powder onto the supply plate and subsequently the conveyor. The conveyor is a V-shaped channel which transports the powder to the delivery tubing. The volume of the powder delivered is given by the amplitude of oscillation. The construction of the plate and the conveyor secures a constant flow of powder while mitigating the influence of uneven grain size distribution. The whole system is filled with carrier gas which helps to accelerate the powder inside the delivery tubing. The system is able to work at an overpressure of up to 15 bar. The upper limit for the powder flow volume is 60 $cm^3min^{-1}$, the lower limit is defined by the least powder flow mass of 0.5 $gmin^{-1}$.


**Fig. 30 TruLaser Cell 3000 machine [107]**

**Fig. 31 Flowmotion powder delivery module [174]**

Quasi-static tensile testing of the samples was conducted for both experimental parts on a custom-made MIAMI testing machine, designed by the Laboratory of Experimental Mechanics at the Inegi research centre in Porto. The load of the tensile specimen was monitored by a Vetek-2t 2 ton load cell. The work load was recorded using a custom-made software, creating a load-over-time table in format of .csv. A constant deformation speed of 1 $mms^{-1}$ was used for all the tests.

The machine is equipped with a contact strain gauge, but it was not used for our strain measurement. To achieve more accurate data collection, a DIC assembly was set up to monitor the deformation of the sample. This assembly consisted of a Basler Ace acA2500 - 60µm industrial camera, additional illumination and Pylon viewer 6.3.0 software, which processed and recorded the images throughout the tensile testing at a constant frequency. The image sequences were processed using VIC-2D 7 software for strain computation. This computed strain was subsequently synchronized with the load-over-time table using the MATLAB processor, which enabled plotting of Stress-strain curves (SS curves) for each specimen. These were further evaluated and compared to characterize the investigated materials and the technologies.

The fracture surfaces of a selection of the samples were investigated using a Keyence VHX-6000 microscope. However, this was not sufficient for a full evaluation of the fracture characteristics, and a more thorough fractography study could be achieved, preferably using a scanning electron microscope.

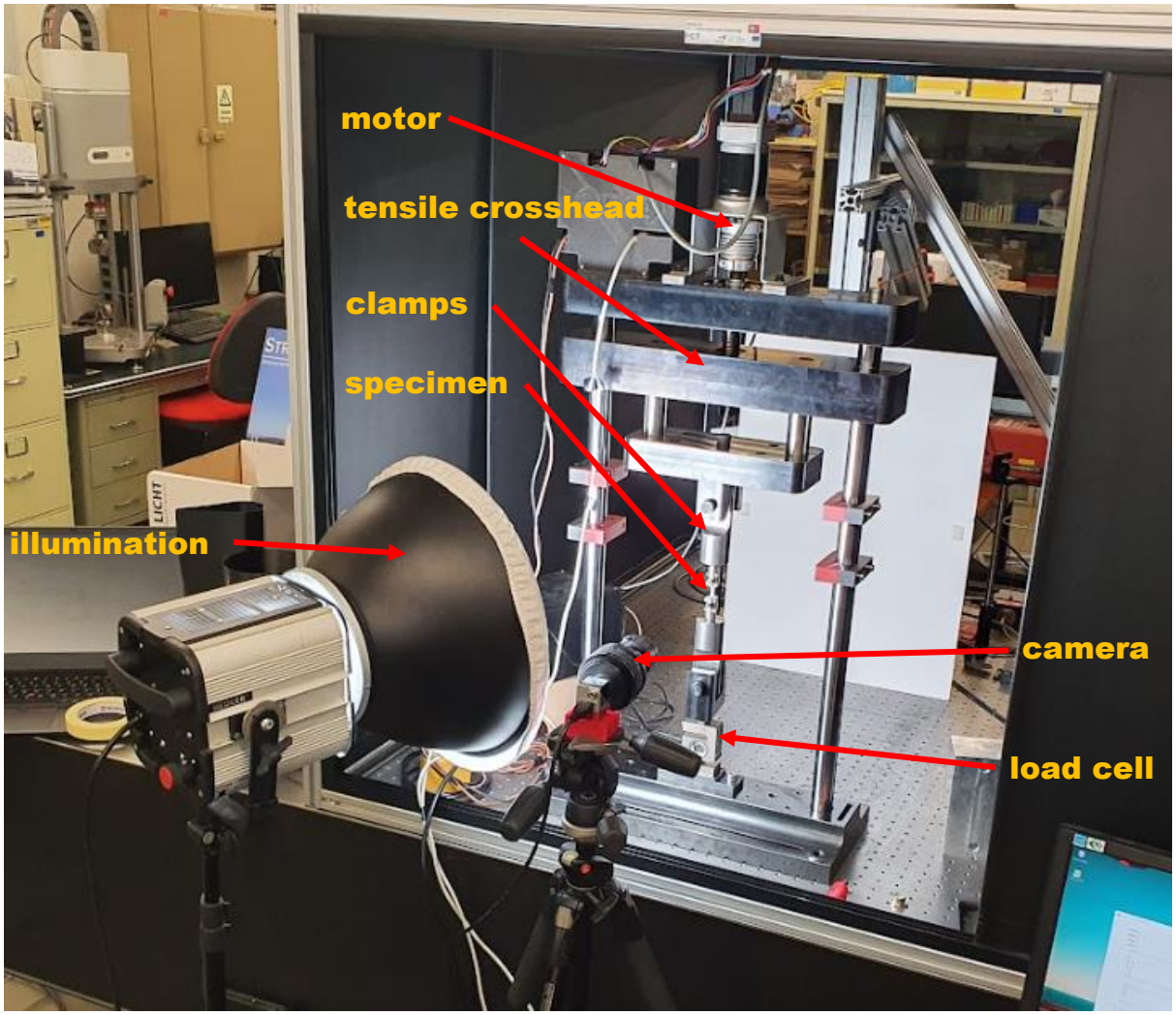


**Fig. 32 Tensile testing assembly**

### 3.4.2 Sample preparation

For the first experimental part, the blocks were printed using default parameters that were optimized by the machine supplier. The blocks were cut from the build platform using an EDM

wire cutter. Subsequently, the blocks were positioned in the milling machine according to the desired final sample orientation (see the schematic below) and the contour of the samples was machined. Finally, an EDM cutter was used to create the individual parts. For the technical drawing see attachment nr. 7. For the manufacturing process instructions see attachment nr. 8.

**Tab. 1 SLM process parameters**

| Material | Laser Power [W] | Scanning speed [$mms^{-1}$] | Layer thickness [µm] | Hatch spacing [µm] | Shielding Gas speed [$ms^{-1}$] | Scanning strategy |
|---|---|---|---|---|---|---|
| 316L | 220 | 700 | 30 | 120 | 2,1 | Chessboard (5 x 5 mm) |
| C300 | 223 | 800 | 30 | 120 | 2,1 | Chessboard (5 x 5 mm) |

**Tab. 2 LMD process parameters**

| Material | Laser Power [W] | Scanning speed [$mms^{-1}$] | Powder feed [$gmin^{-1}$] | Laser spot diameter [mm] | Track overlap [%] | Carrier gas flow [$lmin^{-1}$] | Shielding gas flow [$lmin^{-1}$] | Scanning strategy |
|---|---|---|---|---|---|---|---|---|
| 316L | 1130 | 1000 | 10 | 3 | 50 | 5 | 12 | bidirectional |
| C300 | 1200 | 1000 | 10 | 3 | 50 | 5 | 12 | bidirectional |

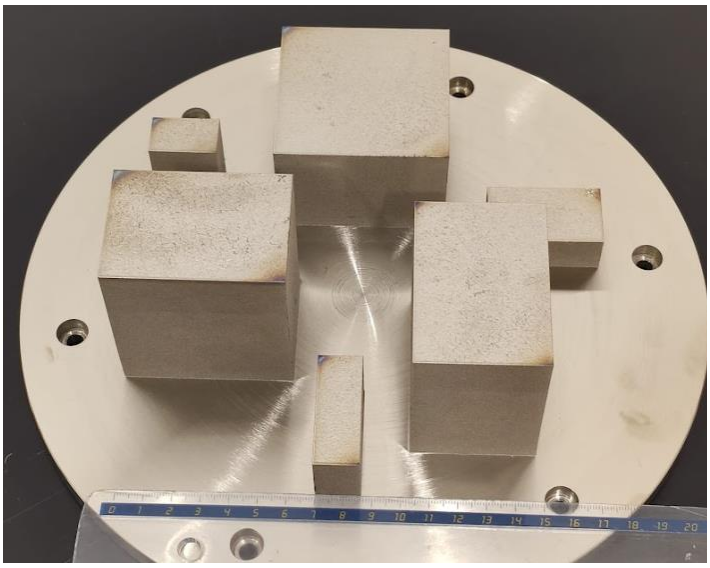

**Fig. 33 Blocks printed with the SLM technology**

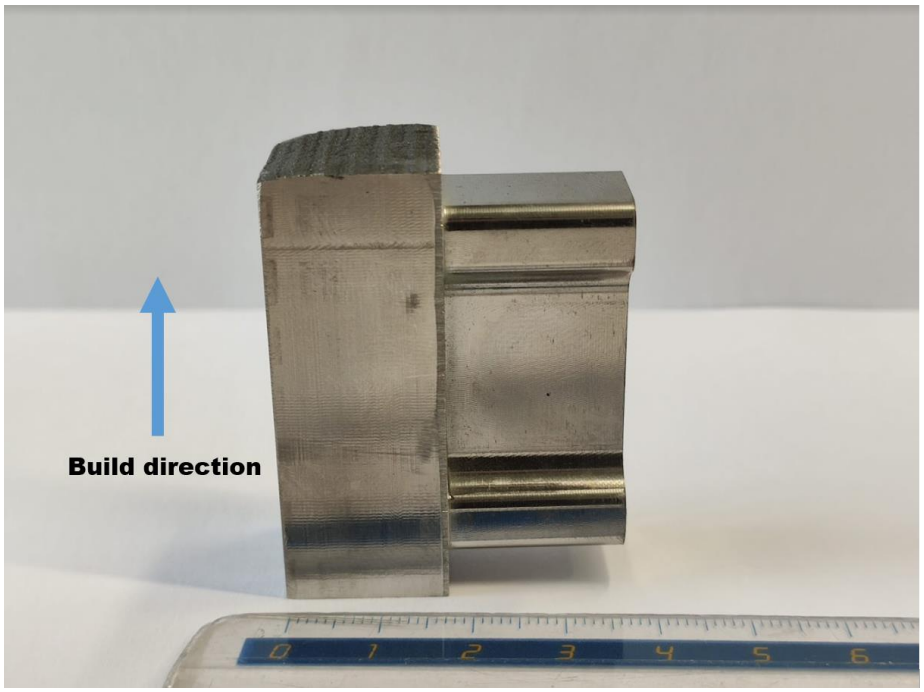


**Fig. 34 Samples cut out from a block printed with LMD technology in the „Z“ direction prior to EDM slicing**

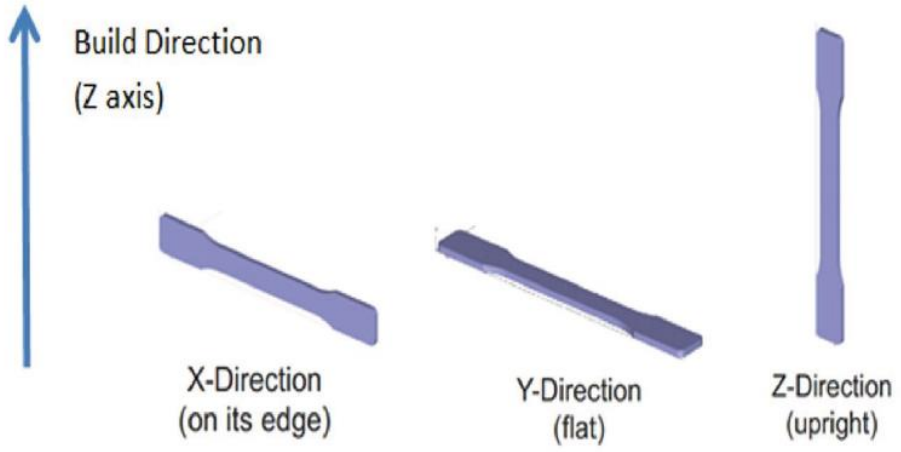


**Fig. 35 Sample direction schematic**

For the DIC analysis, the samples needed to be covered with a speckle pattern. The principle of DIC analysis is the calculation of the displacement from two images of the object taken before and after deformation. To do this, the image is divided into smaller areas called subsets. Each subset is then found in the second picture and its displacement from the original is calculated. To reliably identify the matching subsets in between images, they need to be easy to distinguish from one another and unique. Therefore, the speckle pattern needs to be sufficiently fine, random have a high degree of contrast with the background. To achieve this, one face of the sample was painted white using a powder-based spray paint, and subsequently covered in a black speckle pattern using an airbrush gun. This is a common technique for preparing of samples for DIC analysis [175].

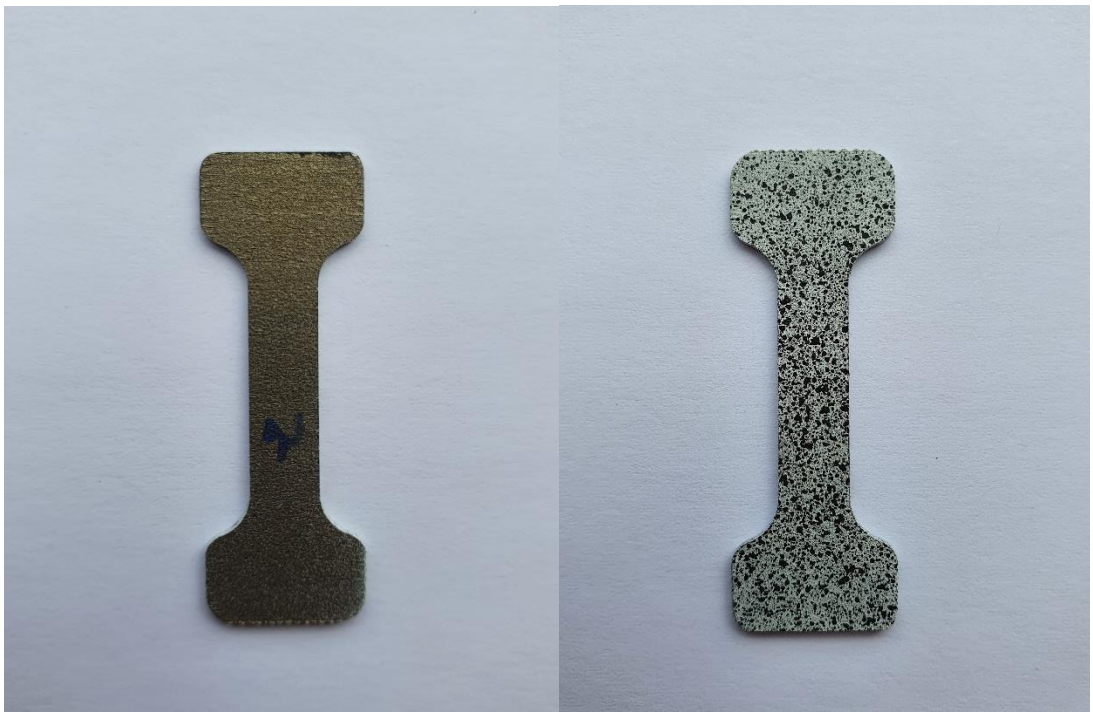

**Fig. 36 Tensile specimen; left: as manufactured, right: prepared for DIC**

The second part of the experiment was conducted based on the knowledge gained from this testing. The goal was to create a Central Composite Design testing of the LMD process parameters. During this DoE specimens were manufactured using a combination of SLM and LMD technology, which will be subsequently investigated. The SLM parts of the specimens were printed using the default parameter set recommended by the machine supplier. The result of this DoE will be an optimal set of parameters for this combined process, and these parameters will be later used for manufacturing a the specific component – a hot-forming tool. C300 was used for the part created by SLM, and TS700 was used for the LMD part, with respect to the final component composition.

For this phase, combined specimens of C300 and TS700 were manufactured using different technologies for each part. First, blocks of C300 were manufactured using SLM with the same procedure and process parameters (see tab. 1) as the parts for the first experimental part. These were subsequently positioned in the LMD machine and a block of TS700 was deposited on top of them using LMD technology.

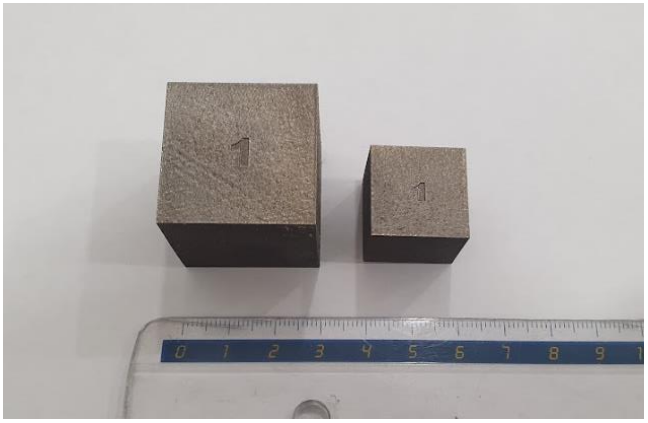


**Fig. 37 C300 Blocks printed with SLM**

For this deposition, different parameter sets were used according to a DoE table generated for the CCD. Factors and levels needed to be chosen to create the DoE table of parameter sets. Laser power, scanning speed and powder feed were chosen as the factors, with three levels each, based on the importance of different parameters. This created the Three-level Full-factorial Design. Additionally, star points were introduced to create a Central Composite Design.

Since no recommendations for the parameters were available from the machine supplier, the level values had to be estimated based on the experience of the machine operator. Initially, six parameter sets were chosen in the expected process window and used to print several layers of the material on a blank part. These deposited layers were observed during the print and visually evaluated after the deposition process. The result can be seen in the figure below.

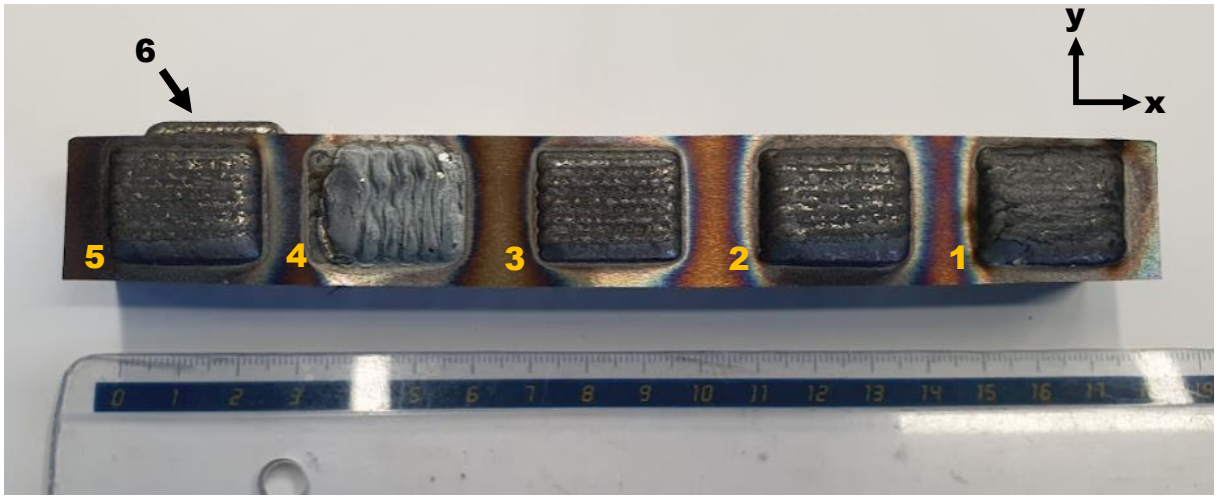


**Fig. 38 Parameter testing for estimation of CCD levels - top view**

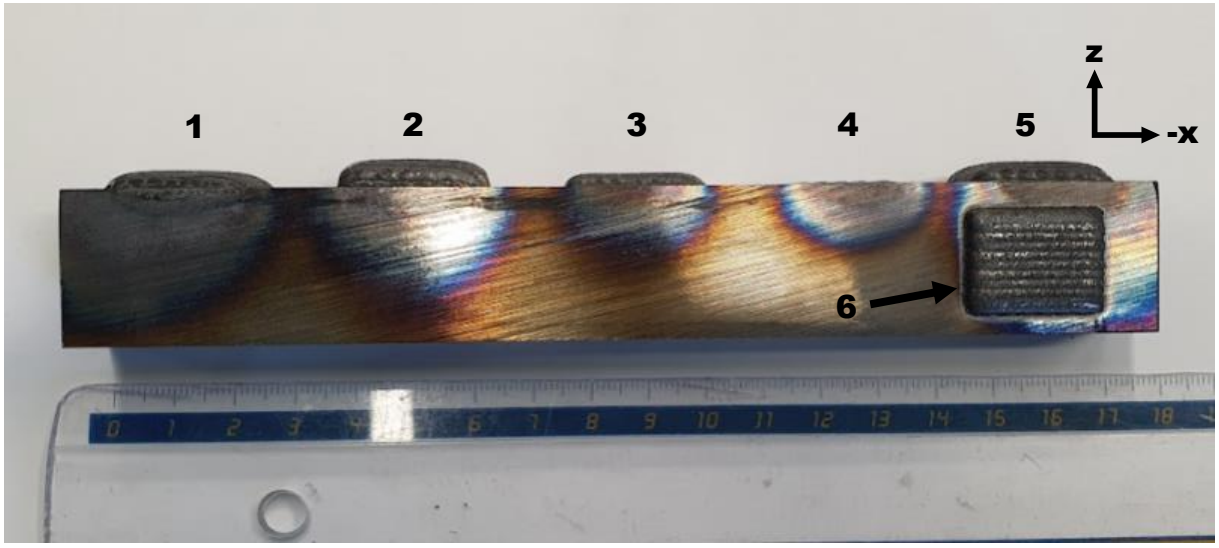


**Fig. 39 Parameter testing for estimation of CCD levels - side view**

**Tab. 3 Parameters picked for estimation of CCD levels**

| Run Nr. | Laser Power [W] | Scanning speed [mms$^{-1}$] | Powder feed [gmin$^{-1}$] | Laser spot diameter [mm] | Track overlap [%] | Carrier gas flow [lmin$^{-1}$] | Shielding gas flow [lmin$^{-1}$] |
|---|---|---|---|---|---|---|---|
| 1 | 2000 | 1000 | 10 | 3 | 50 | 5 | 12 |
| 2 | 1500 | 750 | 12,5 | | | | |
| 3 | 1000 | 1000 | 10 | | | | |
| 4 | 2000 | 1000 | 5 | | | | |
| 5 | 1300 | 800 | 10 | | | | |
| 6 | 800 | 750 | 10 | | | | |

Parameter set 1 showed signs of excessive heat input, as the deposit surface was uneven, the edges showed severe edge effects and the area of coloration due to HAZ was relatively large. Set 2 showed a significantly great achieved layer thickness and more promising surface quality. Sets 3 and 6 showed similar results, where the edges show a low degree of material falling on the edges, but the individual weld beads are not properly connected on the sides. This implies the possibility of insufficient melting. Set 4 had to be terminated prematurely, because the low powder feed caused insufficient heat absorption by the bulk material and the excess reflected energy might have damaged the machine optics. Set 5 showed similar results to set 2 with a more even surface and thinner layers.

Based on this observations and machine operator's experience, the three levels for the Factorial design were selected as shown in the table below. Axial points were then introduced to create a Circumscribed CCD by using the formula [176]:

$$\alpha = (2^k)^{0.25} = (2^3)^{0.25} = 1.6818 \doteq 1.7 \quad (3)$$

*$\alpha$ – axial points level value, k – number of factors*

The value of $\alpha$ was rounded up to give reasonable values for the process parameters. The resulting values were used to create a DoE table with twenty runs in a randomized run order using Minitab® [177] software. For the complete DoE table see attachment nr. 1.

**Tab. 4 Final CCD values**

| $\alpha$ = 1,7 | Level - $\alpha$ | Level -1 | Level 0 | Level +1 | Level + $\alpha$ |
|---|---|---|---|---|---|
| Laser Power [W] | 790 | 1000 | 1300 | 1600 | 1810 |
| Scanning speed [mms$^{-1}$] | 560 | 700 | 900 | 1100 | 1240 |
| Powder feed [gmin$^{-1}$] | 5,75 | 7,5 | 10 | 12,5 | 14,25 |

The TS700 blocks were deposited on top of the C300 cubes according to the DoE table. The C300 cubes were positioned so that the LMD build direction was perpendicular to the build direction of the SLM cubes, which matches the planned orientation setup of the final component. The control parameters of the process matched the previous LMD processes (see tab.2 and tab.3).

The manufacturing process started by setting up the machine and powder delivery system. It was necessary to calibrate the powder feed before the print. The C300 cubes were placed in the machine and the nozzle was positioned using a real-time camera imaging inside the nozzle assembly. After stabilizing the powder flow, the process started depositing the material according to the program. The default layer height was set to 0,7 mm, but was subsequently adjusted during the process, according to the real layer height. This was done by stopping the process after every sixth layer and readjusting the nozzle distance from the surface. These readjusting procedures took approximately two minutes on average. There was also a five-second idle time between individual layers to avoid local overheating. The process continued until a sufficient amount (height) of material (at least 25 mm), was deposited. Depending on the real layer height for each parameter set, this was between 30 to 72 layers.

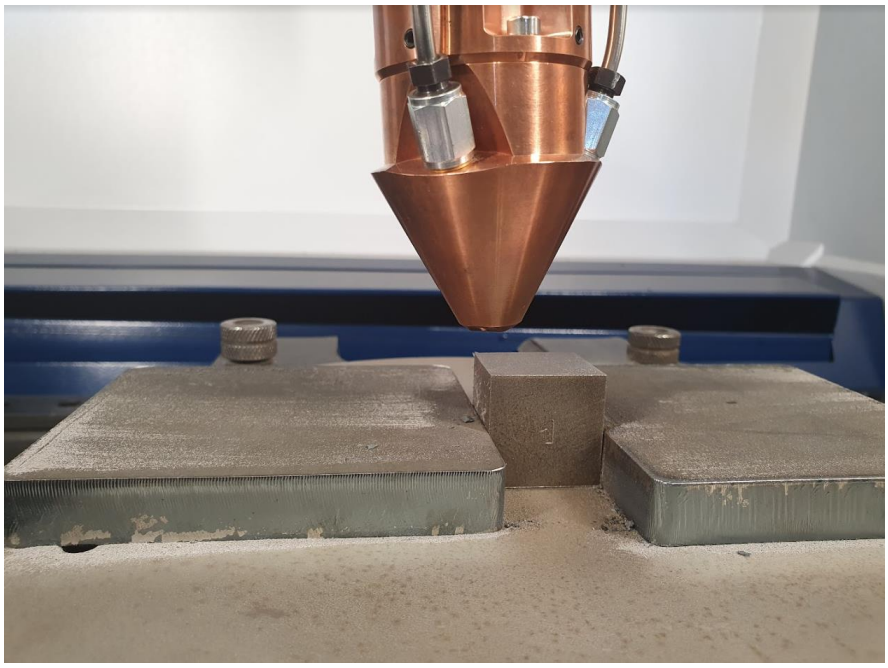

**Fig. 40 SLM blocks ready for the LMD of TS700**

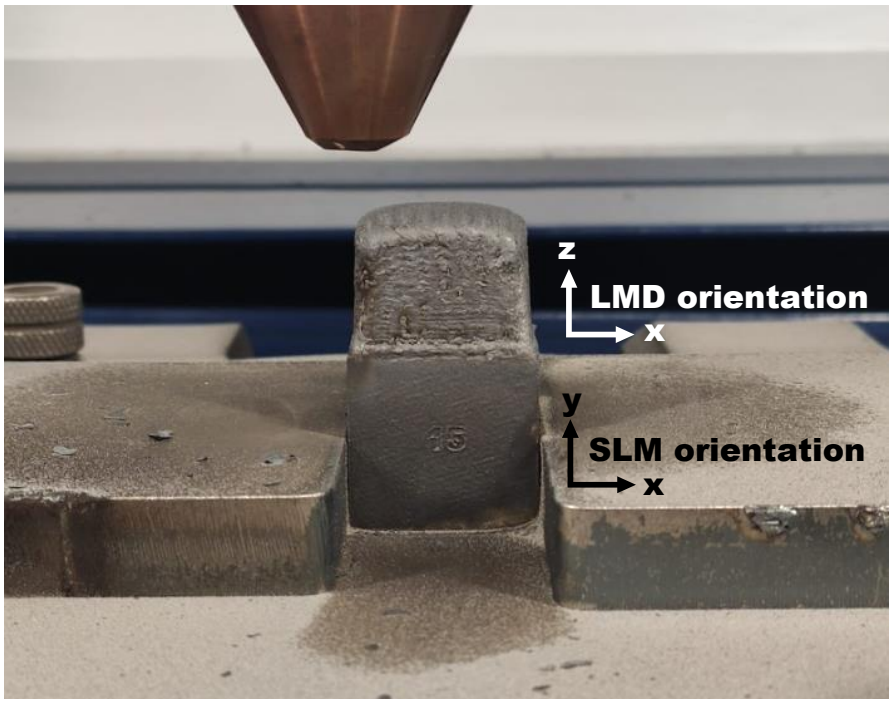


**Fig. 41 Combined block of C300 and TS700 created by SLM and LMD respectively**

Tensile specimens were then manufactured from the combined blocks in a similar way as before. Careful positioning of the parts for the machining was necessary, as it was an intention to have the material interface, e.g. the edge of the original C300 cube, in the middle of the area of interest. The parts were numbered according to their run order for identification and also to indicate, which side of the sample is made out of which material (see attachment nr. 8).

Lastly, the samples were again painted white and covered with a speckle pattern for the DIC.

# 4 Results and discussion

The tensile testing resulted in a series of tensile diagrams (SS curves), from which certain material characteristics were expressed. The main focus was on evaluating and comparing the material ductility, e.g. ultimate strain at failure, and ultimate strength of the material to investigate the differences between both technologies. Determining the yield strength was not a purpose of this work, but it would be most likely determined as Rp0,2, as it was not clearly distinguishable in the diagrams. The values of ultimate stress and Strain at failure were further compared using bar graphs.

## 4.1 316L results

Examples of the resulting SS curves and corresponding fractures are shown below, as well as examples of the fracture images from the light microscopy. Complete data including measured values are listed in attachments nr. 2, 3 and 5.

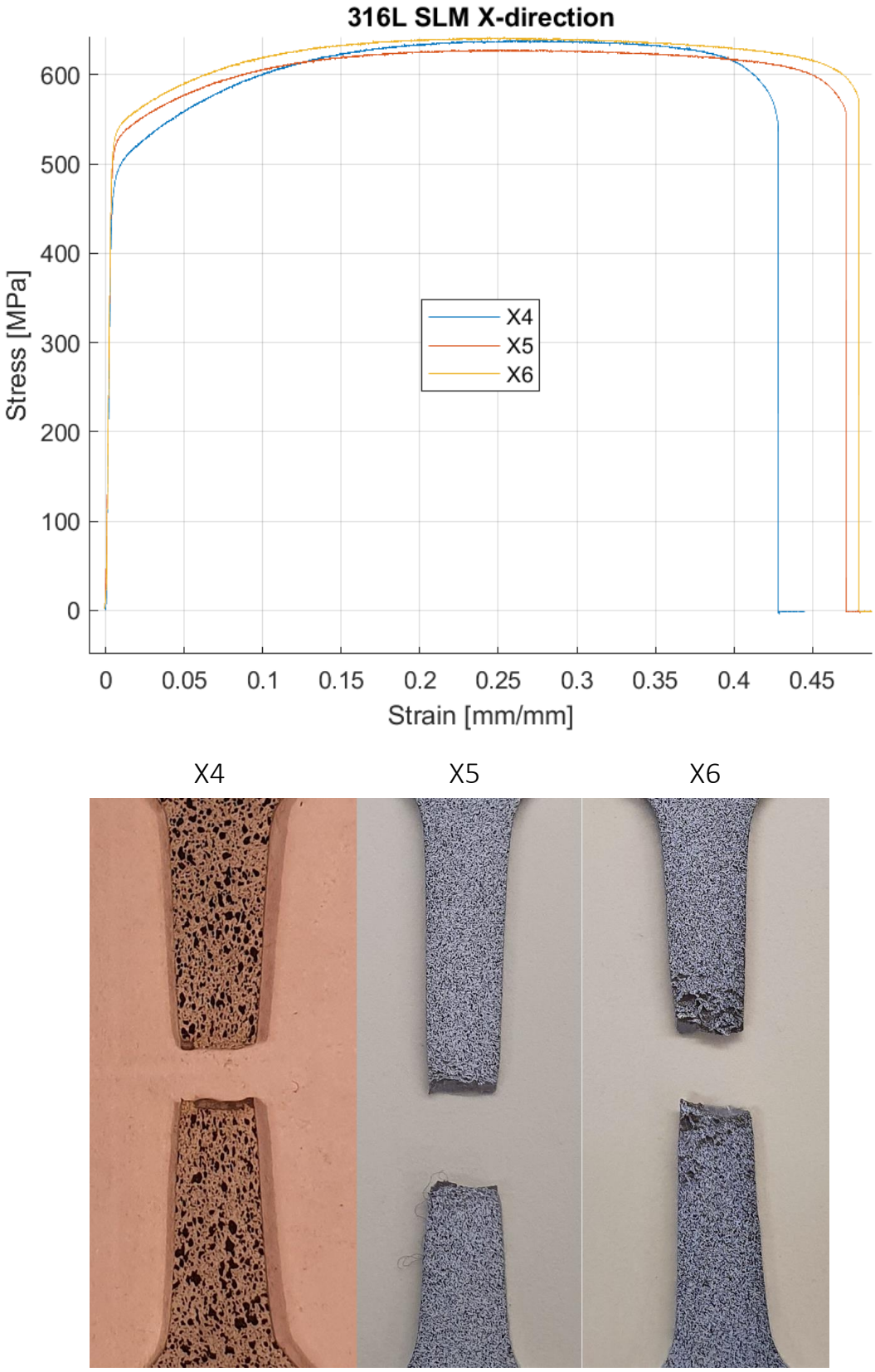


**Fig. 42 SS curves of 316L SLM X-direction samples with fractures**

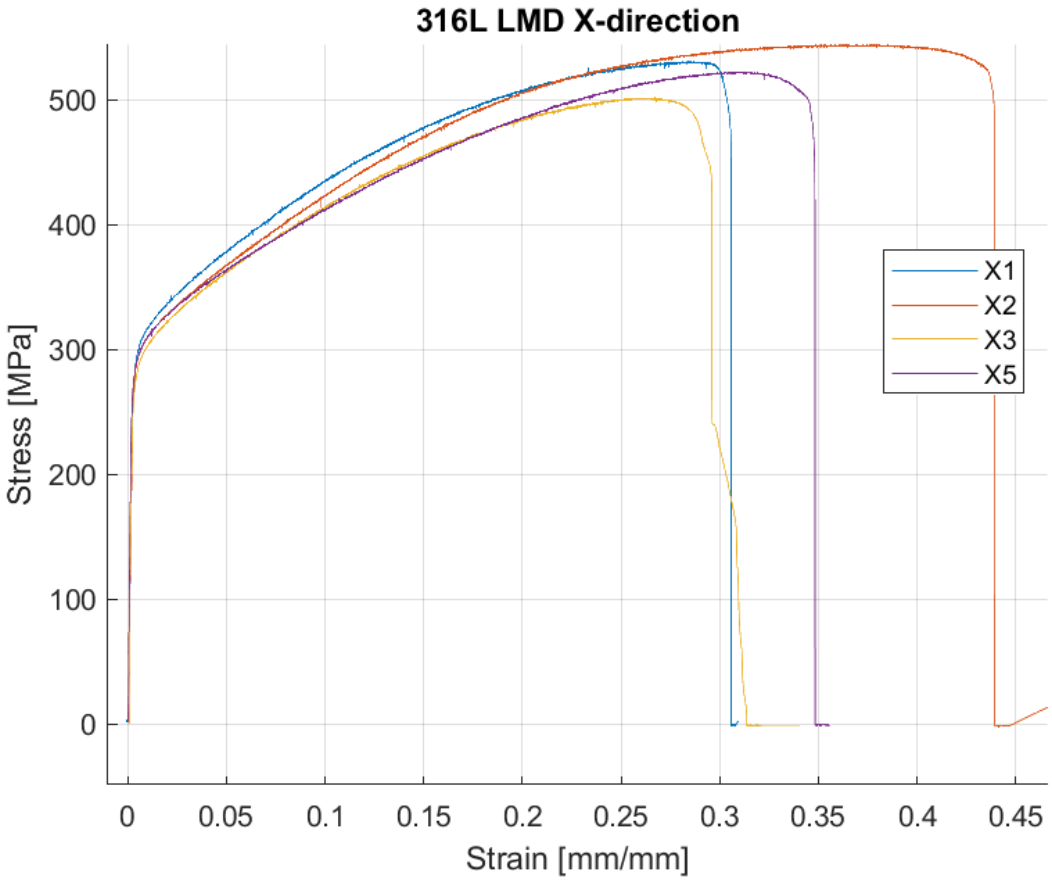



**Fig. 43 SS curves of 316L LMD X-direction samples with fractures**

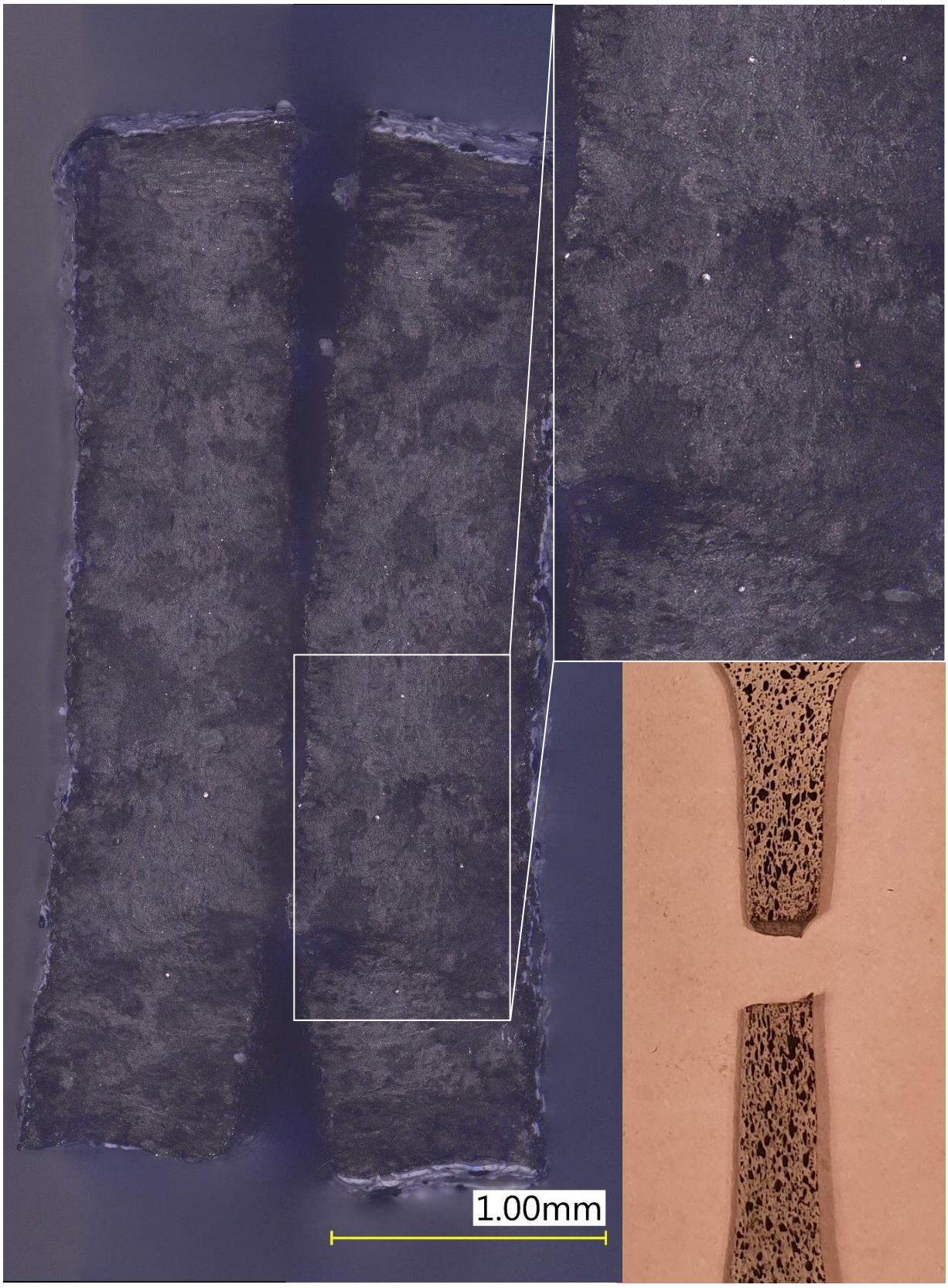


**Fig. 44 Fracture surface of a 316L SLM Y-direction sample**

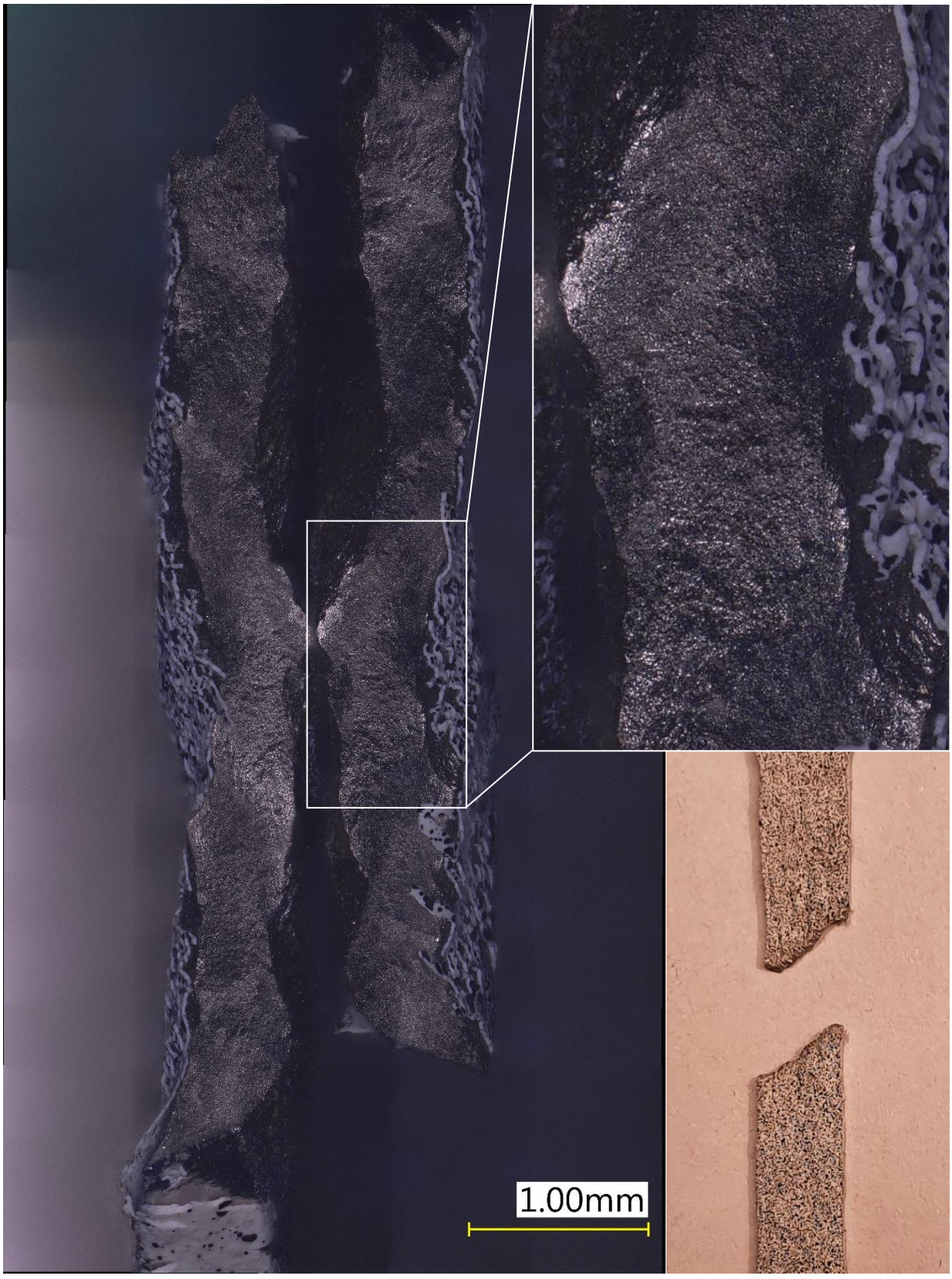


**Fig. 45 Fracture surface of a 316L LMD Y-direction sample**

Significant dissimilarities were observed between the two technologies for 316L. Besides the obvious difference in ultimate strength, the SLM specimens also exhibited more even necking, which occurred only in one place, where it eventually resulted in failure. On the other hand, the surface of the LMD samples deformed unevenly at random places on the specimens, especially on their sides. Although the fractures look in the end very similar to the SLM samples, they were hard to predict and caused more variation in the ultimate strain. The effect of surface coarsening was most severe for the LMD X-direction samples.

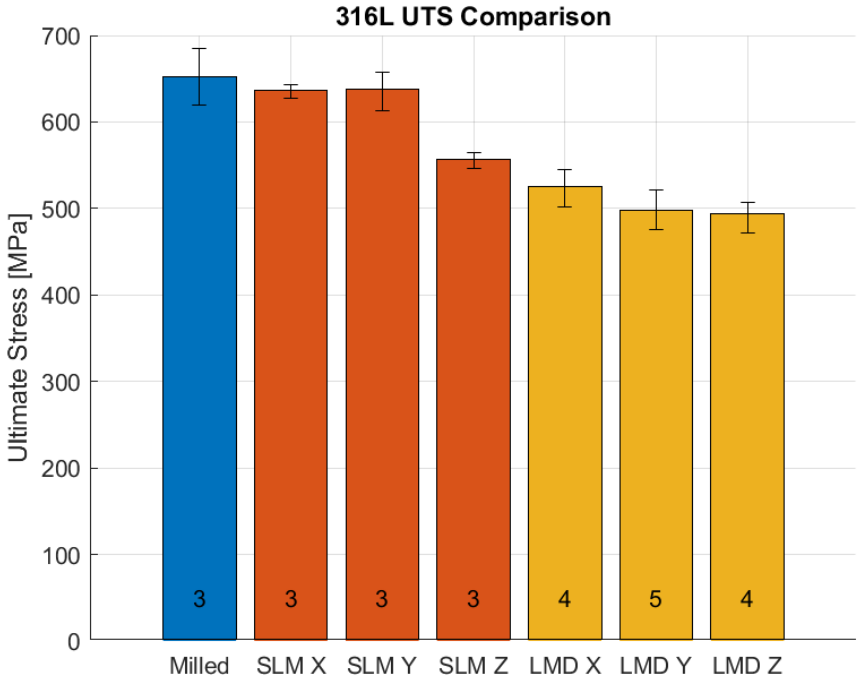


**Fig. 46 316L Ultimate strength comparison**

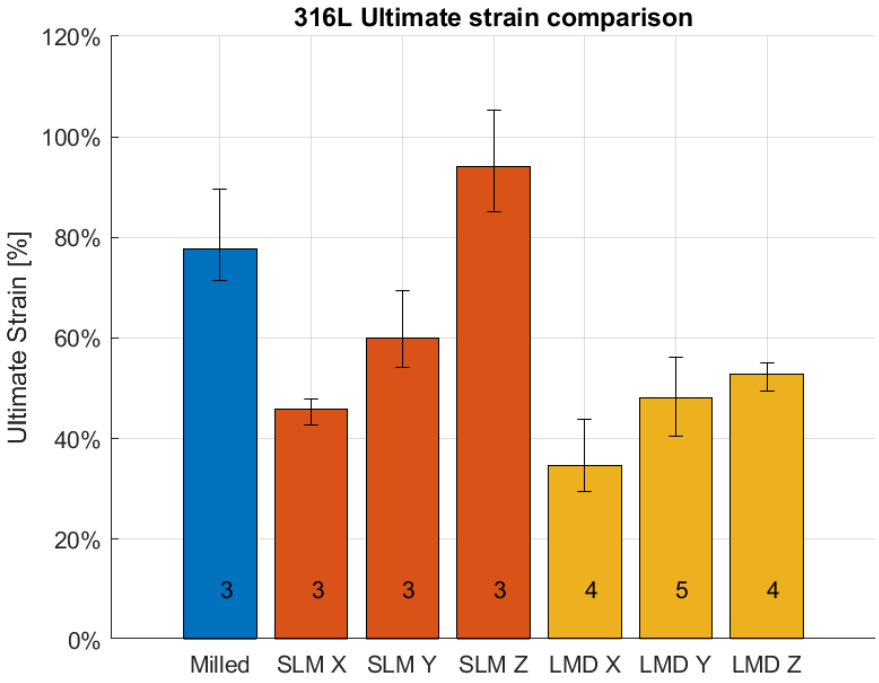


**Fig. 47 316L Ultimate strain comparison**

**Tab. 5 Comparison of average resulting values for 316L**

| 316L | Mean UTS [Mpa] | Mean strain at failure [%] | Mean Young's modulus [Mpa] |
|---|---|---|---|
| SLM X | 636.26837 | 45.97 | 135055.0638 |
| SLM Y | 637.61950 | 60.04 | 248352.3307 |
| SLM Z | 556.57367 | 93.99 | 121710.5292 |
| LMD X | 524.93523 | 34.72 | 107780.9754 |
| LMD Y | 497.60980 | 48.27 | 115194.1833 |
| LMD Z | 493.37155 | 52.88 | 131654.5071 |
| Milled (conventional) | 652.30127 | 77.69 | 137860.1287 |

The fracture imaging showed the significant uneven deformation of the samples. It also showed, that the SLM samples exhibited a greater reduction of the area, which corresponds with the overall higher ductility. Inclusions of around 15-30 μm were observed in the fracture surface of the LMD samples, while the SLM and conventional samples did not.

After the testing and evaluation, the following conclusions were made:

- 316L performed better in SLM than LMD technology for both ultimate strength and strain at failure. This may be due to uneven necking of the LMD specimens during the tensile testing, which was probably caused by a coarser weld bead structure. Also, high energy input may introduce the formation of brittle phases at the grain boundaries, further weakening the material.
- 316L showed slight anisotropy in terms of strength, where the Z-direction performed worse overall than the other two directions. At the same time, 316L showed significant anisotropy in terms of strain, where the Z-direction showed the highest ductility. This contrast implies, that the anisotropy is most likely caused by the different grain orientations, while brittle phase formation had a lesser impact, as it would be expected to lower both strength and ductility in the Z-direction.
- 316L showed relatively consistent results, both for stress and strain measurement. The SS curves varied for both technologies – while the LMD samples were closer to the conventional material, the SLM samples exhibited higher yield strength and different strengthening curve shapes. The SLM Z-direction samples differed the most, with the highest ductility but very little deformation strengthening.
- Results showed that the as-built 316L achieve the property values of conventionally wrought material and that the build orientation can trade-off the ductility for higher strength. The SLM samples had on average 93.50% of the strength of the concentional material, while the LMD had on average 77.5%. Their fractures were of irregular shape, mostly plastic with significant necking.

## 4.2 C300 results

Examples of the resulting SS curves and corresponding fractures are shown below, as well as examples of the fracture images from the light microscopy. Complete data including measured values are listed in attachments nr. 2, 4 and 6.

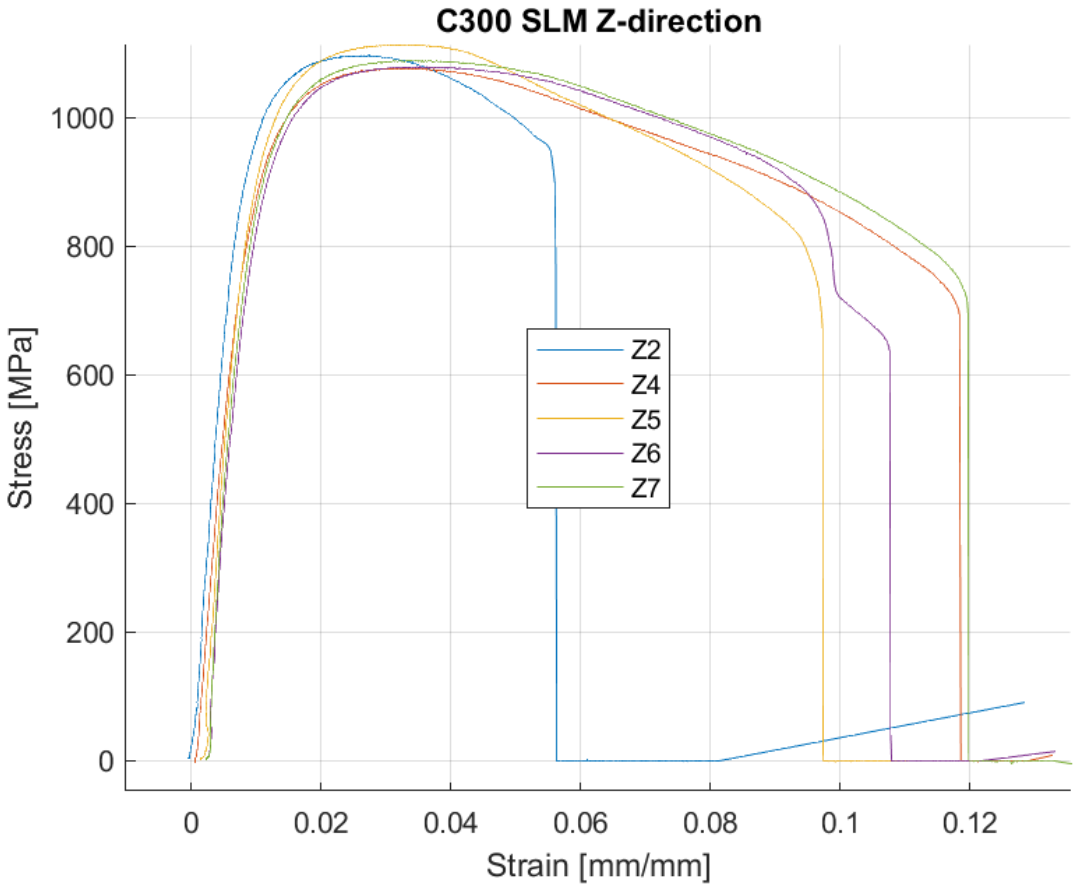


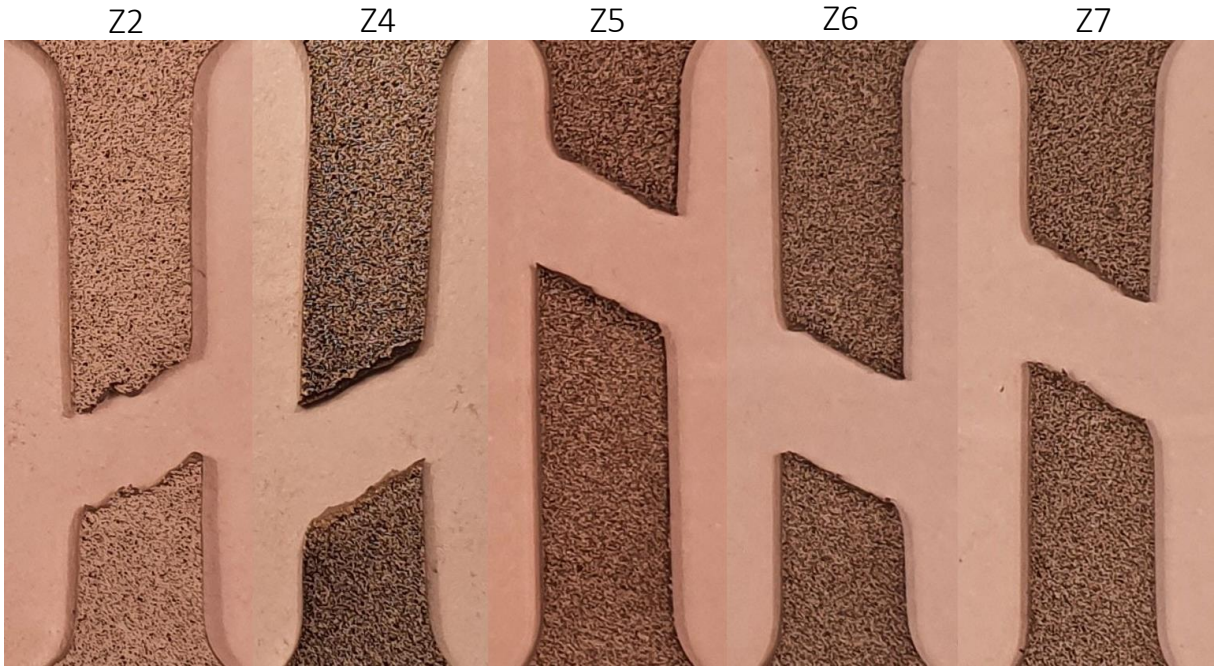


**Fig. 48 Fracture surface of a c300 SLM Z-direction sample**

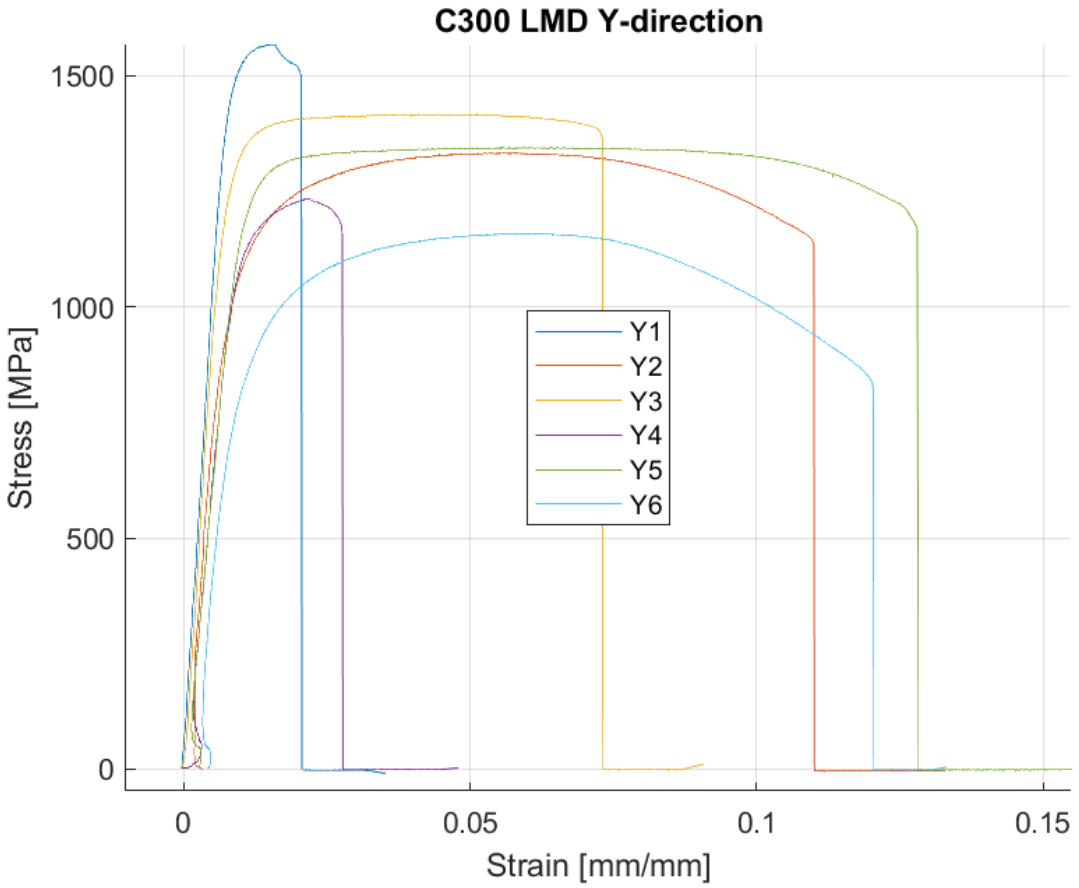


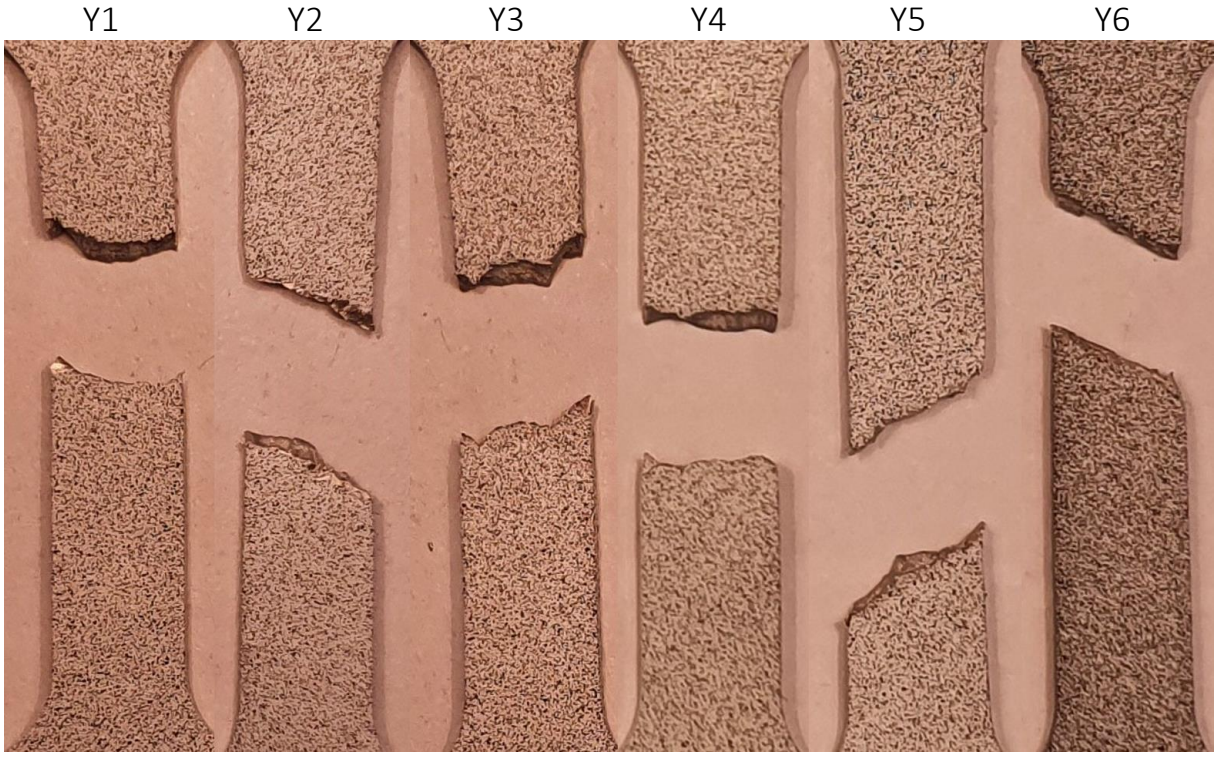


**Fig. 49 Fracture surface of a c300 LMD Y-direction sample**

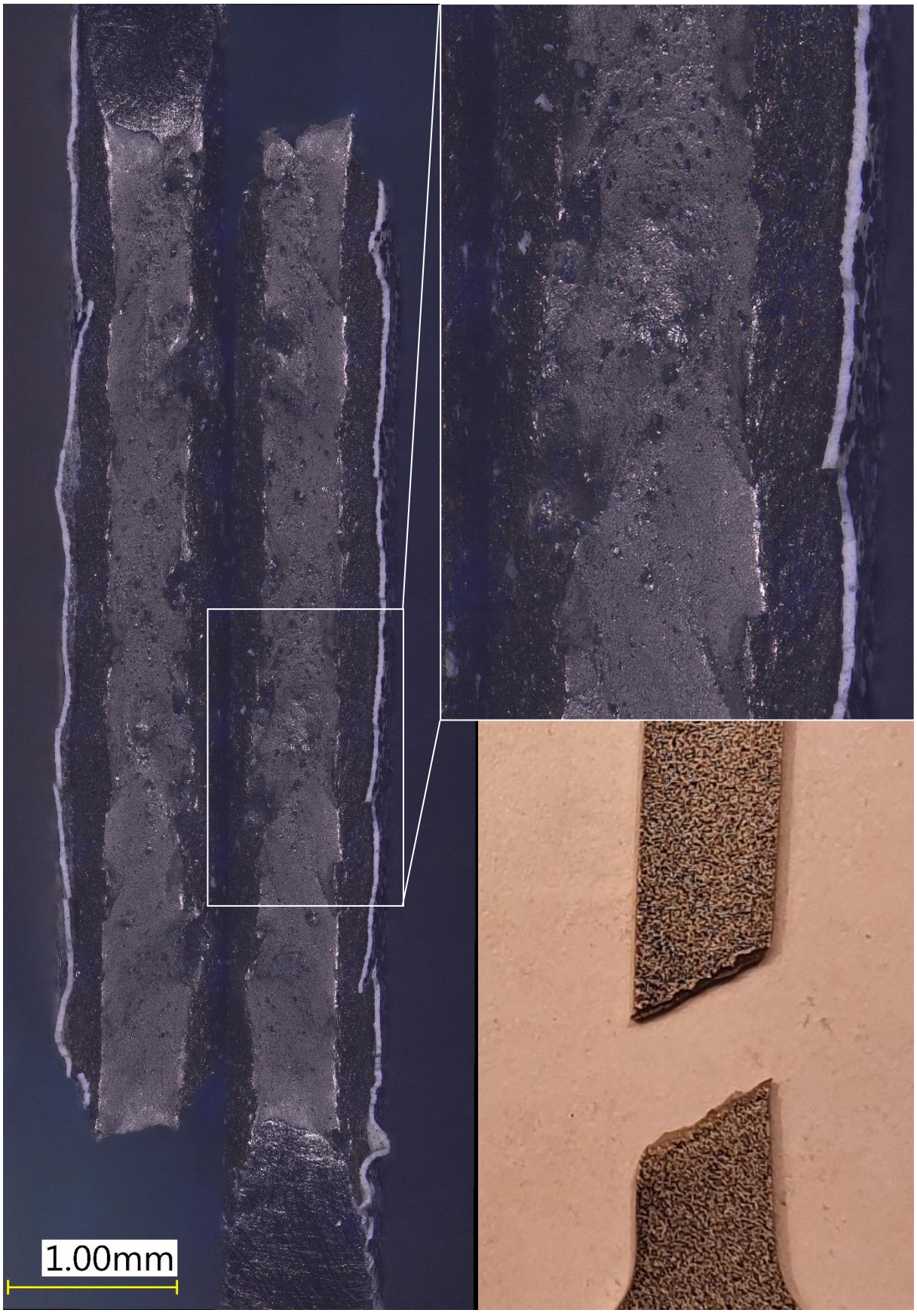


**Fig. 50 Fracture surface of a C300 SLM Z-direction sample**

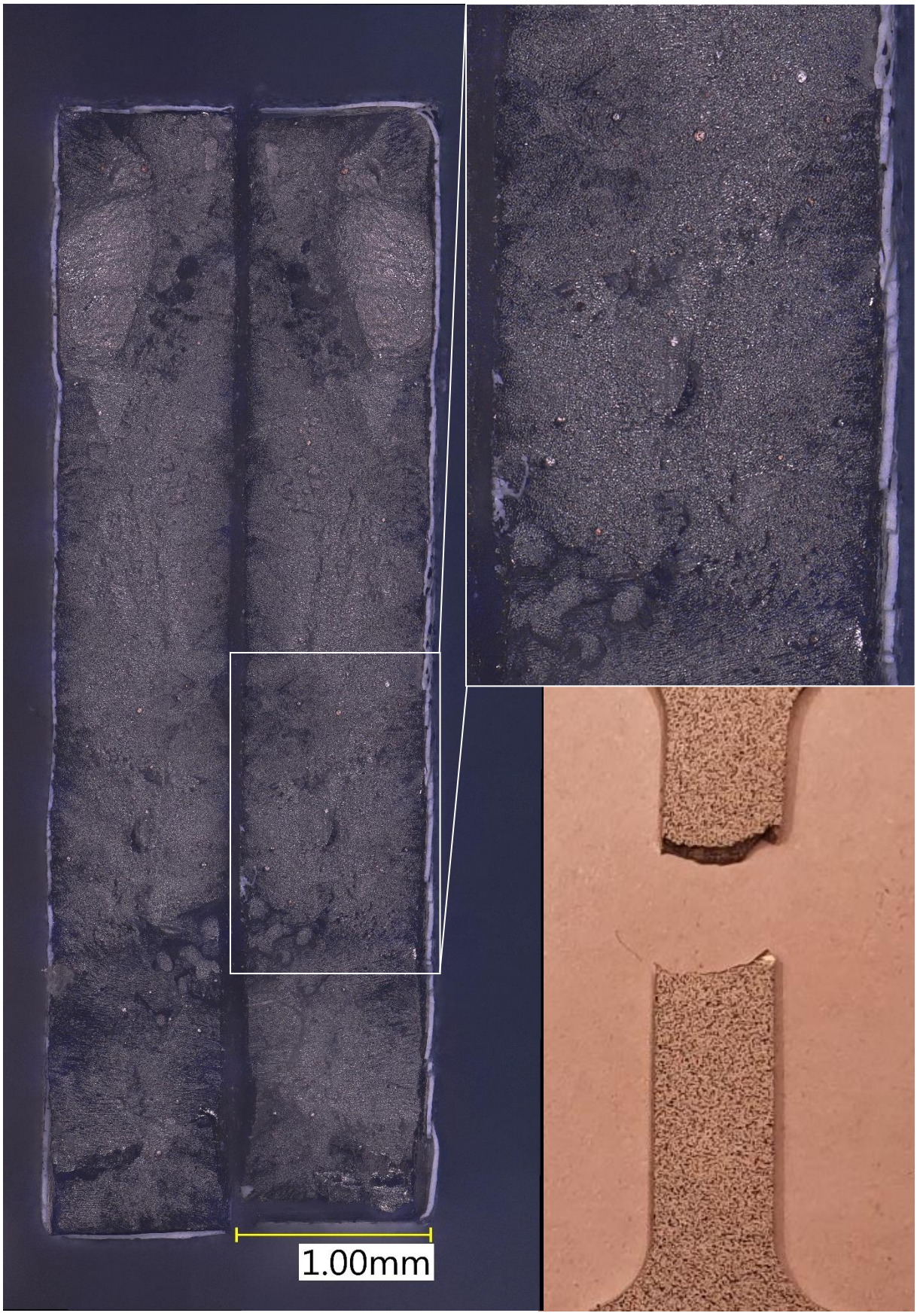


**Fig. 51 Fracture surface of a C300 LMD Y-direction sample**

This material also exhibited differences between the technologies. The main issue during testing and evaluation of the results was the high rate of premature failures of the LMD samples. Unlike the SLM samples, the LMD ones often showed irregular fracture shapes without significant necking. From the recorded image sequences could be observed, that the parts that showed higher ultimate strains also showed significant necking in the 45° shear region. These differences were most severe for the LMD Y-direction samples, that showed a lot of variation in strength, strain and shape of the strengthening curves as well as the whole diagram.

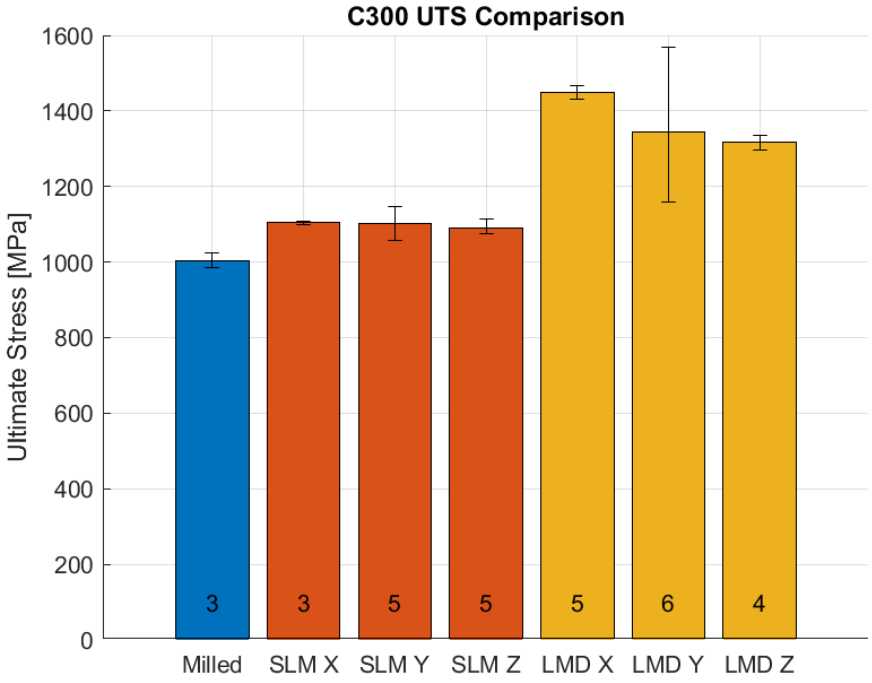


**Fig. 52 C300 Ultimate strength comparison**

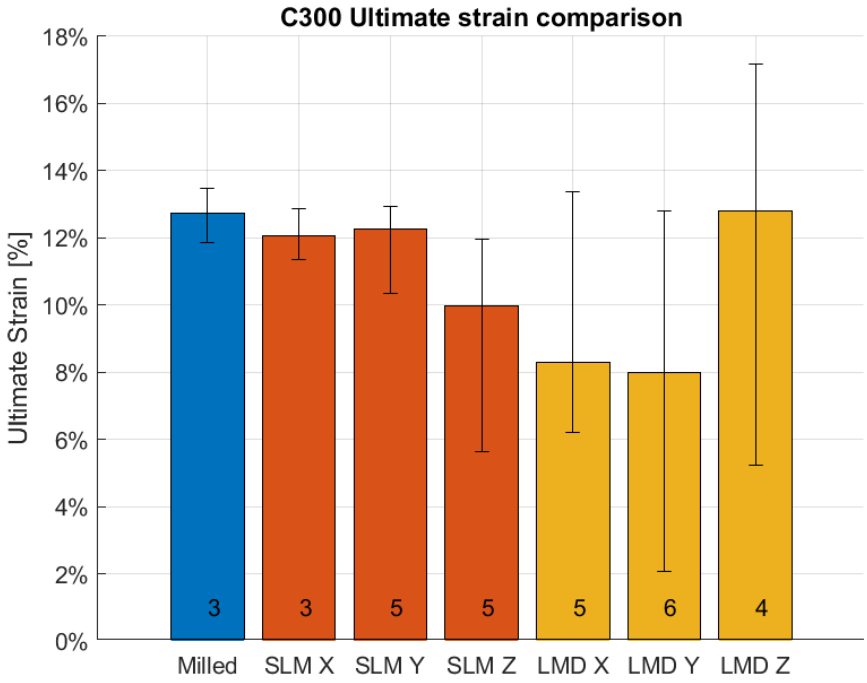


**Fig. 53 C300 Ultimate strain comparison**

**Tab. 6 Comparison of average resulting values for C300**

| C300 | Mean UTS [Mpa] | Mean strain at failure [%] | Mean Young's modulus [Mpa] |
|---|---|---|---|
| SLM X | 1103.57800 | 12.05 | 112299.1433 |
| SLM Y | 1102.65610 | 12.27 | 115303.9135 |
| SLM Z | 1091.00924 | 9.98 | 101021.6180 |
| LMD X | 1449.87486 | 8.30 | 146477.4679 |
| LMD Y | 1342.89695 | 8.00 | 126128.3594 |
| LMD Z | 1318.12290 | 12.82 | 130734.5116 |
| Milled (conventional) | 1004.61060 | 12.73 | 78167.6877 |

The fracture imaging showed significantly higher reduction of area in the SLM samples, which is again in agreement with the higher Strain at failure and therefore ductility. Inclusions were observed in the facture surfaces of the SLM samples of around 20 – 30 μm. The LMD samples showed smaller irregularities. These could be inclusions as well as porosities.

After the testing and evaluation, following conclusions were made:

- C300 performed better in LMD than SLM in terms of ultimate strength, but worse in strain at failure, while both technologies exceed the strength of conventionally wrought material. This is attributed to partial precipitation and aging due to increased temperature during the building process.
- C300 showed little to no anisotropy in the SLM specimens. The LMD samples showed a slight anisotropy, where the Z-direction shows the lowest strength but the highest ductility, similar to 316L.
- C300 showed less consistent results, especially in terms of strain measurement. The results showed many obviously premature failures. Those usually occurred above the yield point, but caused high dispersion of the results of the strain measurement. A feasible explanation is that both technologies introduce defects such as pores and inclusions into the material. Due to low ductility, the material is presumably more notch sensitive and prone to fail prematurely due to fracture initiation at those stress concentration points.
- The C300 SS curves for the SLM technology were very similar to the conventional material, while the LMD exhibited higher yield strength as well as a different character of their strengthening curves.
- The stable fractures of C300 samples showed a plastic shear mechanism in the 45° angle to the loading direction, with little to no necking. The premature failure fractures were of irregular shapes with a brittle character.
- Results showed that the as-built C300 can exceed the property values of conventionally wrought material with an impact of the building orientation on the resulting ductility. The SLM samples had on average 109,4% of the strength of the conventional material, while the LMD had on average 136,4%.

# 5 Conclusion

The presented work focused on two different technologies of additive manufacturing – Selective Laser Melting and Laser Metal Deposition, as well as testing of the materials processed by them and their resulting characteristics.

The research part dealt with the problematics of metal 3D printing in general. First, its role in the industrial world was presented. The scope of different metal AM techniques was listed and also set in the context of the official ASTM standardization system. Further on, the work focused on the description of SLM and LMD, as they were significant for the framework of the experimental part of the thesis. Their common principles were discussed and compared. The metallic powders as an input of the process were briefly discussed, as well as different materials commonly used for the powder-based AM processes.

Both technologies were then thoroughly described in order to provide knowledge necessary for understanding the problematics of the experimental part. Phenomena specific for each of them were identified and discussed. The benefits and drawbacks of each technology were formulated and compared. Concerning the process development process discussed in the experimental part, special attention was paid to expressing the importance of specific process parameters and their influence on the respective process. As material quality assessment of the AM parts is of high importance, defect formation mechanisms and defect control methods were presented, along with other relevant challenges. Finally, a chapter regarding joining dissimilar materials was compiled, as well as a chapter containing a necessary introduction to DoE statistical techniques and their practical use.

The experimental part consisted of two phases – the first one investigating the differences between the two discussed technologies using material testing, and the second one dealing with the preparation of DoE and manufacturing of testing specimens using a combination of the two technologies.

For the first experimental phase, the testing samples were manufactured, prepared and subsequently subjected to quasi-static tensile testing using a custom testing machine. A Digital Image Correlation setup was used for the measurement of the sample deformation and strain to ensure higher measurement accuracy. The MATLAB computational engine was used to process the measurement data and create a visual representation of the testing, i.e. tensile diagrams (stress-strain curves). A selection of specimens was also subjected to light microscopy, which proved to be insufficient as a tool for fracture surface investigation, but supported the proposal of using Scanning Electron Microscope Fractography for forthcoming testing. The testing identified significant differences between the technologies used in terms of as-build material properties, which were then discussed.

The second experimental phase consisted mostly of preparing the Central Composite Design with the intention of optimizing the LMD parameters for the manufacturing of a combined hot-work tool with conformal cooling channels. First the parameter window was estimated in order to appropriately select the levels for the CCD factors. Then the combined samples and tensile specimens were manufactured. Due to a delay in a related project schedule, the testing was not realized in time to include the testing results in this work. However, they will be presented within the project deliverables later.

A further suggestion is to perform another DoE to investigate samples made in discussed manner using metallographic methods. This would confirm or disprove assumptions above and give a more detailed insight into the problematics.

This thesis fulfilled most of its original goals and is of importance not only for the companies involved in the project realization, but also for a greater scope of future work focused on investigation of AM parts and their testing. It also provides comprehensive information about the benefits and drawbacks of combining the SLM and LMD technologies, and suggests new ways for their effective utilization in today's industrial world.

# References

[1] J. Zhang and Y.-G. Jung, *Overview of additive manufacturing process*. Cambridge, MA: Butterworth-Heinemann, 2018.

[2] A. Selema, M. N. Ibrahim, and P. Sergeant, 'Metal Additive Manufacturing for Electrical Machines: Technology Review and Latest Advancements', *Energies*, vol. 15, no. 3, Art. no. 3, Jan. 2022, doi: 10.3390/en15031076.

[3] 'The advantages of 3D printing', *Hubs*. https://www.hubs.com/knowledge-base/advantages-3d-printing/ (accessed Jan. 26, 2022).

[4] J. Zhu, H. Zhou, C. Wang, L. Zhou, S. Yuan, and W. Zhang, 'A review of topology optimization for additive manufacturing: Status and challenges', *Chin. J. Aeronaut.*, vol. 34, no. 1, pp. 91–110, Jan. 2021, doi: 10.1016/j.cja.2020.09.020.

[5] 'Bastech Uses 3D-Printed Conformal Cooling Inserts to Reduce Costs and Time', *3D Systems*, Jan. 19, 2017. https://www.3dsystems.com/learning-center/case-studies/conformal-cooling-ready-prime-time (accessed Feb. 01, 2022).

[6] 'Best Metal 3D Printers of 2021 – Buyer's Guide', *All3DP Pro*, Nov. 04, 2021. https://all3dp.com/1/3d-metal-3d-printer-metal-3d-printing/ (accessed Nov. 18, 2021).

[7] P. Peyre, M. Dal, S. Pouzet, and O. Castelnau, 'Simplified numerical model for the laser metal deposition additive manufacturing process', *J. Laser Appl.*, vol. 29, p. 022304, May 2017, doi: 10.2351/1.4983251.

[8] T. Kurzynowski, E. Chlebus, B. Kuźnicka, and J. Reiner, 'Parameters in Selective Laser Melting for processing metallic powders', *Proc. SPIE*, vol. 8239, p. 823914, Feb. 2012, doi: 10.1117/12.907292.

[9] 'Conduction Mode vs. Keyhole Mode Laser Welding', *EWI*, Feb. 20, 2015. https://ewi.org/conduction-mode-vs-keyhole-mode-laser-welding/ (accessed Nov. 18, 2021).

[10] 'Heat conduction welding | TRUMPF'. https://www.trumpf.com/en_US/solutions/applications/laser-welding/heat-conduction-welding/ (accessed Nov. 18, 2021).

[11] R. Fabbro, 'Melt pool and keyhole behaviour analysis for deep penetration laser welding', *J. Phys. Appl. Phys.*, vol. 43, no. 44, Art. no. 44, Nov. 2010, doi: 10.1088/0022-3727/43/44/445501.

[12] V. Gunenthiram, P. Peyre, M. Schneider, M. Dal, F. Coste, and R. Fabbro, 'Analysis of laser–melt pool–powder bed interaction during the selective laser melting of a stainless steel', *J. Laser Appl.*, vol. 29, no. 2, Art. no. 2, May 2017, doi: 10.2351/1.4983259.

[13] I. Yadroitsev, A. Gusarov, I. Yadroitsava, and I. Smurov, 'Single track formation in selective laser melting of metal powders', *J. Mater. Process. Technol.*, vol. 210, no. 12, Art. no. 12, Sep. 2010, doi: 10.1016/j.jmatprotec.2010.05.010.

[14] E. Kivirasi, H. Piili, and P. Ylander, 'An Approach for a Better Understanding of Spattering Phenomena: Spatter Analysis System Development for Direct Metal Laser Sintering', Oct. 2018.

[15] D. Dagel, G. Grossetete, and D. O. Maccallum, 'Measurement of Laser Weld Temperatures for 3D Model Input', Sandia National Lab. (SNL-NM), Albuquerque, NM (United States), SAND2016-10703, Oct. 2016. doi: 10.2172/1330607.

[16] H. Brooks, A. Rennie, T. Abram, J. McGovern, and F. Caron, 'Variable Fused Deposition Modelling - analysis of benefits, concept design and tool path generation', 2011, pp. 511–517. doi: 10.1201/b11341-83.

[17] O. D. Neikov, D. V. Lotsko, and V. G. Gopienko, 'Powder Characterization and Testing', p. 38, 2019.

[18] 'Metal Powders: Particle Characterization :: Microtrac.com'. https://www.microtrac.com/applications/knowledge-base/particle-characterization-of-metal-powders/ (accessed Feb. 03, 2022).

[19] 'Powder for selective laser melting', *Inside Metal Additive Manufacturing*. http://www.insidemetaladditivemanufacturing.com/1/post/2014/10/the-role-of-super-powders-in-slm.html (accessed Feb. 03, 2022).

[20] J. Montero, A. Rodriguez, J. Amado, and A. Yáñez, 'Inspection of Powder Flow During LMD Deposition by High Speed Imaging', *Phys. Procedia*, vol. 83, pp. 1319–1328, Dec. 2016, doi: 10.1016/j.phpro.2016.08.139.

[21] 'Metal 3D printing materials and DMLS materials |EOS GmbH'. https://www.eos.info/en/additive-manufacturing/3d-printing-metal/dmls-metal-materials (accessed Feb. 22, 2022).

[22] 'Materials Used in Selective Laser Melting (SLM) - Matmatch'. https://matmatch.com/learn/material/materials-used-in-selective-laser-melting-slm (accessed Feb. 22, 2022).

[23] 'Explore Metals Used in 3D Printing', *SLM Solutions*. https://www.slm-solutions.com/products-and-solutions/powders/ (accessed Feb. 22, 2022).

[24] S. Das, D. L. Bourell, and S. S. Babu, 'Metallic materials for 3D printing', *MRS Bull.*, vol. 41, no. 10, pp. 729–741, 2016, doi: 10.1557/mrs.2016.217.

[25] 'Laser metal deposition (LMD) | TRUMPF'. https://www.trumpf.com/en_INT/solutions/applications/additive-manufacturing/laser-metal-deposition-lmd/ (accessed Nov. 23, 2021).

[26] 'Pow(d)erFinder® | Höganäs'. https://www.hoganas.com/en/powder-technologies/powderfinder/ (accessed Apr. 05, 2022).

[27] M. Shellabear and O. Nyrhilä, 'DMLS – DEVELOPMENT HISTORY AND STATE OF THE ART', *Lane 2004 Conf.*, p. 12, Sep. 2004.

[28] 'DMLS Technology for Metal 3D Printer'. https://www.eos.info/en/industrial-3d-printing/additive-manufacturing-how-it-works/dmls-metal-3d-printing (accessed Nov. 16, 2021).

[29] S. Rahmati, '10.12 - Direct Rapid Tooling', in *Comprehensive Materials Processing*, S. Hashmi, G. F. Batalha, C. J. Van Tyne, and B. Yilbas, Eds. Oxford: Elsevier, 2014, pp. 303–344. doi: 10.1016/B978-0-08-096532-1.01013-X.

[30] 'Metal Additive Manufacturing', *3T additive manufacturing*, Mar. 27, 2019. https://www.3t-am.com/metal-additive-manufacturing (accessed Nov. 16, 2021).

[31] X. Shi *et al.*, 'Performance of High Layer Thickness in Selective Laser Melting of Ti6Al4V', *Materials*, vol. 9, no. 12, p. 975, Dec. 2016, doi: 10.3390/ma9120975.

[32] P. G. Martinho, 'Chapter 9 - Rapid manufacturing and tooling', in *Design and Manufacturing of Plastics Products*, A. S. Pouzada, Ed. William Andrew Publishing, 2021, pp. 381–456. doi: 10.1016/B978-0-12-819775-2.00008-5.

[33] V. Griffiths, J. Scanlan, M. H. Eres, A. Martinez-Sykora, and P. Chinchapatnam, 'Cost-driven build orientation and bin packing of parts in Selective Laser Melting (SLM)', *Eur J Oper Res*, 2019, doi: 10.1016/j.ejor.2018.07.053.

[34] 'eos-m-290-description.pdf'. Accessed: Feb. 21, 2022. [Online]. Available: https://engineering.cmu.edu/next/_files/documents/eos-m-290-description.pdf

[35] R. Ding *et al.*, 'Effect of Shielding Gas Volume Flow on the Consistency of Microstructure and Tensile Properties of 316L Manufactured by Selective Laser Melting', *Metals*, vol. 11, no. 2, Art. no. 2, Feb. 2021, doi: 10.3390/met11020205.

[36] C. Pauzon, E. Hryha, P. Forêt, and L. Nyborg, 'Effect of argon and nitrogen atmospheres on the properties of stainless steel 316 L parts produced by laser-powder bed fusion', *Mater. Des.*, vol. 179, p. 107873, Oct. 2019, doi: 10.1016/j.matdes.2019.107873.

[37] J. Reijonen, A. Revuelta, T. Riipinen, K. Ruusuvuori, and P. Puukko, 'On the effect of shielding gas flow on porosity and melt pool geometry in laser powder bed fusion additive manufacturing', *Addit. Manuf.*, vol. 32, p. 101030, Mar. 2020, doi: 10.1016/j.addma.2019.101030.

[38] M. Schniedenharn, F. Wiedemann, and J. Schleifenbaum, 'Visualization of the shielding gas flow in SLM machines by space-resolved thermal anemometry', *Rapid Prototyp. J.*, 2018, doi: 10.1108/RPJ-07-2017-0149.

[39] 'A Novel Approach to Support Structures Optimized for Heat Dissipation in SLM by Combining Process Simulation with Topology Optimization', *C-Therm Technologies Ltd.* https://ctherm.com/resources/tech-library/a-novel-approach-to-support-structures-optimized-for-heat-dissipation-in-slm-by-combining-process-simulation-with-topology-optimization/ (accessed Feb. 21, 2022).

[40] C. Li, Z. Y. Liu, X. Y. Fang, and Y. B. Guo, 'Residual Stress in Metal Additive Manufacturing', *Procedia CIRP*, vol. 71, pp. 348–353, Jan. 2018, doi: 10.1016/j.procir.2018.05.039.

[41] 'Small Metal 3D Printer specialized for Medical Products'. https://www.eos.info/en/additive-manufacturing/3d-printing-metal/eos-metal-systems/eos-m-100 (accessed Nov. 16, 2021).

[42] 'Concept Laser_X Line_Machine | GE Additive'. https://www.ge.com/additive/additive-manufacturing/machines/dmlm-machines/x-line-2000r (accessed Nov. 17, 2021).

[43] B. Cheng, J. Lydon, K. Cooper, V. Cole, P. Northrop, and K. Chou, 'Melt Pool Dimension Measurement In Selective Laser Melting Using Thermal Imaging', 2017. https://www.semanticscholar.org/paper/Melt-Pool-Dimension-Measurement-In-Selective-Laser-Cheng-Lydon/81084c89f6bb161f5e743343f147621aa7038803 (accessed Sep. 02, 2021).

[44] 'HBD-350 / 350T_HBD Metal 3D Printer, Additive Manufacturing 3D Printing, Metal Printing, Best 3D Printer Metal, 3D Printing'.

https://en.hb3dp.com/product/21.html?gclid=Cj0KCQiA95aRBhCsARIsAC2xvfyYgq2JuQH88lZlyFhwOZ2q75ngClw4KqqBgRMIQWqGcTyu7-vX2J8aAoIrEALw_wcB (accessed Mar. 07, 2022).

[45] R. plc, 'Renishaw: RenAM 500 Metal additive manufacturing systems', *Renishaw*. http://www.renishaw.com/en/renam-500-metal-additive-manufacturing-3d-printing-systems--37011 (accessed Mar. 07, 2022).

[46] 'Fraunhofer opens "world's largest SLM facility" in Aachen Germany', *3D Printing Industry*, Jun. 14, 2017. https://3dprintingindustry.com/news/fraunhofer-opens-worlds-largest-slm-facility-aachen-germany-115961/ (accessed Nov. 16, 2021).

[47] 'Lightweight design with additive manufacturing | EOS'. https://www.eos.info/en/industrial-3d-printing/advantages/lightweight-structures (accessed Feb. 11, 2022).

[48] 'AM: good for making lightweight metal auto parts, less so for mass production'. https://www.thefabricator.com/additivereport/article/additive/am-good-for-making-lightweight-metal-auto-parts-less-so-for-mass-production (accessed Feb. 11, 2022).

[49] 'Metal Additive Manufacturing for Healthcare', *SLM Solutions*. https://www.slm-solutions.com/industries/healthcare/ (accessed Feb. 11, 2022).

[50] S. Cosma, 'Manufacturing of implants by selective laser melting', *Balneo Res. J.*, vol. 3, pp. 85–90, Sep. 2012, doi: 10.12680/balneo.2012.1034.

[51] Department of Prosthetic Dental Medicine, Faculty of Dental Medicine, Medical University of Varna, Bulgaria., D. Dzhendov, and T. Dikova, 'APPLICATION OF SELECTIVE LASER MELTING IN MANUFACTURING OF FIXED DENTAL PROSTHESES', *J. IMAB - Annu. Proceeding Sci. Pap.*, vol. 22, no. 4, pp. 1414–1417, Dec. 2016, doi: 10.5272/jimab.2016224.1414.

[52] 'Additive Manufacturing - Aviation and Aeronautics', *SLM Solutions*. https://www.slm-solutions.com/industries/aerospace-and-defense/ (accessed Feb. 11, 2022).

[53] 'Aerospace 3D printing applications', *Hubs*. https://www.hubs.com/knowledge-base/aerospace-3d-printing-applications/ (accessed Feb. 11, 2022).

[54] 'Metal Additive Manufacturing for Automotive', *SLM Solutions*. https://www.slm-solutions.com/industries/automotive/ (accessed Feb. 11, 2022).

[55] 'Conformal cooling: How Additive Manufacturing benefits injection moulding', *Metal Additive Manufacturing*, Sep. 01, 2018. https://www.metal-am.com/articles/how-3d-printing-is-increasing-efficiency-and-quality-in-the-injection-moulding-industry/ (accessed Feb. 11, 2022).

[56] 'Conformal Cooling', *3D Systems*, Sep. 23, 2019. https://www.3dsystems.com/conformal-cooling (accessed Feb. 01, 2022).

[57] A. Masmoudi, R. Bolot, and C. Coddet, 'Investigation of the laser–powder–atmosphere interaction zone during the selective laser melting process', *J. Mater. Process. Technol.*, vol. 225, pp. 122–132, Nov. 2015, doi: 10.1016/j.jmatprotec.2015.05.008.

[58] U. Scipioni Bertoli, A. J. Wolfer, M. J. Matthews, J.-P. R. Delplanque, and J. M. Schoenung, 'On the limitations of Volumetric Energy Density as a design parameter for Selective Laser Melting', *Mater. Des.*, vol. 113, pp. 331–340, Jan. 2017, doi: 10.1016/j.matdes.2016.10.037.

[59] A. Metel, M. Stebulyanin, S. Fedorov, and A. Okunkova, 'Power Density Distribution for Laser Additive Manufacturing (SLM): Potential, Fundamentals and Advanced Applications', *Technologies*, vol. 7, p. 5, Dec. 2018, doi: 10.3390/technologies7010005.

[60] F. Mazzucato, A. Aversa, R. Doglione, S. Biamino, A. Valente, and M. Lombardi, 'Influence of Process Parameters and Deposition Strategy on Laser Metal Deposition of 316L Powder', *Metals*, vol. 9, p. 1160, Oct. 2019, doi: 10.3390/met9111160.

[61] V. Gunenthiram *et al.*, 'Experimental analysis of spatter generation and melt-pool behavior during the powder bed laser beam melting process', *J. Mater. Process. Technol.*, vol. 251, pp. 376–386, Jan. 2018, doi: 10.1016/j.jmatprotec.2017.08.012.

[62] M. J. Matthews, G. Guss, S. A. Khairallah, A. M. Rubenchik, P. J. Depond, and W. E. King, 'Denudation of metal powder layers in laser powder bed fusion processes', *Acta Mater.*, vol. 114, pp. 33–42, Aug. 2016, doi: 10.1016/j.actamat.2016.05.017.

[63] H. J. Niu and I. T. H. Chang, 'Instability of scan tracks of selective laser sintering of high speed steel powder', *Scr. Mater.*, vol. 41, no. 11, Art. no. 11, Nov. 1999, doi: 10.1016/S1359-6462(99)00276-6.

[64] M. F. Sadali, M. Z. Hassan, F. Ahmad, H. Yahaya, and Z. A. Rasid, 'Influence of selective laser melting scanning speed parameter on the surface morphology, surface roughness, and micropores for manufactured Ti6Al4V parts', *J. Mater. Res.*, vol. 35, no. 15, pp. 2025–2035, Aug. 2020, doi: 10.1557/jmr.2020.84.

[65] B. Nguyen, N. Luu, M. L. S. Nai, Z. Zhu, Z. Chen, and J. Wei, 'The role of powder layer thickness on the quality of SLM printed parts', *Arch. Civ. Mech. Eng.*, vol. 18, pp. 948–955, Jul. 2018, doi: 10.1016/j.acme.2018.01.015.

[66] V. Sh. Sufiiarov, A. A. Popovich, E. V. Borisov, I. A. Polozov, D. V. Masaylo, and A. V. Orlov, 'The Effect of Layer Thickness at Selective Laser Melting', *Procedia Eng.*, vol. 174, pp. 126–134, Jan. 2017, doi: 10.1016/j.proeng.2017.01.179.

[67] A. Simchi, 'Direct laser sintering of metal powders: Mechanism, kinetics and microstructural features', *Mater. Sci. Eng. A*, vol. 428, no. 1, Art. no. 1, Jul. 2006, doi: 10.1016/j.msea.2006.04.117.

[68] D. Gu and Y. Shen, 'Balling phenomena in direct laser sintering of stainless steel powder: Metallurgical mechanisms and control methods', *Mater. Des.*, vol. 30, no. 8, Art. no. 8, Sep. 2009, doi: 10.1016/j.matdes.2009.01.013.

[69] S. A. Khairallah, A. T. Anderson, A. Rubenchik, and W. E. King, 'Laser powder-bed fusion additive manufacturing: Physics of complex melt flow and formation mechanisms of pores, spatter, and denudation zones', *Acta Mater.*, vol. 108, pp. 36–45, Apr. 2016, doi: 10.1016/j.actamat.2016.02.014.

[70] B. Zhang, Y. Li, and Q. Bai, 'Defect Formation Mechanisms in Selective Laser Melting: A Review', *Chin. J. Mech. Eng.*, vol. 30, no. 3, Art. no. 3, May 2017, doi: 10.1007/s10033-017-0121-5.

[71] P. Karimi, 'SLM additive manufacturing of Alloy 718 Effect of process parameters on microstructure and properties', 2016. doi: 10.13140/RG.2.2.25434.64963.

[72] X. Zhou, X. Liu, D. Zhang, Z. Shen, and W. Liu, 'Balling phenomena in selective laser melted tungsten', *J. Mater. Process. Technol.*, vol. 222, pp. 33–42, Aug. 2015, doi: 10.1016/j.jmatprotec.2015.02.032.

[73] D. Wang *et al.*, 'Mechanisms and characteristics of spatter generation in SLM processing and its effect on the properties', *Mater. Des.*, vol. 117, pp. 121–130, Mar. 2017, doi: 10.1016/j.matdes.2016.12.060.

[74] D. Gu *et al.*, 'Densification behavior, microstructure evolution, and wear performance of selective laser melting processed commercially pure titanium', *Acta Mater.*, vol. 60, no. 9, pp. 3849–3860, May 2012, doi: 10.1016/j.actamat.2012.04.006.

[75] Z. Chen, S. Cao, X. Wu, and C. H. J. Davies, '13 - Surface roughness and fatigue properties of selective laser melted Ti–6Al–4V alloy', in *Additive Manufacturing for the Aerospace Industry*, F. Froes and R. Boyer, Eds. Elsevier, 2019, pp. 283–299. doi: 10.1016/B978-0-12-814062-8.00015-7.

[76] T. Hirata, T. Kimura, and T. Nakamoto, 'Effects of hot isostatic pressing and internal porosity on the performance of selective laser melted AlSi10Mg alloys', *Mater. Sci. Eng. A*, vol. 772, p. 138713, Jan. 2020, doi: 10.1016/j.msea.2019.138713.

[77] W. Yi, H. Chen, Y. Wu, Y. Chen, and H. Li, 'Effect of Deposition Strategy on Fatigue Behavior of Laser Melting Deposition 12CrNi2 Alloy Steel', in *2019 IEEE 4th Optoelectronics Global Conference (OGC)*, Sep. 2019, pp. 5–8. doi: 10.1109/OGC.2019.8925011.

[78] H. Isaac, 'Method of forming structures wholly of fusion deposited weld metal', US2299747A, Oct. 27, 1942 Accessed: Mar. 14, 2022. [Online]. Available: https://patents.google.com/patent/US2299747/en

[79] R. M. Mahamood, *Laser Metal Deposition Process of Metals, Alloys, and Composite Materials*. Cham: Springer International Publishing, 2018. doi: 10.1007/978-3-319-64985-6.

[80] B. Graf, S. Ammer, A. Gumenyuk, and M. Rethmeier, 'Design of Experiments for Laser Metal Deposition in Maintenance, Repair and Overhaul Applications', *Procedia CIRP*, vol. 11, pp. 245–248, Dec. 2013, doi: 10.1016/j.procir.2013.07.031.

[81] S. L. Sing, C. F. Tey, J. H. K. Tan, S. Huang, and W. Y. Yeong, '2 - 3D printing of metals in rapid prototyping of biomaterials: Techniques in additive manufacturing', in *Rapid Prototyping of Biomaterials (Second Edition)*, R. Narayan, Ed. Woodhead Publishing, 2020, pp. 17–40. doi: 10.1016/B978-0-08-102663-2.00002-2.

[82] '3D printing composite materials: A comprehensive review - ScienceDirect'. https://www.sciencedirect.com/science/article/pii/B9780128205129000137 (accessed Nov. 17, 2021).

[83] G. P. Halada and C. R. Clayton, 'Chapter 19 - The Intersection of Design, Manufacturing, and Surface Engineering', in *Handbook of Environmental Degradation of Materials (Third Edition)*, M. Kutz, Ed. William Andrew Publishing, 2018, pp. 397–422. doi: 10.1016/B978-0-323-52472-8.00019-8.

[84] 'Additive Manufacturing: New Process Improves Speed and Reliability', *siemens.com Global Website*. https://new.siemens.com/global/en/company/stories/research-technologies/additivemanufacturing/additive-manufacturing-laser-metal-deposition.html (accessed Nov. 23, 2021).

[85] 'Wire vs. Powder', *Production Engineering*. https://www.productionengineering.com (accessed Mar. 22, 2022).

[86] R. Mahamood, E. Akinlabi, D. M. Shukla, and S. Pityana, 'Material Efficiency of Laser Metal Deposited Ti6Al4V: Effect of Laser Power', *Eng. Lett.*, vol. 21, pp. 18–22, Feb. 2013.

[87] J. Kelbassa, 'Wire vs. Powder in LMD'.

[88] B. Shen, B. Du, M. Wang, N. Xiao, Y. Xu, and S. Hao, 'Comparison on Microstructure and Properties of Stainless Steel Layer Formed by Extreme High-Speed and Conventional Laser Melting Deposition', *Front. Mater.*, vol. 6, Oct. 2019, doi: 10.3389/fmats.2019.00248.

[89] M. Valentin, C. Arnaud, and R. Kling, 'Additive manufacturing by wire based laser metal deposition', in *Laser 3D Manufacturing VI*, San Francisco, United States, Mar. 2019, p. 19. doi: 10.1117/12.2510074.

[90] J. Arrizubieta, J. Ruiz, S. Martínez, E. Ukar, and A. Lamikiz, 'Intelligent nozzle design for the Laser Metal Deposition process in the Industry 4.0', *Procedia Manuf.*, vol. 13, pp. 1237–1244, Dec. 2017, doi: 10.1016/j.promfg.2017.09.043.

[91] J. Arrizubieta, I. Tabernero, J. Ruiz, A. Lamikiz, S. Martínez, and E. Ukar, 'Continuous Coaxial Nozzle Design for LMD based on Numerical Simulation', *Phys. Procedia*, vol. 56, pp. 429–438, Dec. 2014, doi: 10.1016/j.phpro.2014.08.146.

[92] J. Hao, Q. Meng, C. Li, Z. Li, and D. Wu, 'Effects of tilt angle between laser nozzle and substrate on bead morphology in multi-axis laser cladding', *J. Manuf. Process.*, vol. 43, pp. 311–322, Jul. 2019, doi: 10.1016/j.jmapro.2019.04.025.

[93] 'What is Directed Energy Deposition (DED)?', *Markforged*. https://markforged.com/resources/learn/3d-printing-basics/3d-printing-processes/what-is-directed-energy-deposition-ded (accessed Mar. 14, 2022).

[94] S. Sreekanth, 'Laser-Directed Energy Deposition: Influence of Process Parameters and Heat-Treatments', p. 90, 2020.

[95] 'DED Printer - Magic 800 : Industrial DED 3D Printer For Very Large Parts', *AddUp*. https://addupsolutions.com/machines/ded/magic-800/ (accessed Mar. 24, 2022).

[96] Ruiz, Jose, 'Study of the Influence of Shielding Gases on Laser Metal Deposition of Inconel 718 Superalloy', *ResearchGate*. https://www.researchgate.net/figure/Laser-Metal-Deposition-LMD-experiments-process-parameters_tbl2_326955906 (accessed Nov. 17, 2021).

[97] J. Elmer, J. Vaja, H. Carlton, and R. Pong, 'The Effect of Ar and N-2 Shielding Gas on Laser Weld Porosity in Steel, Stainless Steels, and Nickel', *Weld. J.*, vol. 94, pp. 313s–325s, Oct. 2015.

[98] 'Unique applications of Laser Metal Deposition technolog', *Inside Metal Additive Manufacturing*. http://www.insidemetaladditivemanufacturing.com/1/post/2015/07/unique-applications-of-laser-metal-deposition-technology.html (accessed Mar. 22, 2022).

[99] L. J. Kumar and C. G. K. Nair, 'Laser metal deposition repair applications for Inconel 718 alloy', *Mater. Today Proc.*, vol. 4, no. 10, pp. 11068–11077, Jan. 2017, doi: 10.1016/j.matpr.2017.08.068.

[100] 'LMD a Game-changer for Parts Production and Repair | Electronics360'. https://electronics360.globalspec.com/article/12185/lmd-a-game-changer-for-parts-production-and-repair (accessed Mar. 22, 2022).

[101] T. Petrat, B. Graf, A. Gumenyuk, and M. Rethmeier, 'Laser Metal Deposition as Repair Technology for a Gas Turbine Burner Made of Inconel 718', *Phys. Procedia*, vol. 83, pp. 761–768, Dec. 2016, doi: 10.1016/j.phpro.2016.08.078.

[102] A. Dass and A. Moridi, 'State of the Art in Directed Energy Deposition: From Additive Manufacturing to Materials Design', *Coatings*, vol. 9, no. 7, Art. no. 7, Jul. 2019, doi: 10.3390/coatings9070418.

[103] D.-G. Ahn, 'Directed Energy Deposition (DED) Process: State of the Art', *Int. J. Precis. Eng. Manuf.-Green Technol.*, vol. 8, no. 2, pp. 703–742, Mar. 2021, doi: 10.1007/s40684-020-00302-7.

[104] K. Shah, I. ul Haq, A. Khan, S. A. Shah, M. Khan, and A. J. Pinkerton, 'Parametric study of development of Inconel-steel functionally graded materials by laser direct metal deposition', *Mater. Des. 1980-2015*, vol. 54, pp. 531–538, Feb. 2014, doi: 10.1016/j.matdes.2013.08.079.

[105] A. Ben-Artzy *et al.*, 'Compositionally graded SS316 to C300 Maraging steel using additive manufacturing', *Mater. Des.*, vol. 201, p. 109500, Mar. 2021, doi: 10.1016/j.matdes.2021.109500.

[106] B. E. Carroll *et al.*, 'Functionally graded material of 304L stainless steel and inconel 625 fabricated by directed energy deposition: Characterization and thermodynamic modeling', *Acta Mater.*, vol. 108, pp. 46–54, Apr. 2016, doi: 10.1016/j.actamat.2016.02.019.

[107] 'TruLaser Cell 3000'. https://www.trumpf.com/en_INT/products/machines-systems/laser-welding-systems-and-the-arc-welding-cell/trulaser-cell-3000/ (accessed Mar. 24, 2022).

[108] 'Directed Energy Deposition (DED): A Complete Guide', *3DSourced*, Jan. 13, 2021. https://www.3dsourced.com/3d-printing-technologies/directed-energy-deposition/ (accessed Mar. 24, 2022).

[109] S. Oliari, A. S. D'Oliveira, and M. Schulz, 'Additive Manufacturing of H11 with Wire-Based Laser Metal Deposition', *Soldag. Insp.*, vol. 22, Dec. 2017, doi: 10.1590/0104-9224/si2204.06.

[110] W. A. Ayoola, W. J. Suder, and S. W. Williams, 'Parameters controlling weld bead profile in conduction laser welding', *J. Mater. Process. Technol.*, vol. 249, pp. 522–530, Nov. 2017, doi: 10.1016/j.jmatprotec.2017.06.026.

[111] S. Ocylok, E. Alexeev, S. Mann, A. Weisheit, K. Wissenbach, and I. Kelbassa, 'Correlations of Melt Pool Geometry and Process Parameters During Laser Metal Deposition by Coaxial Process Monitoring', *Phys. Procedia*, vol. 56, pp. 228–238, Dec. 2014, doi: 10.1016/j.phpro.2014.08.167.

[112] 'TruPrint Series 3000 | TRUMPF'. https://www.trumpf.com/en_CA/products/machines-systems/additive-production-systems/truprint-3000/ (accessed Feb. 11, 2022).

[113] S. Donadello, M. Motta, A. G. Demir, and B. Previtali, 'Monitoring of laser metal deposition height by means of coaxial laser triangulation', *Opt. Lasers Eng.*, vol. 112, pp. 136–144, Jan. 2019, doi: 10.1016/j.optlaseng.2018.09.012.

[114] R. M. Mahamood, E. T. Akinlabi, and S. Akinlabi, 'Laser power and Scanning Speed Influence on the Mechanical Property of Laser Metal Deposited Titanium-Alloy', *Lasers Manuf. Mater. Process.*, vol. 2, no. 1, pp. 43–55, Mar. 2015, doi: 10.1007/s40516-014-0003-y.

[115] R. M. Mahamood and E. T. Akinlabi, 'Effect of Laser Power on Surface Finish during Laser Metal Deposition Process', p. 5, 2014.

[116] I. Burkhardt, R. Visone, S. Riekehr, M. W. Rackel, N. Kashaev, and J. Enz, 'Parameter development and characterization of laser metal deposited Ti alloy powders for use at elevated temperatures', *Procedia CIRP*, vol. 74, pp. 176–179, Jan. 2018, doi: 10.1016/j.procir.2018.08.088.

[117] X. Wang, L. Q. Li, J. Qu, and W. Tao, 'Microstructure and mechanical properties of laser metal deposited AlSi10Mg alloys', *Mater. Sci. Technol.*, vol. 35, pp. 1–10, Oct. 2019, doi: 10.1080/02670836.2019.1674022.

[118] G. Li *et al.*, 'Experimental Investigation on Laser Metal Deposition of Ti-6Al-4V Alloy with Coaxial Local Shielding Gas Nozzle', *J. Mater. Eng. Perform.*, vol. 29, pp. 1–9, Nov. 2020, doi: 10.1007/s11665-020-05283-x.

[119] J. Cao, F. Liu, X. Lin, C. Huang, J. Chen, and W. Huang, 'Effect of overlap rate on recrystallization behaviors of Laser Solid Formed Inconel 718 superalloy', *Opt. Laser Technol.*, vol. 45, pp. 228–235, Feb. 2013, doi: 10.1016/j.optlastec.2012.06.043.

[120] M.-N. Bold, J. Zielinski, S. Ziegler, and J. H. Schleifenbaum, 'Study of LMD of Inconel 718 on Inclined Planes: Influence of Inclination on Width and Height of Deposited Material', Social Science Research Network, Rochester, NY, SSRN Scholarly Paper ID 3785875, Feb. 2021. doi: 10.2139/ssrn.3785875.

[121] Y. rye Choi, S. Sun, Q. Liu, M. Brandt, and M. Qian, 'Influence of deposition strategy on the microstructure and fatigue properties of Laser Metal Deposited Ti-6Al-4V powder on Ti-6Al-4V substrate', *Int. J. Fatigue*, vol. 130, p. 105236, Aug. 2019, doi: 10.1016/j.ijfatigue.2019.105236.

[122] D. Svetlizky *et al.*, 'Directed energy deposition (DED) additive manufacturing: Physical characteristics, defects, challenges and applications', *Mater. Today*, vol. 49, pp. 271–295, Oct. 2021, doi: 10.1016/j.mattod.2021.03.020.

[123] M. Liu, A. Kumar, S. Bukkapatnam, and M. Kuttolamadom, 'A Review of the Anomalies in Directed Energy Deposition (DED) Processes & Potential Solutions - Part Quality & Defects', *Procedia Manuf.*, vol. 53, pp. 507–518, Jan. 2021, doi: 10.1016/j.promfg.2021.06.093.

[124] V. Kratochvílová, L. Zemanová, F. Vlašic, and P. Mazal, 'Study of Initial Stages of Fatigue Process in Selective Laser Melting Material Using Acoustic Emission Method', *Solid State Phenom.*, vol. 258, pp. 477–480, Dec. 2016, doi: 10.4028/www.scientific.net/SSP.258.477.

[125] J. Chen, W. Hou, X. Wang, S. Chu, and Z. Yang, 'Microstructure, porosity and mechanical properties of selective laser melted AlSi10Mg', *Chin. J. Aeronaut.*, vol. 33, no. 7, pp. 2043–2054, Jul. 2020, doi: 10.1016/j.cja.2019.08.017.

[126] Y. Liu, Y. Yang, S. Mai, D. Wang, and C. Song, 'Investigation into spatter behavior during selective laser melting of AISI 316L stainless steel powder', *Mater. Des.*, vol. 87, pp. 797–806, Dec. 2015, doi: 10.1016/j.matdes.2015.08.086.

[127] L. Kučerová, I. Zetková, A. Jandová, and M. Bystrianský, 'Microstructural characterisation and in-situ straining of additive-manufactured X3NiCoMoTi 18-9-5 maraging steel', *Mater. Sci. Eng. A*, vol. 750, pp. 70–80, Mar. 2019, doi: 10.1016/j.msea.2019.02.041.

[128] 'Mechanické vlastnosti materiálů připravovaných pomocí procesu SLM; Ing. Marek Doubrava ( 2018 - 117622) – VUT'. https://www.vut.cz/studenti/zav-prace/detail/117622 (accessed Nov. 11, 2021).

[129] N. Kumar, W. Yuan, and R. S. Mishra, 'Chapter 2 - A Framework for Friction Stir Welding of Dissimilar Alloys and Materials', in *Friction Stir Welding of Dissimilar Alloys and Materials*, N. Kumar, W. Yuan, and R. S. Mishra, Eds. Butterworth-Heinemann, 2015, pp. 15–33. doi: 10.1016/B978-0-12-802418-8.00002-3.

[130] N. Kumar, W. Yuan, and R. S. Mishra, 'Chapter 1 - Introduction', in *Friction Stir Welding of Dissimilar Alloys and Materials*, N. Kumar, W. Yuan, and R. S. Mishra, Eds. Butterworth-Heinemann, 2015, pp. 1–13. doi: 10.1016/B978-0-12-802418-8.00001-1.

[131] 'Welding_Handbook_WELDING_SCIENCE_AND_TEC.pdf'. Accessed: Jan. 25, 2022. [Online]. Available: http://blog.aku.edu.tr/cakmakkaya/files/2020/03/Welding_Handbook_WELDING_SCIENCE_AND_TEC.pdf

[132] '5. Process Improvement'. https://www.itl.nist.gov/div898/handbook/pri/pri.htm (accessed Jan. 17, 2022).

[133] 'What is DOE? Design of Experiments Basics for Beginners', *Sartorius*. https://www.sartorius.com/en/knowledge/science-snippets/what-is-doe-design-of-experiments-basics-for-beginners-507170 (accessed Jan. 12, 2022).

[134] 'Trial and error', *Wikipedia*. Jan. 18, 2022. Accessed: Jan. 19, 2022. [Online]. Available: https://en.wikipedia.org/w/index.php?title=Trial_and_error&oldid=1066413843

[135] 'Design of experiments'. https://www.jmp.com/en_au/statistics-knowledge-portal/what-is-design-of-experiments.html (accessed Jan. 19, 2022).

[136] J. Tošenovský, 'PLÁNOVÁNÍ EXPERIMENTŮ', p. 223, 2012.

[137] 'What are response surface designs, central composite designs, and Box-Behnken designs?' https://support.minitab.com/en-us/minitab/18/help-and-how-to/modeling-statistics/doe/supporting-topics/response-surface-designs/response-surface-central-composite-and-box-behnken-designs/#what-is-a-central-composite-design (accessed Jan. 19, 2022).

[138] 'Analysis Of Variance (ANOVA) | Introduction, Types & Techniques', *Analytics Vidhya*, Jan. 15, 2018. https://www.analyticsvidhya.com/blog/2018/01/anova-analysis-of-variance/ (accessed Jan. 12, 2022).

[139] H. Liu, L. Wei, J. Bao, Z. Xing, B. Song, and C. Lei, 'Numerical and Experimental Investigation into Hot Forming of Ultra High Strength Steel Sheet', *J. Mater. Eng. Perform.*, vol. 20, pp. 1–10, Feb. 2011, doi: 10.1007/s11665-010-9641-1.

[140] P. Danielczyk and I. Wróbel, 'Analysis of Hot Stamping Tool Cooling System—A Case Study', *Materials*, vol. 14, no. 11, Art. no. 11, Jan. 2021, doi: 10.3390/ma14112759.

[141] H. Hoffmann, H. So, and H. Steinbeiss, 'Design of Hot Stamping Tools with Cooling System', *CIRP Ann.*, vol. 56, no. 1, pp. 269–272, 2007, doi: 10.1016/j.cirp.2007.05.062.

[142] 'How Carbon Affects the Quality of Steel Weldability and Hardness', *Analyzing Metals*, Aug. 18, 2020. https://www.thermofisher.com/blog/metals/how-carbon-affects-the-quality-of-steel-weldability-and-hardness/ (accessed May 16, 2022).

[143] O. Elin, S. Stefan, M. Taoran, P. Sebastian, L. Christophe, and A. Johanna, 'Microstructure and Properties of SLM High Speed Steel', Jan. 2021, doi: 10.20944/preprints202101.0624.v1.

[144] 'Alloy Steel Maraging 300 | Vascomax® C300 Alloy Steel'. https://www.magellanmetals.com/maraging-c300-vascomax-300 (accessed Nov. 08, 2021).

[145] 'Rickard Metals | C300 Maraging Steel', Oct. 22, 2014. https://rickardmetals.com/products/alloy-steel/c300-maraging-steel/ (accessed Nov. 08, 2021).

[146] 'Maraging 300 | Vascomax® 300 | AMS 6514'. https://www.smithmetal.com/grade-c300.htm (accessed Nov. 08, 2021).

[147] 'AISI Grade 18Ni (300) Maraging Steel, Aged, sheet, tested transverse, 6 mm'. http://www.matweb.com/search/datasheet_print.aspx?matguid=550702a40aa64761b8296d5ffffc47c7 (accessed Nov. 09, 2021).

[148] bolzano.cz, 'Technická podpora nástrojové oceli | Bolzano'. https://bolzano.cz/technicka-podpora/technicka-podpora-nastrojovych-oceli/ (accessed Nov. 11, 2021).

[149] 'maraging, nanoprecipitates, TWIP, TRIP, AHSS,stainless steel, high Mn steel, manganese, austenite,ultra fine grained steel, atom probe tomography'. http://www.dierk-raabe.com/martensite-alloys-and-transformations/maraging-trip-steels/ (accessed Nov. 09, 2021).

[150] 'ATI C-200TM/C-250TM/C-300TM/C-350TM Alloys .The maraging steels are also exceptionally stable during - [PDF Document]', *fdocuments.in*. https://fdocuments.in/document/ati-c-200tmc-250tmc-300tmc-350tm-alloys-the-maraging-steels-are-also-exceptionally.html (accessed Nov. 11, 2021).

[151] 'SSA Documents'. https://www.ssa-corp.com/documents/Data%20Sheet%20Maraging.pdf (accessed Nov. 09, 2021).

[152] W. M. Garrison, 'Martensitic Non-stainless Steels: High Strength and High Alloy', in *Encyclopedia of Materials: Science and Technology*, K. H. J. Buschow, R. W. Cahn, M. C. Flemings, B. Ilschner, E. J. Kramer, S. Mahajan, and P. Veyssière, Eds. Oxford: Elsevier, 2001, pp. 5197–5202. doi: 10.1016/B0-08-043152-6/00903-7.

[153] A. P. Mouritz, Ed., '11 - Steels for aircraft structures', in *Introduction to Aerospace Materials*, Woodhead Publishing, 2012, pp. 232–250. doi: 10.1533/9780857095152.232.

[154] F. Tariq, M. Shifa, and R. A. Baloch, 'Effect of Overaging Conditions on Microstructure and Mechanical Properties of Maraging Steel', *Met. Sci. Heat Treat.*, vol. 62, no. 3, pp. 188–194, Jul. 2020, doi: 10.1007/s11041-020-00535-y.

[155] F. Cajner, D. Landek, and V. Leskovšek, 'Surface modifications of maraging steels used in the manufacture of moulds and dies', *Mater. Tehnol.*, vol. 44, pp. 85–91, Mar. 2010.

[156] 'Maraging Steel 300 / C300 (UNS K93120) - Aircraft Materials'. https://www.aircraftmaterials.com/data/nickel/C300.html (accessed Nov. 09, 2021).

[157] C. Félix-Martínez, J. Ibarra-Medina, D. A. Fernández-Benavides, L. A. Cáceres-Díaz, and J. M. Alvarado-Orozco, 'Effect of the parametric optimization and heat-treatment on the 18Ni-300 maraging steel microstructural properties manufactured by directed energy deposition', *Int. J. Adv. Manuf. Technol.*, vol. 115, no. 11, pp. 3999–4020, Aug. 2021, doi: 10.1007/s00170-021-07320-y.

[158] C. Turk, H. Zunko, C. Aumayr, H. Leitner, and M. Kapp, 'Advances in Maraging Steels for Additive Manufacturing', *BHM Berg- Hüttenmänn. Monatshefte*, vol. 164, no. 3, pp. 112–116, Mar. 2019, doi: 10.1007/s00501-019-0835-z.

[159] C. Tan, K. Zhou, W. Ma, P. Zhang, M. Liu, and T. Kuang, 'Microstructural evolution, nanoprecipitation behavior and mechanical properties of selective laser melted high-performance grade 300 maraging steel', *Mater. Des.*, vol. 134, pp. 23–34, Nov. 2017, doi: 10.1016/j.matdes.2017.08.026.

[160] K. Kempen, E. Yasa, L. Thijs, J.-P. Kruth, and J. Van Humbeeck, 'Microstructure and mechanical properties of Selective Laser Melted 18Ni-300 steel', *Phys. Procedia*, vol. 12, pp. 255–263, Jan. 2011, doi: 10.1016/j.phpro.2011.03.033.

[161] 'Tool Steels- Chromium Hot-Work Steels', *AZoM.com*, Jul. 10, 2012. https://www.azom.com/article.aspx?ArticleID=6149 (accessed May 17, 2022).

[162] 'High Speed Steel | H13 Steel | H13 | H13 Technical Data'. https://hudsontoolsteel.com/technical-data/steelH3 (accessed May 18, 2022).

[163] 'Hot Work Tool Steels :: Total Materia Article'. https://www.totalmateria.com/page.aspx?ID=CheckArticle&site=kts&NM=234 (accessed May 17, 2022).

[164] Aubert&Duval, 'Pearl® Micro TS700, powder for additive manufacturing', https://www.aubertduval.com/wp-media/uploads/2021/11/TS700_PearlMicro_V0_AM_GB.pdf, (accesed Jan. 2022)

[165] Interview with representative of Aubert&Duval, On the matter of powder materials for additive manufacturing, Nov. 2021 .

[166] S. Taylor and H. R. Kotadia, 'Microstructural evolution of 316L austenitic stainless steel during in-situ biaxial deformation and annealing', *Mater. Charact.*, vol. 163, p. 110288, May 2020, doi: 10.1016/j.matchar.2020.110288.

[167] A. Kosmac, *Surface hardening of stainless steels*. Brussels: Euro Inox, 2015. Accessed: May 16, 2022. [Online]. Available: http://www.euro-inox.org/pdf/map/Surface_Hardening_EN.pdf

[168] 'SAE 316L stainless steel', *Wikipedia*. Feb. 02, 2022. Accessed: May 16, 2022. [Online]. Available: https://en.wikipedia.org/w/index.php?title=SAE_316L_stainless_steel&oldid=1069382296

[169] '316 vs 316L Stainless Steel: What's the Difference?', *Bergsen Metal*, Jan. 12, 2021. https://bergsen.com/316-vs-316l-stainless-steel/ (accessed May 16, 2022).

[170] H.-L. Ming *et al.*, 'Microstructure, Residual Strain and Stress Corrosion Cracking Behavior in 316L Heat-Affected Zone', *Acta Metall. Sin. Engl. Lett.*, vol. 29, no. 9, pp. 848–858, Sep. 2016, doi: 10.1007/s40195-016-0461-7.

[171] B. A. AlMangour, 'Additive Manufacturing of High-Performance 316L Stainless Steel Nanocomposites via Selective Laser Melting', UCLA, 2017. Accessed: May 18, 2022. [Online]. Available: https://escholarship.org/uc/item/4jp76591

[172] S. Sarafan *et al.*, 'Benchmarking of 316L Stainless Steel Manufactured by a Hybrid Additive/Subtractive Technology', *J. Manuf. Mater. Process.*, vol. 6, no. 2, Art. no. 2, Apr. 2022, doi: 10.3390/jmmp6020030.

[173] 'Stainless steel for metal 3D printers| EOS GmbH'. https://www.eos.info/en/additive-manufacturing/3d-printing-metal/dmls-metal-materials/stainless-steel (accessed May 18, 2022).

[174] 'Powder Feeder', *Medicoat*. https://medicoat.com/system-engineering/powder-feeder/ (accessed May 20, 2022).

[175] 'DIC: Digital Image Correlation Strain analysis | SEIKA Digital Image Corporation.' https://www.seika-di.com/en/measurement/dic.html (accessed May 20, 2022).

[176] S. Bhattacharya, *Central Composite Design for Response Surface Methodology and Its Application in Pharmacy*. IntechOpen, 2021. doi: 10.5772/intechopen.95835.

[177] 'Data Analysis, Statistical & Process Improvement Tools', *wwwSite*. https://www.minitab.com/content/www/websites/en-us.html (accessed May 23, 2022).

# ATTACHMENT nr. 1

# DoE table for the LMD of combined specimens

| Factors | LMD parameters | Level -1 | Level 0 | Level 1 | α = 1.7 |
|---|---|---|---|---|---|
| A | Laser Power [W] | 1000 | 1300 | 1600 | |
| B | Scanning velocity [mm/min] | 700 | 900 | 1100 | |
| C | Powder flow rate [g/min] | 7.5 | 10 | 12.5 | |

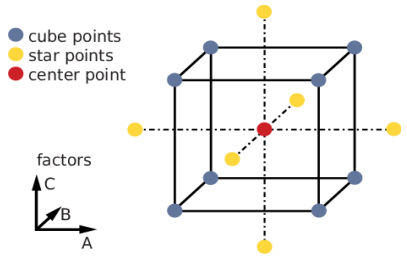


| StdOrder | RunOrder | PtType | Blocks | A | B | C | StdOrder | RunOrder | PtType | Blocks | Power | Scan. Velocity | Powder feed |
|---|---|---|---|---|---|---|---|---|---|---|---|---|---|
| 17 | 1 | 0 | 1 | 0 | 0 | 0 | 17 | 1 | 0 | 1 | 1300 | 900 | 10 |
| 18 | 2 | 0 | 1 | 0 | 0 | 0 | 18 | 2 | 0 | 1 | 1300 | 900 | 10 |
| 12 | 3 | -1 | 1 | 0 | α | 0 | 12 | 3 | -1 | 1 | 1300 | 1240 | 10 |
| 7 | 4 | 1 | 1 | -1 | 1 | 1 | 7 | 4 | 1 | 1 | 1000 | 1100 | 12.5 |
| 19 | 5 | 0 | 1 | 0 | 0 | 0 | 19 | 5 | 0 | 1 | 1300 | 900 | 10 |
| 2 | 6 | 1 | 1 | 1 | -1 | -1 | 2 | 6 | 1 | 1 | 1600 | 700 | 7.5 |
| 9 | 7 | -1 | 1 | -α | 0 | 0 | 9 | 7 | -1 | 1 | 790 | 900 | 10 |
| 6 | 8 | 1 | 1 | 1 | -1 | 1 | 6 | 8 | 1 | 1 | 1600 | 700 | 12.5 |
| 15 | 9 | 0 | 1 | 0 | 0 | 0 | 15 | 9 | 0 | 1 | 1300 | 900 | 10 |
| 11 | 10 | -1 | 1 | 0 | -α | 0 | 11 | 10 | -1 | 1 | 1300 | 560 | 10 |
| 10 | 11 | -1 | 1 | α | 0 | 0 | 10 | 11 | -1 | 1 | 1810 | 900 | 10 |
| 16 | 12 | 0 | 1 | 0 | 0 | 0 | 16 | 12 | 0 | 1 | 1300 | 900 | 10 |
| 13 | 13 | -1 | 1 | 0 | 0 | -α | 13 | 13 | -1 | 1 | 1300 | 900 | 5.75 |
| 14 | 14 | -1 | 1 | 0 | 0 | α | 14 | 14 | -1 | 1 | 1300 | 900 | 14.25 |
| 1 | 15 | 1 | 1 | -1 | -1 | -1 | 1 | 15 | 1 | 1 | 1000 | 700 | 7.5 |
| 8 | 16 | 1 | 1 | 1 | 1 | 1 | 8 | 16 | 1 | 1 | 1600 | 1100 | 12.5 |
| 20 | 17 | 0 | 1 | 0 | 0 | 0 | 20 | 17 | 0 | 1 | 1300 | 900 | 10 |
| 4 | 18 | 1 | 1 | 1 | 1 | -1 | 4 | 18 | 1 | 1 | 1600 | 1100 | 7.5 |
| 3 | 19 | 1 | 1 | -1 | 1 | -1 | 3 | 19 | 1 | 1 | 1000 | 1100 | 7.5 |
| 5 | 20 | 1 | 1 | -1 | -1 | 1 | 5 | 20 | 1 | 1 | 1000 | 700 | 12.5 |

# ATTACHMENT nr. 2

# Table of measured values

| Part | UTS [MPa] | Strain at failure [%] | Young's modulus [Mpa] |
|---|---|---|---|
| 316L_SLM_X4 | 638.4129 | 42.82 | 127356.4925 |
| 316L_SLM_X5 | 627.9089 | 47.12 | 137027.3444 |
| 316L_SLM_X6 | 642.4833 | 47.97 | 140781.3544 |
| 316L_SLM_Y4 | 613.4751 | 69.4 | 345010.9509 |
| 316L_SLM_Y5 | 642.5306 | 56.58 | 224959.587 |
| 316L_SLM_Y6 | 656.8528 | 54.13 | 175086.4543 |
| 316L_SLM_Z4 | 546.442 | 105.4 | 101758.367 |
| 316L_SLM_Z5 | 558.7497 | 85.23 | 123794.7859 |
| 316L_SLM_Z6 | 564.5293 | 91.35 | 139578.4348 |
| 316L_LMD_X1 | 530.9443 | 30.58 | 101057.3015 |
| 316L_LMD_X2 | 544.6448 | 43.88 | 89054.9967 |
| 316L_LMD_X3 | 501.8079 | 29.6 | 101634.1611 |
| 316L_LMD_X5 | 522.3439 | 34.83 | 139377.4424 |
| 316L_LMD_Y1 | 521.4674 | 46.7 | 125839.4341 |
| 316L_LMD_Y2 | 491.2208 | 4064 | 93158.3161 |
| 316L_LMD_Y3 | 509.7287 | 56.45 | 111596.8076 |
| 316L_LMD_Y4 | 490.076 | 47.68 | 126306.9514 |
| 316L_LMD_Y5 | 475.5561 | 49.87 | 119069.4072 |
| 316L_LMD_Z1 | 505.1768 | 49.41 | 126912.4764 |
| 316L_LMD_Z2 | 506.4359 | 55.07 | 195091.6635 |
| 316L_LMD_Z3 | 490.5965 | 52.1 | 65346.6303 |
| 316L_LMD_Z4 | 471.277 | 54.94 | 139267.2582 |
| 316L_M5 | 685.474 | 89.52 | 202492.1382 |
| 316L_M6 | 632.4168 | 72.11 | 105293.5148 |
| 316L_M7 | 639.013 | 71.45 | 105794.7331 |
| C300_SLM_X3 | 1104.6299 | 12.86 | 97184.4727 |
| C300_SLM_X4 | 1098.3938 | 11.36 | 101945.774 |
| C300_SLM_X5 | 1107.7103 | 11.93 | 137767.1831 |
| C300_SLM_Y1 | 1056.5321 | 12.43 | 103954.5897 |
| C300_SLM_Y2 | 1129.28 | 10.35 | 189836.3454 |
| C300_SLM_Y3 | 1071.9056 | 12.75 | 94150.8986 |
| C300_SLM_Y4 | 1147.4464 | 12.85 | 97921.8131 |
| C300_SLM_Y5 | 1108.1164 | 12.95 | 90655.9207 |
| C300_SLM_Z2 | 1096.4113 | 5.62 | 130683.7739 |
| C300_SLM_Z4 | 1076.3755 | 11.84 | 101795.6016 |
| C300_SLM_Z5 | 1113.4451 | 9.73 | 97715.8711 |
| C300_SLM_Z6 | 1080.2938 | 10.76 | 85099.9914 |
| C300_SLM_Z7 | 1088.5205 | 11.97 | 89812.852 |
| C300_LMD_X1 | 1467.1461 | 13.38 | 155873.3922 |
| C300_LMD_X2 | 1430.3973 | 6.19 | 142635.5523 |
| C300_LMD_X3 | 1447.6053 | 6.97 | 128702.0303 |
| C300_LMD_X4 | 1452.9687 | 7.49 | 191048.7948 |
| C300_LMD_X5 | 1451.2569 | 7.47 | 114127.5698 |
| C300_LMD_Y1 | 1567.7157 | 2.06 | 204886.5445 |
| C300_LMD_Y2 | 1333.0482 | 11 | 142969.6735 |
| C300_LMD_Y3 | 1417.7025 | 7.31 | 184637.944 |
| C300_LMD_Y4 | 1233.4707 | 2.78 | 12304.102 |
| C300_LMD_Y5 | 1346.7659 | 12.8 | 123806.5649 |
| C300_LMD_Y6 | 1158.6787 | 12.03 | 88165.3273 |
| C300_LMD_Z1 | 1335.9927 | 5.22 | 143219.8902 |
| C300_LMD_Z2 | 1310.899 | 13.87 | 133371.9668 |
| C300_LMD_Z3 | 1330.5058 | 15.01 | 136256.6446 |
| C300_LMD_Z4 | 1295.0941 | 17.16 | 110089.5446 |
| C300_M1 | 997.3279 | 11.86 | 82845.5986 |
| C300_M2 | 992.6781 | 12.85 | 82951.7033 |
| C300_M3 | 1023.8258 | 13.47 | 68705.7612 |

# ATTACHMENT nr. 3

## Stress – strain curves for the tested 316L specimens

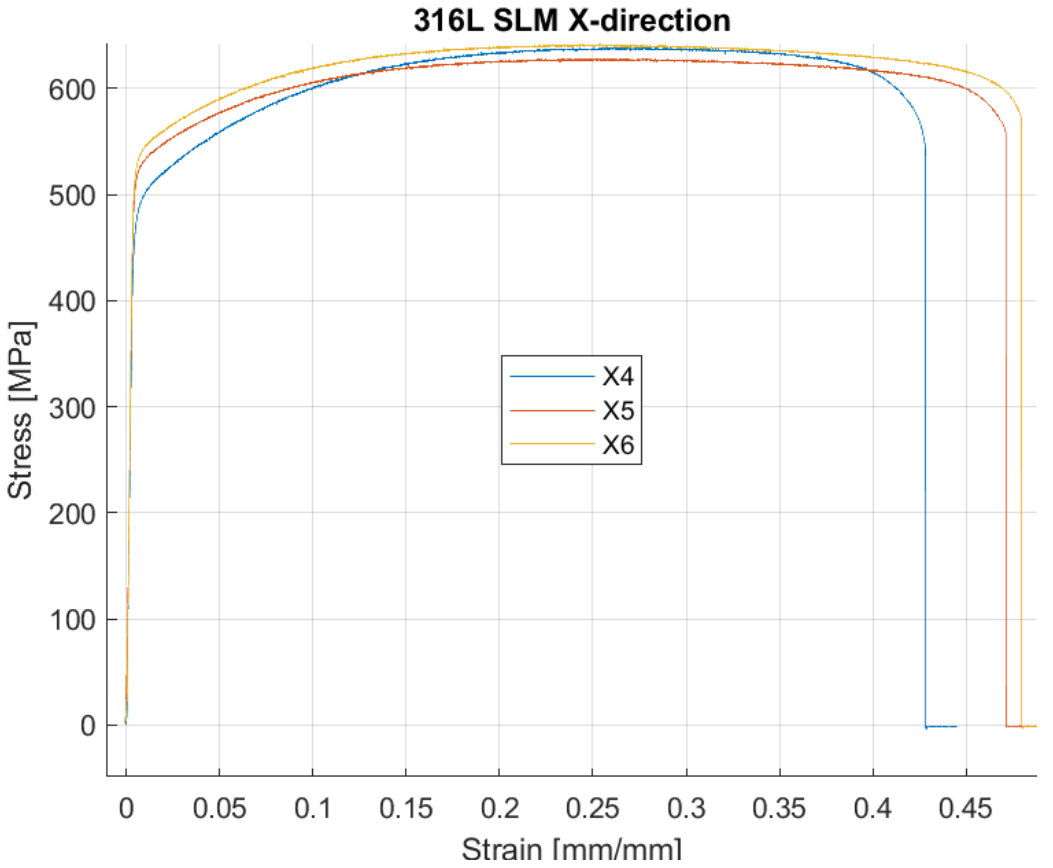
316L SLM X-direction
Stress [MPa]
Strain [mm/mm]
X4
X5
X6

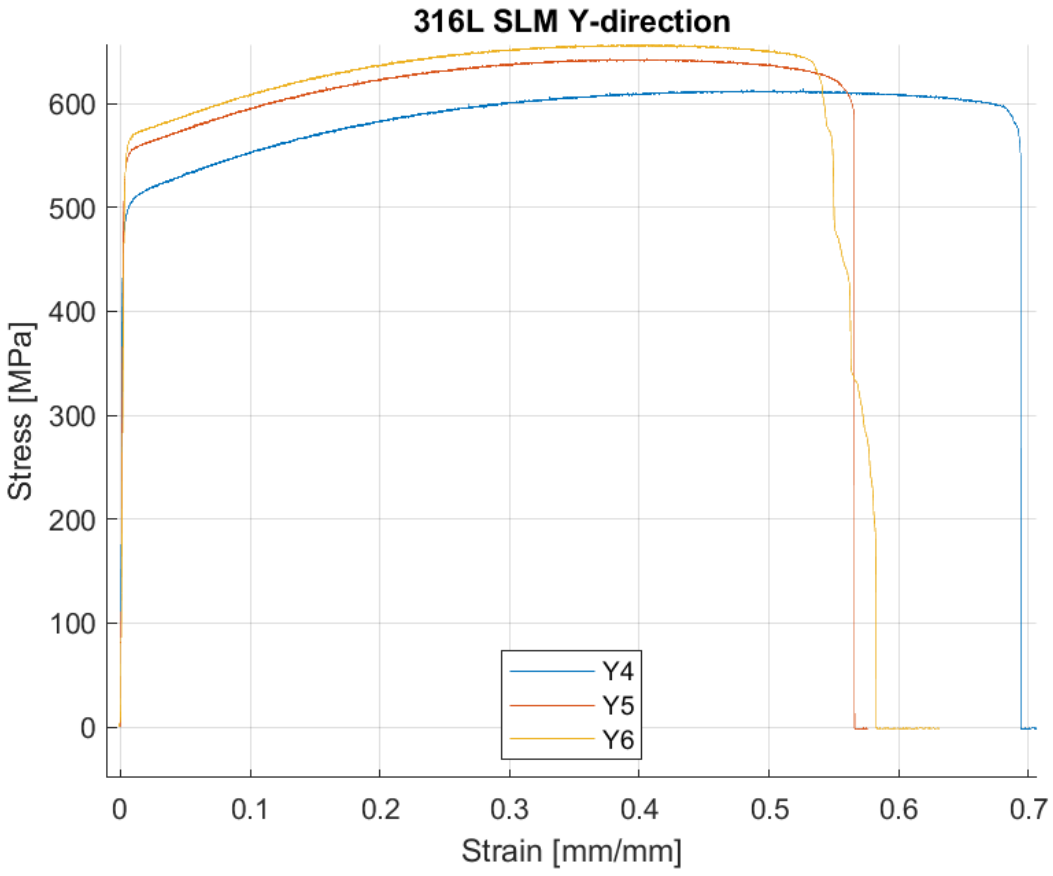
316L SLM Y-direction
Stress [MPa]
Strain [mm/mm]
Y4
Y5
Y6

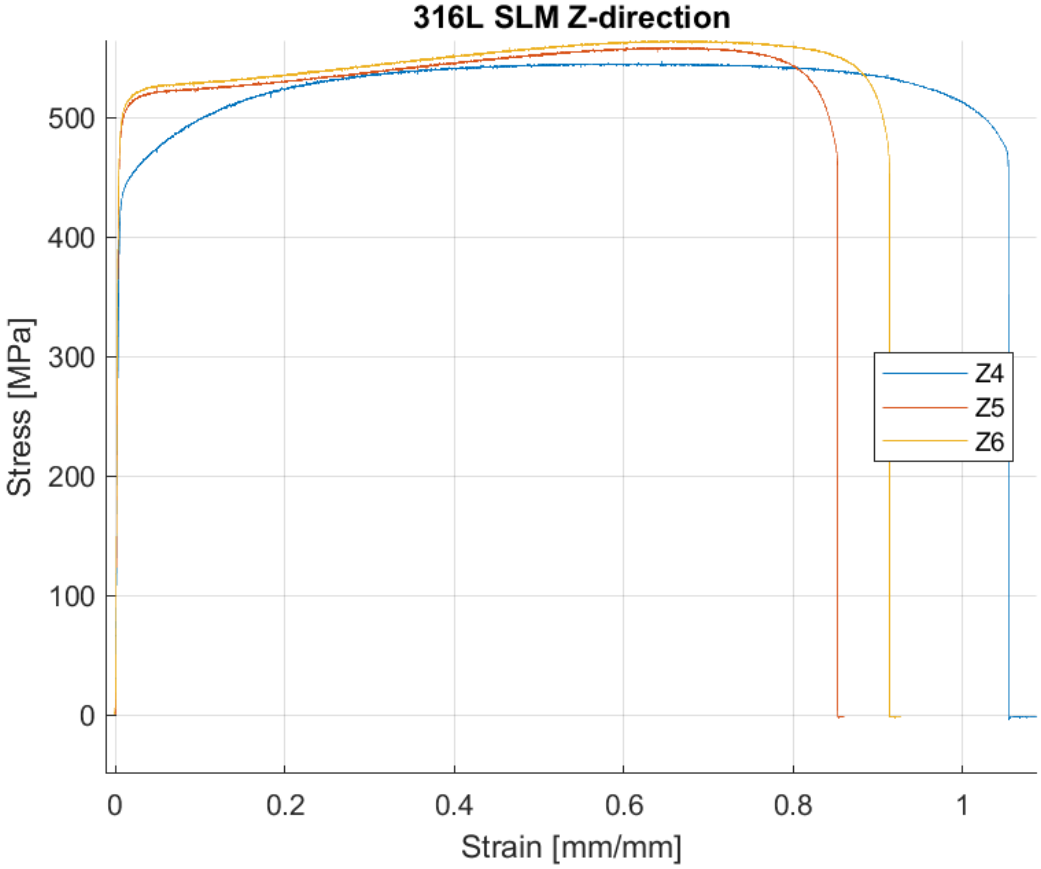
316L SLM Z-direction
Stress [MPa]
Strain [mm/mm]
Z4
Z5
Z6

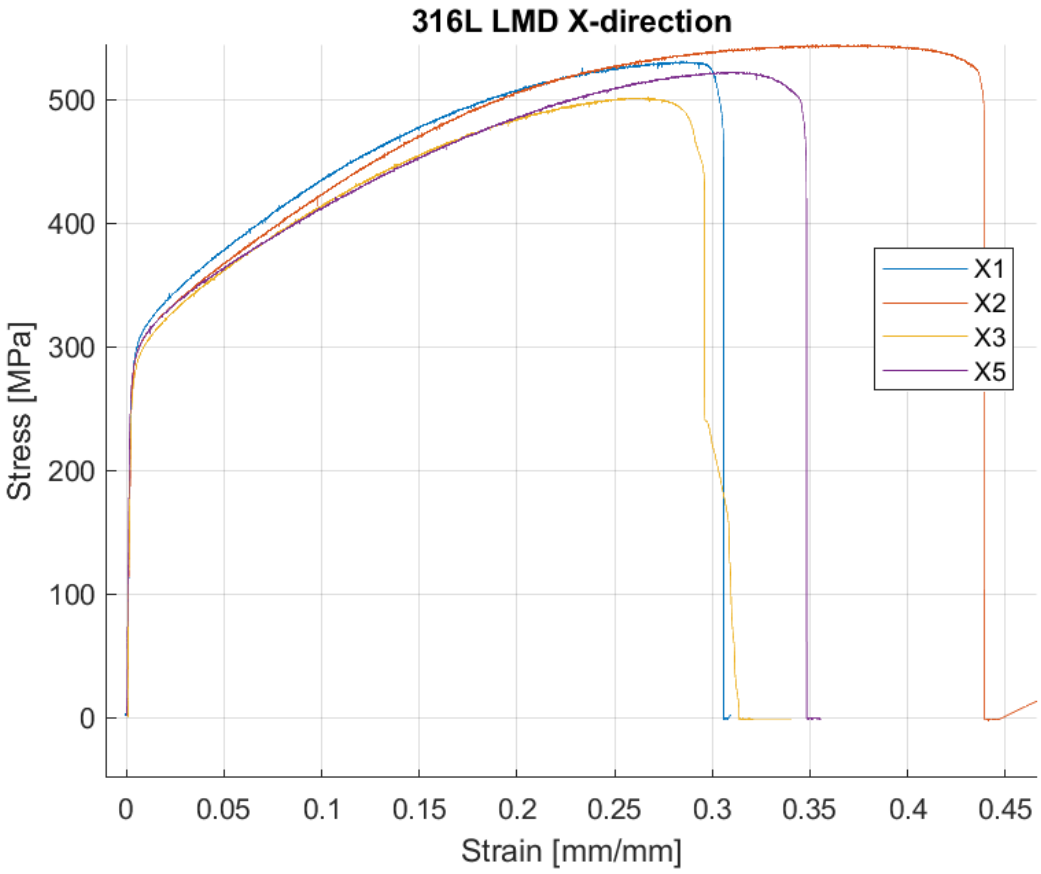
316L LMD X-direction
Stress [MPa]
Strain [mm/mm]
X1
X2
X3
X5

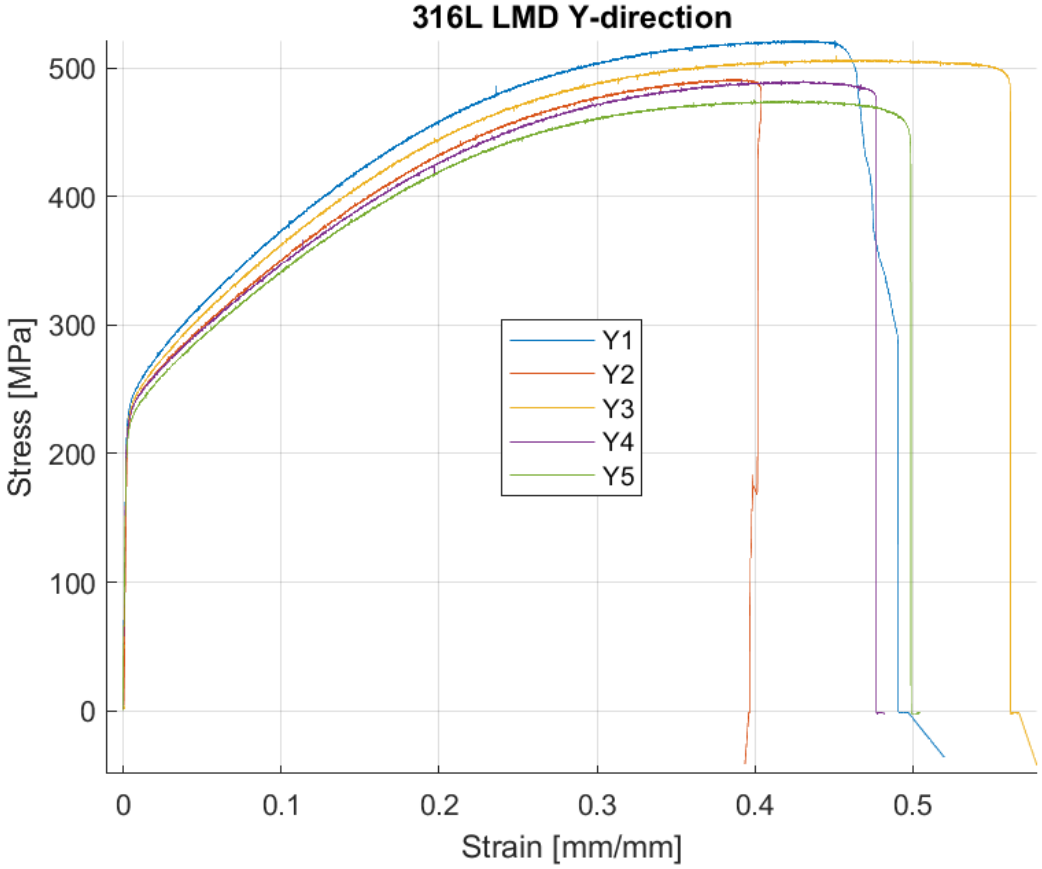
316L LMD Y-direction
Stress [MPa]
Strain [mm/mm]
Y1
Y2
Y3
Y4
Y5
0
100
200
300
400
500
0
0.1
0.2
0.3
0.4
0.5

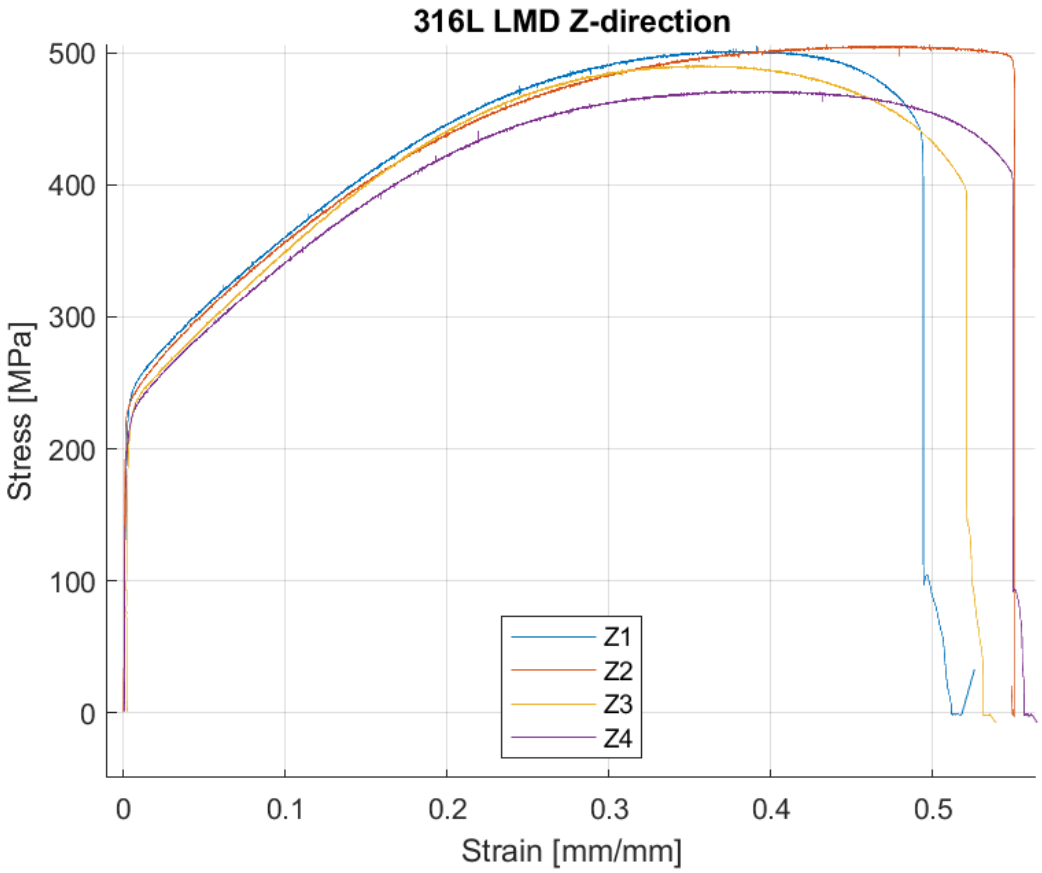
316L LMD Z-direction
Stress [MPa]
Strain [mm/mm]
Z1
Z2
Z3
Z4
0
100
200
300
400
500
0
0.1
0.2
0.3
0.4
0.5

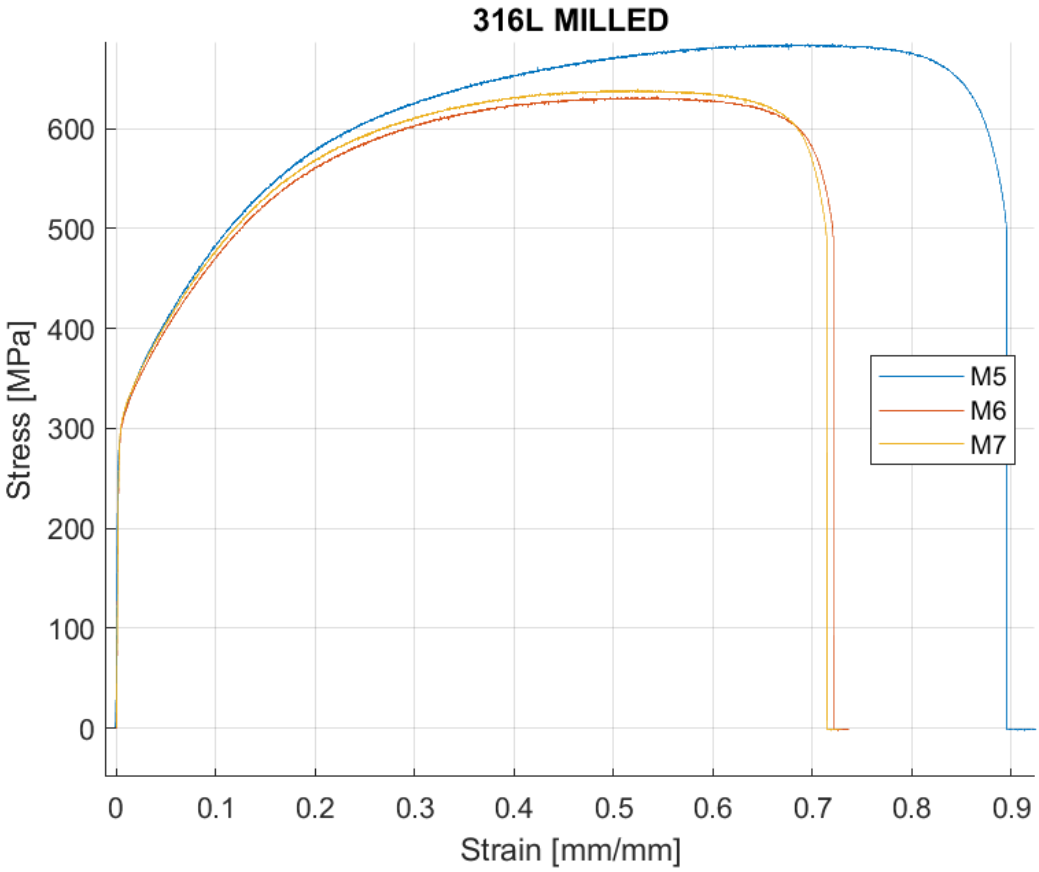
316L MILLED
Stress [MPa]
Strain [mm/mm]
M5
M6
M7

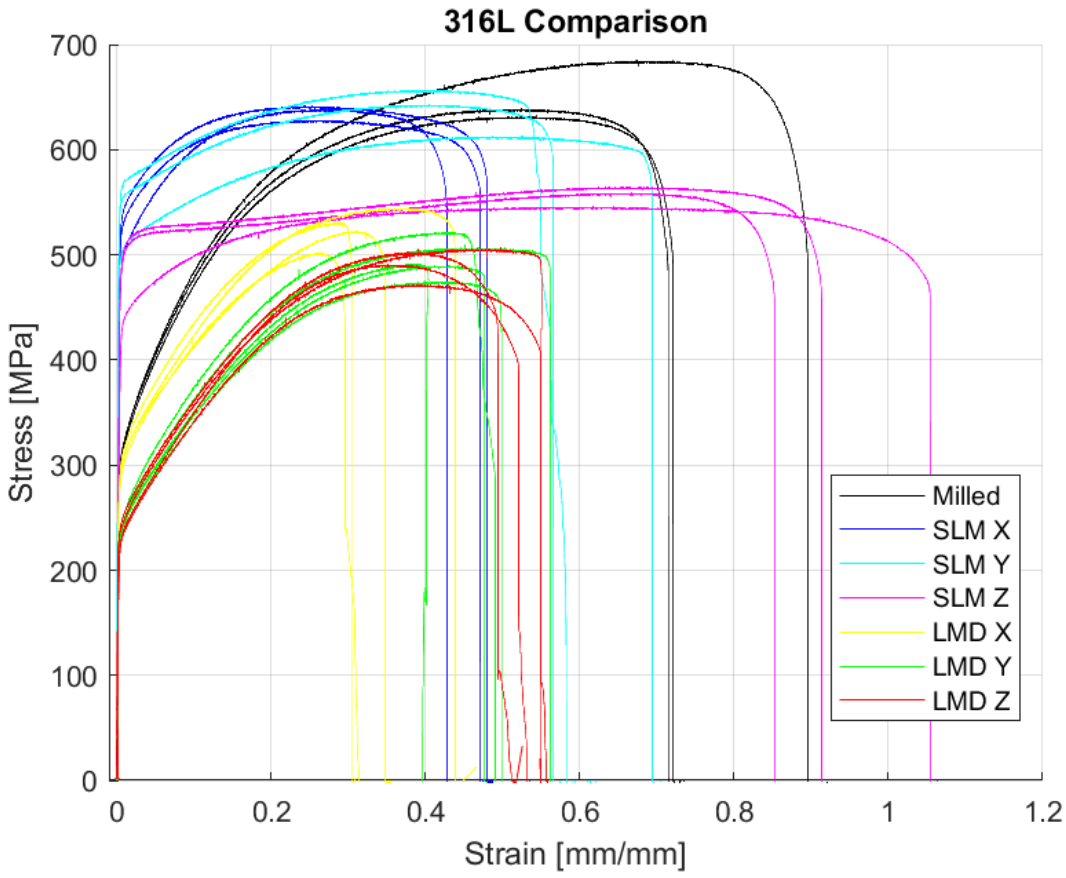
316L Comparison
Stress [MPa]
Strain [mm/mm]
Milled
SLM X
SLM Y
SLM Z
LMD X
LMD Y
LMD Z

# ATTACHMENT nr. 4

## Stress – strain curves for the tested C300 specimens

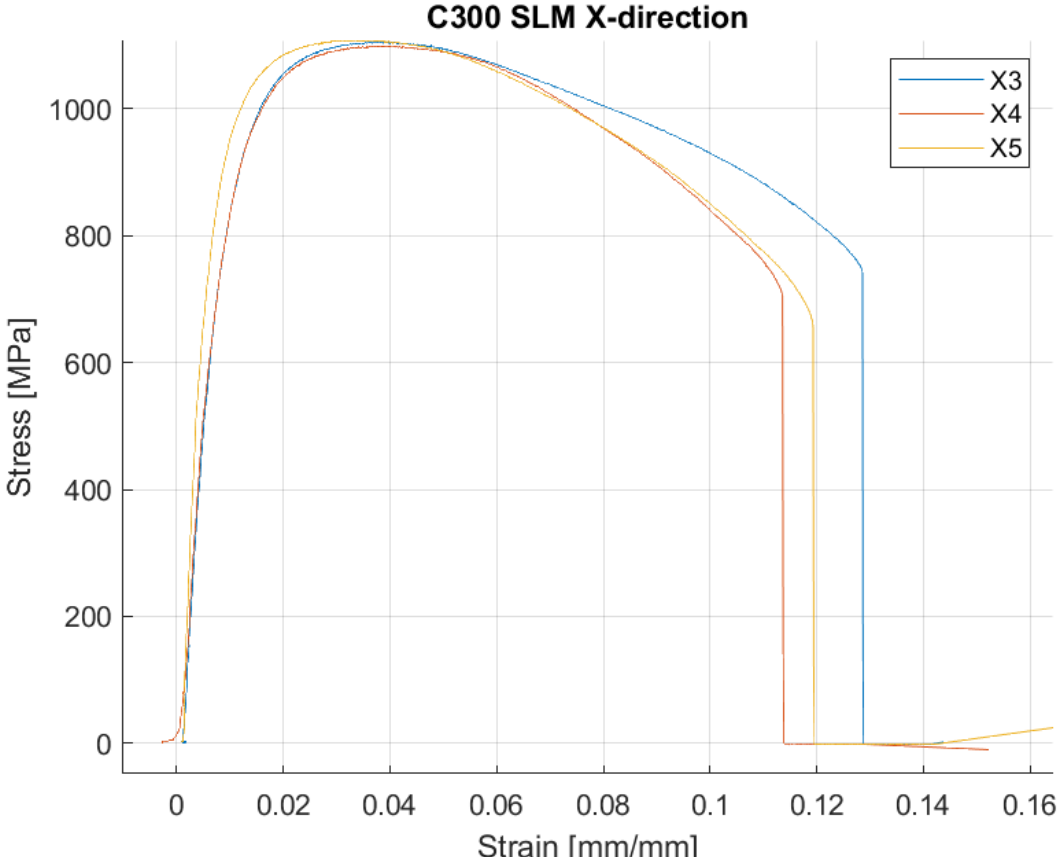
C300 SLM X-direction
X3
X4
X5
Stress [MPa]
Strain [mm/mm]
0
200
400
600
800
1000
0
0.02
0.04
0.06
0.08
0.1
0.12
0.14
0.16

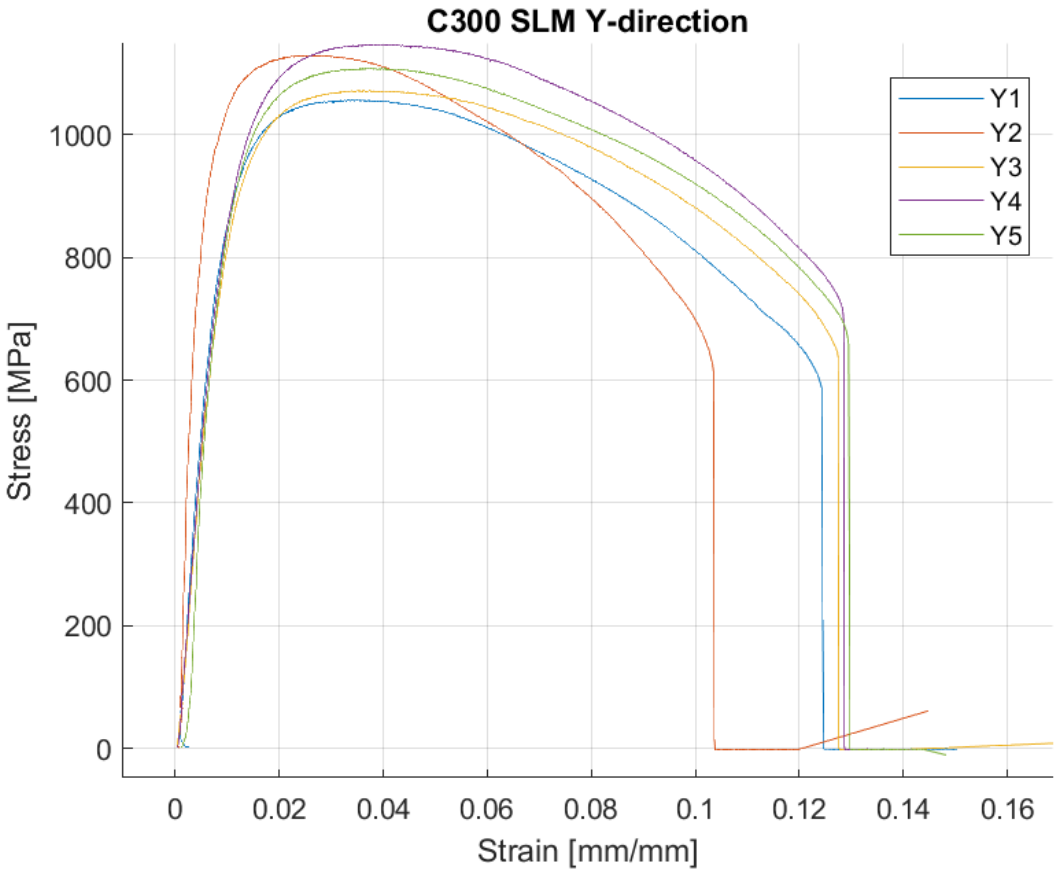
C300 SLM Y-direction
Y1
Y2
Y3
Y4
Y5
Stress [MPa]
Strain [mm/mm]
0
200
400
600
800
1000
0
0.02
0.04
0.06
0.08
0.1
0.12
0.14
0.16

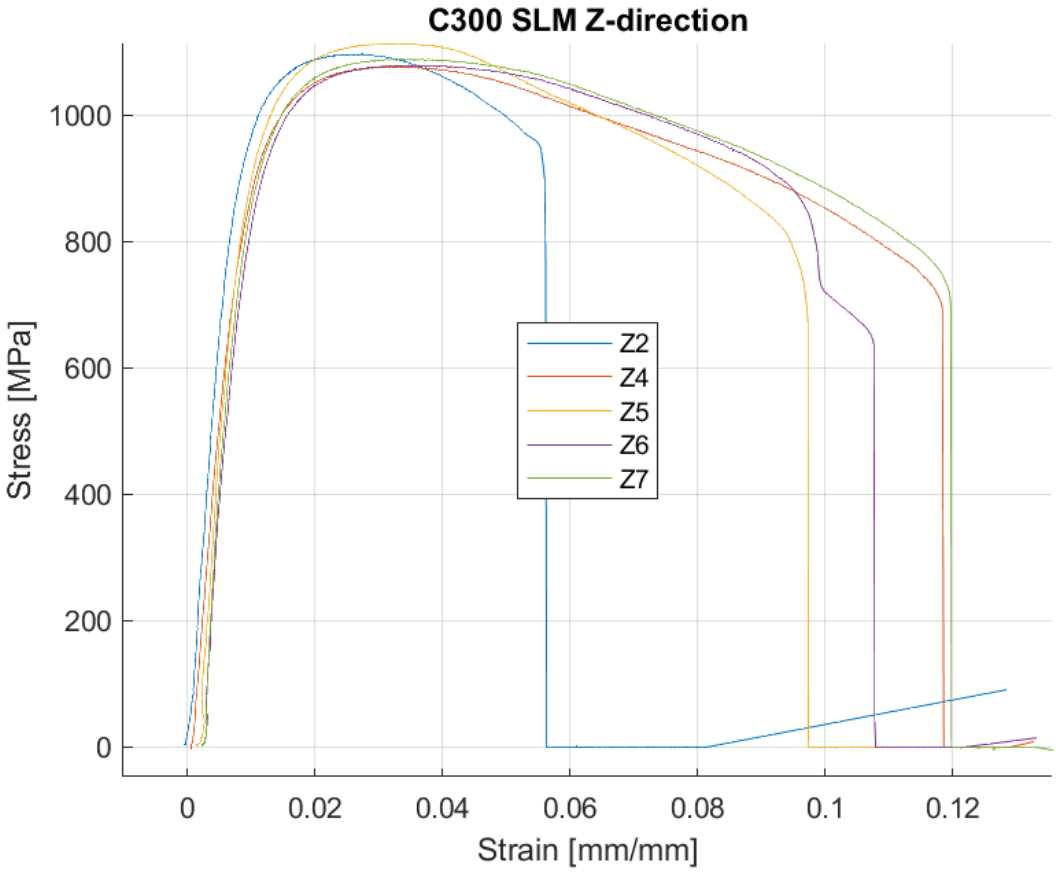
C300 SLM Z-direction
Stress [MPa]
Strain [mm/mm]
Z2
Z4
Z5
Z6
Z7
0
200
400
600
800
1000
0
0.02
0.04
0.06
0.08
0.1
0.12

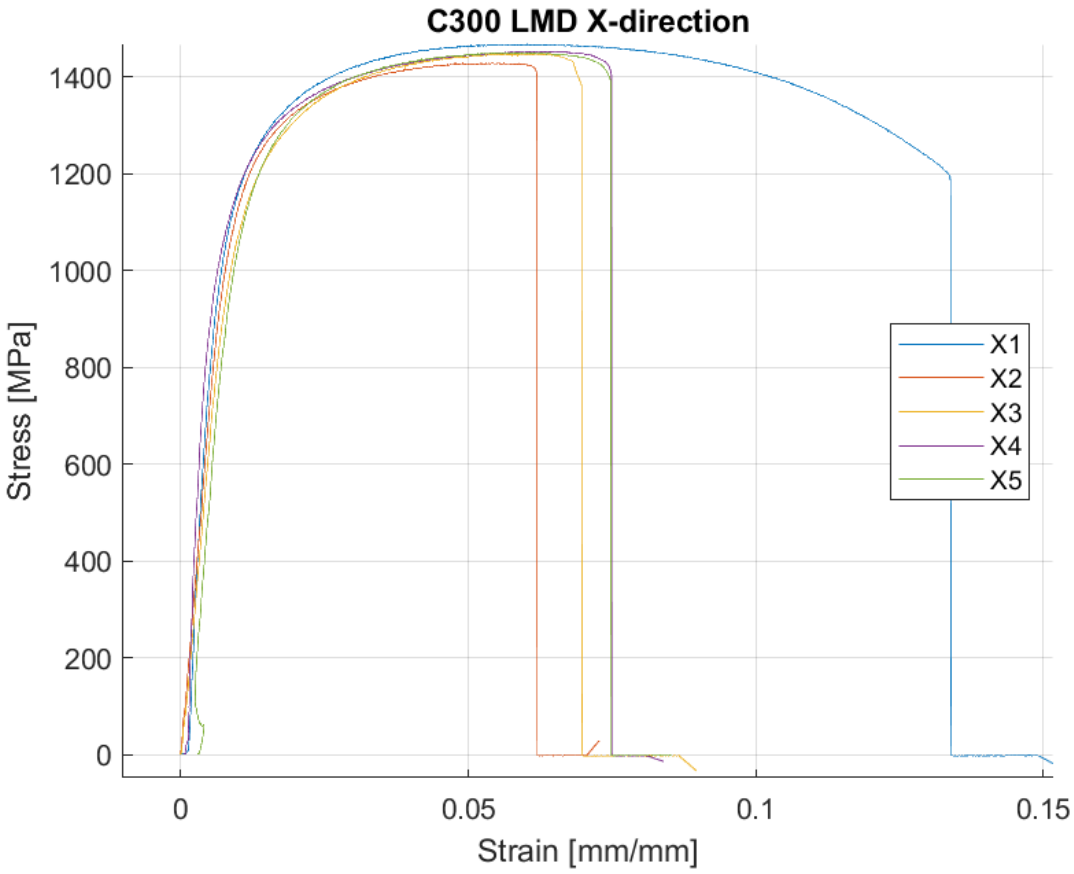
C300 LMD X-direction
Stress [MPa]
Strain [mm/mm]
X1
X2
X3
X4
X5
0
200
400
600
800
1000
1200
1400
0
0.05
0.1
0.15

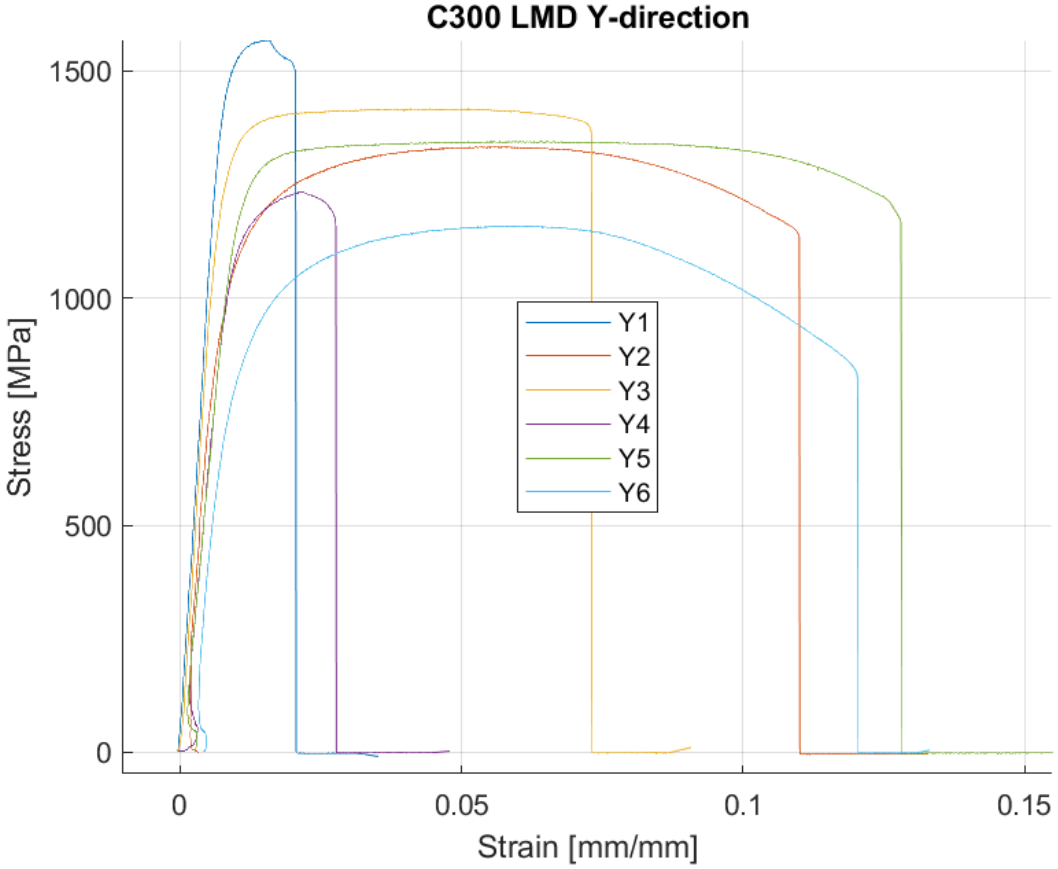
C300 LMD Y-direction
Stress [MPa]
Strain [mm/mm]
Y1
Y2
Y3
Y4
Y5
Y6
0
500
1000
1500
0
0.05
0.1
0.15

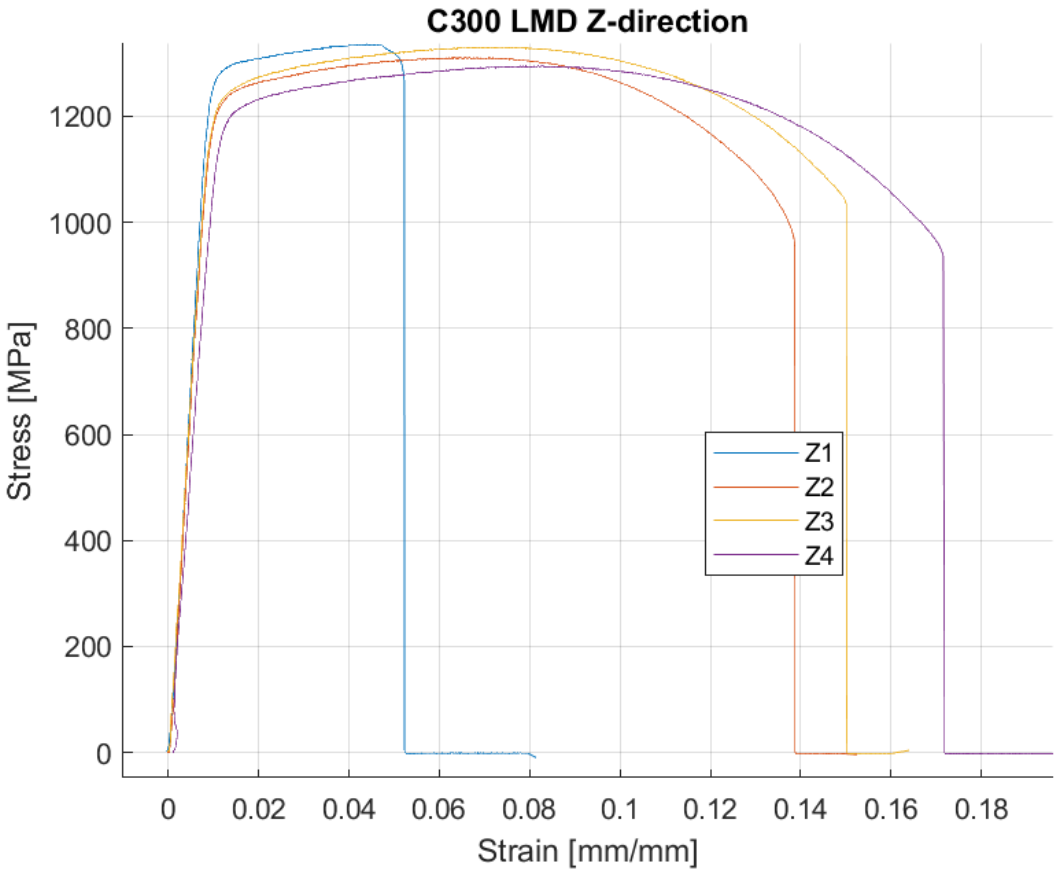
C300 LMD Z-direction
Stress [MPa]
Strain [mm/mm]
Z1
Z2
Z3
Z4
0
200
400
600
800
1000
1200
0
0.02
0.04
0.06
0.08
0.1
0.12
0.14
0.16
0.18

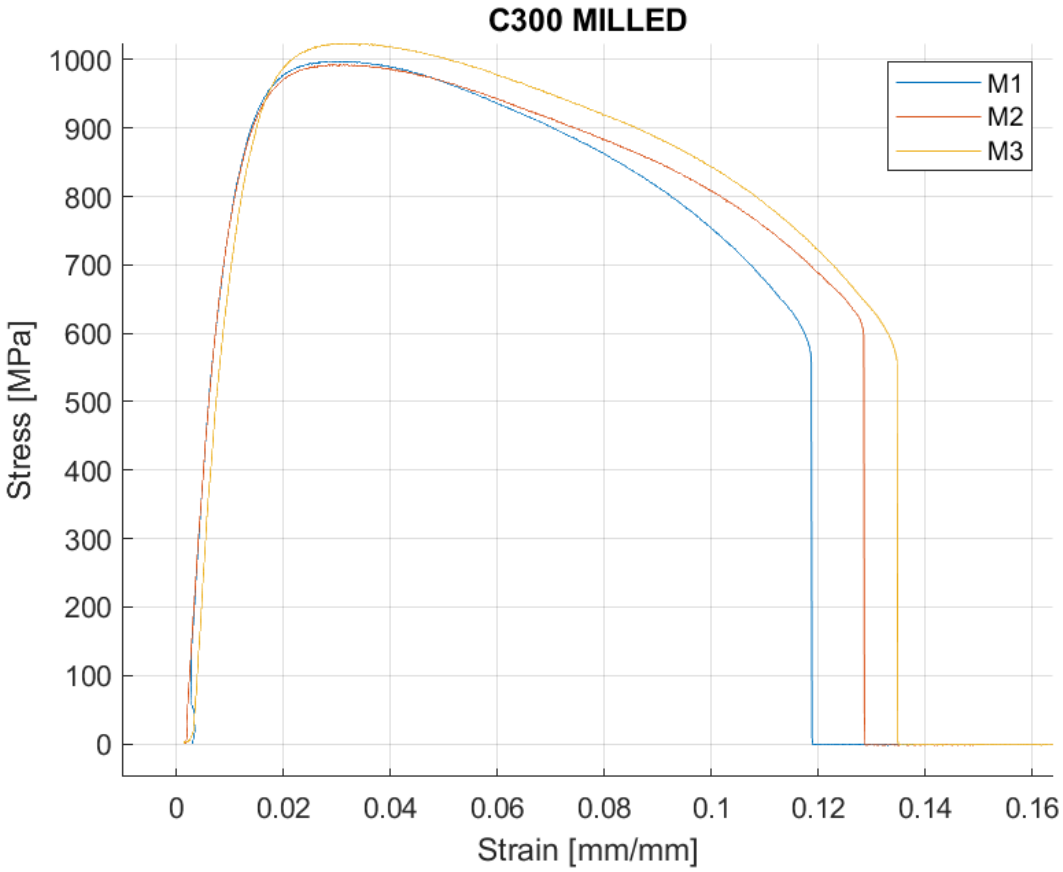
C300 MILLED
M1
M2
M3
Stress [MPa]
Strain [mm/mm]
0
100
200
300
400
500
600
700
800
900
1000
0
0.02
0.04
0.06
0.08
0.1
0.12
0.14
0.16

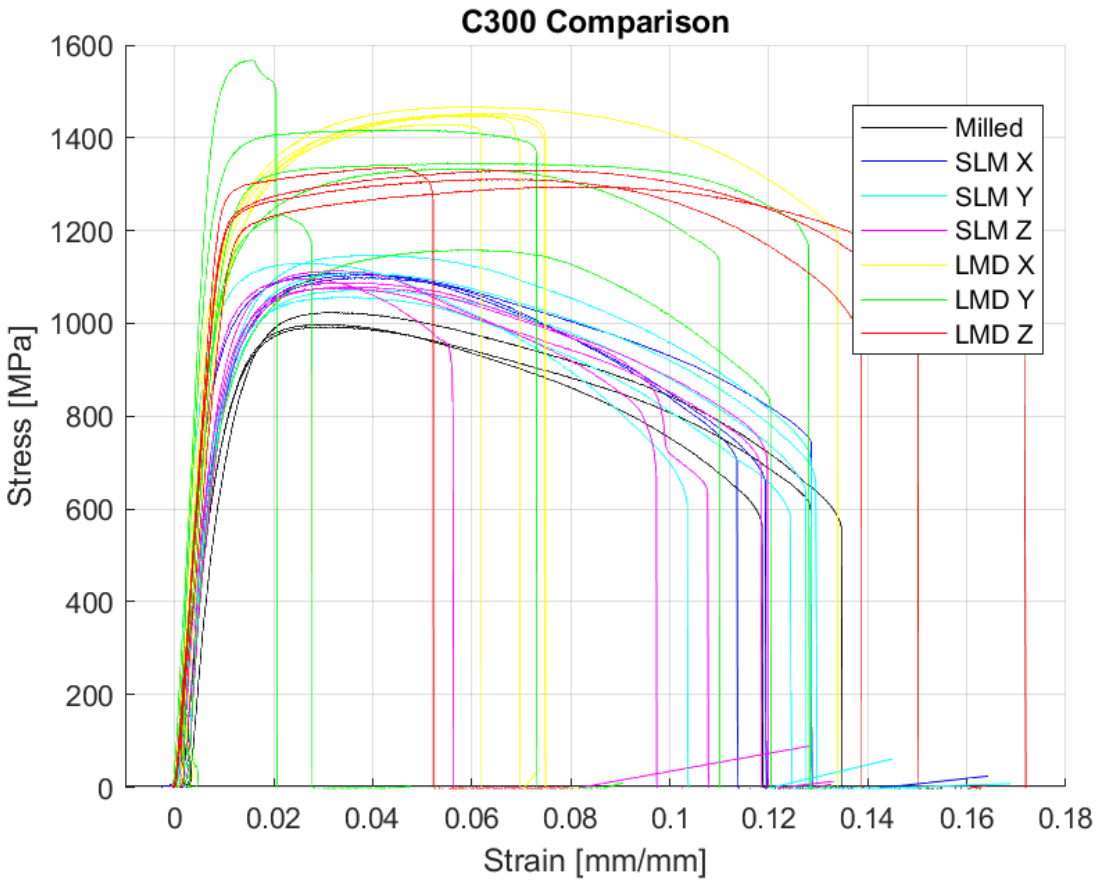
C300 Comparison
Milled
SLM X
SLM Y
SLM Z
LMD X
LMD Y
LMD Z
Stress [MPa]
Strain [mm/mm]
0
200
400
600
800
1000
1200
1400
1600
0
0.02
0.04
0.06
0.08
0.1
0.12
0.14
0.16
0.18

# ATTACHMENT nr. 5

# Fractures of the 316L specimens

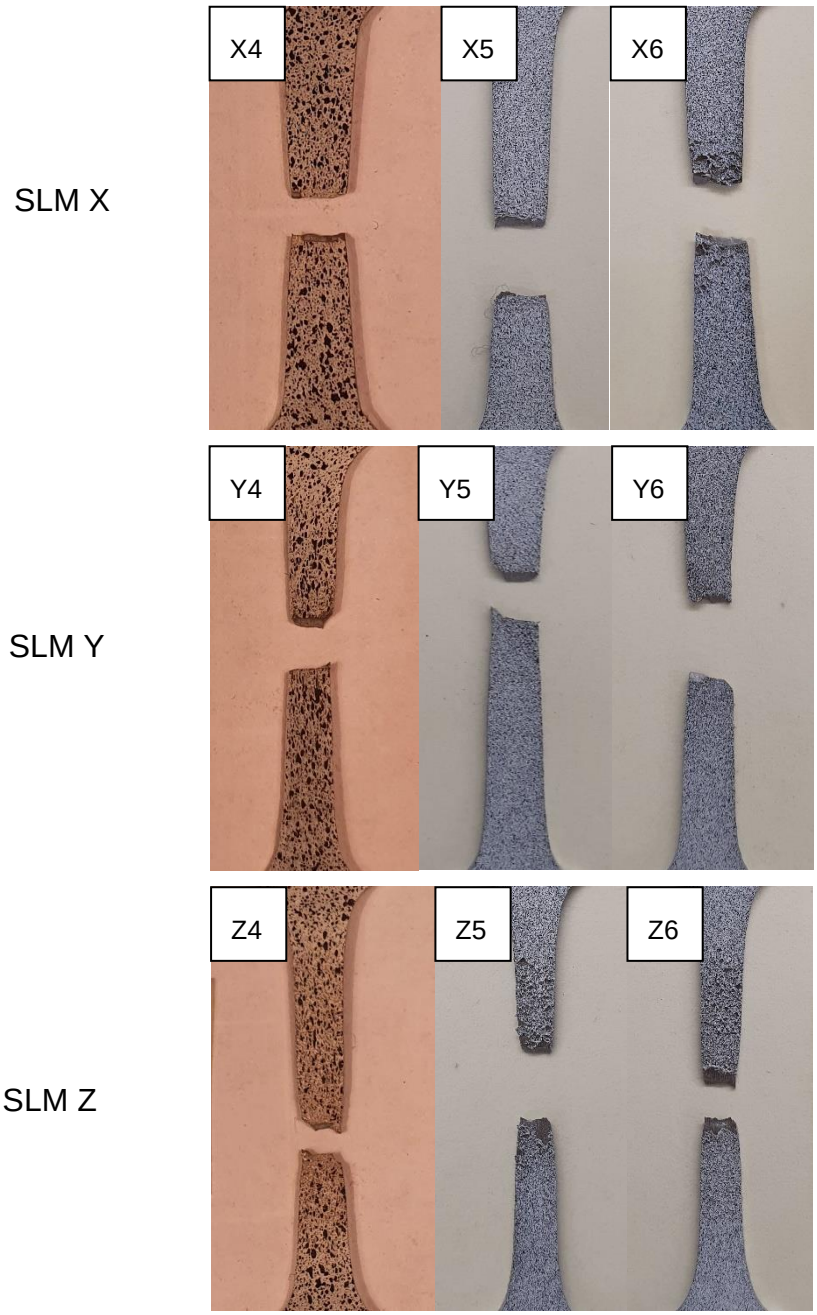
SLM X
X4
X5
X6
SLM Y
Y4
Y5
Y6
SLM Z
Z4
Z5
Z6

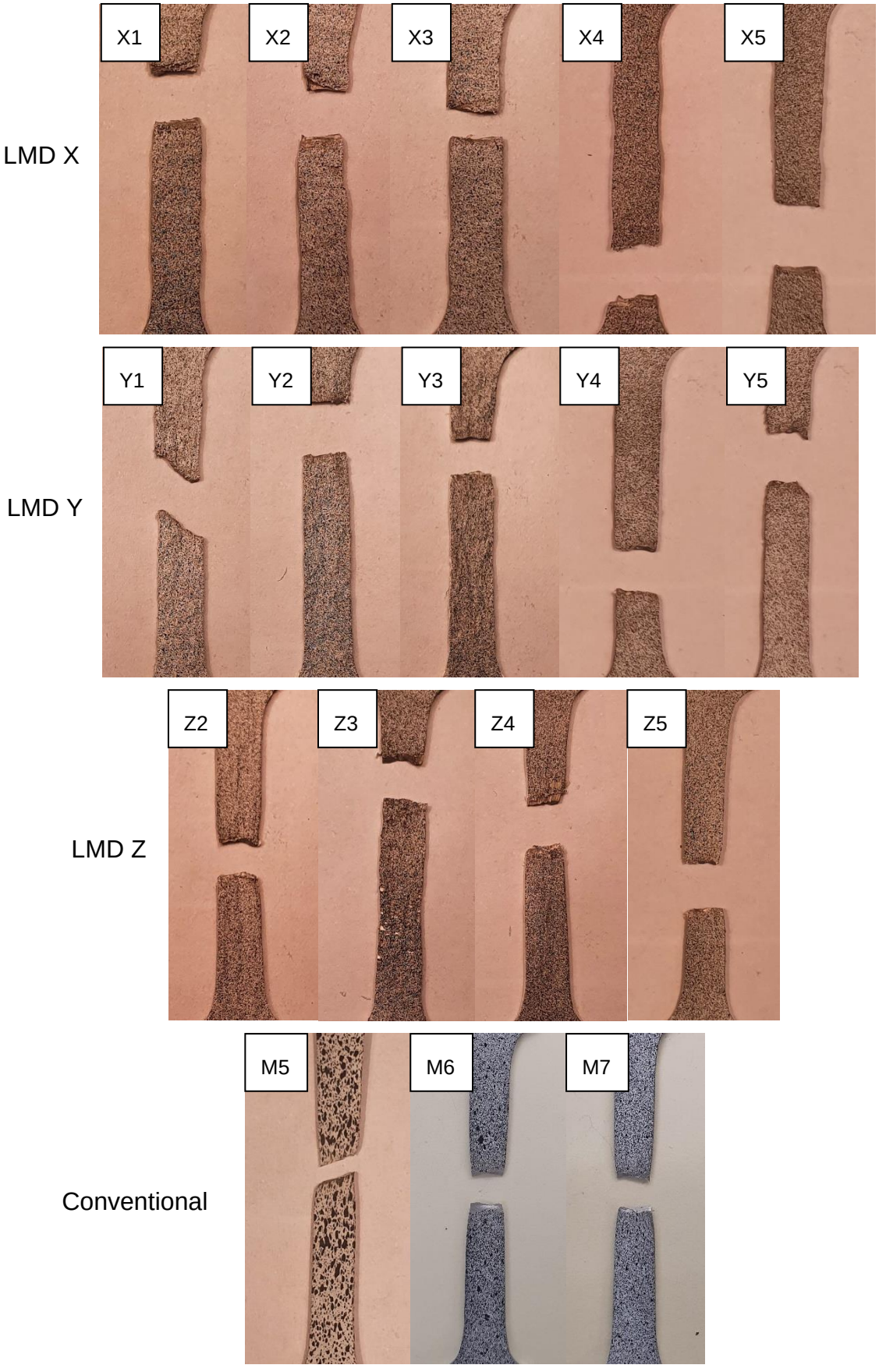
LMD X
X1
X2
X3
X4
X5
LMD Y
Y1
Y2
Y3
Y4
Y5
LMD Z
Z2
Z3
Z4
Z5
Conventional
M5
M6
M7

# ATTACHMENT nr. 6

# Fractures of the C300 specimens

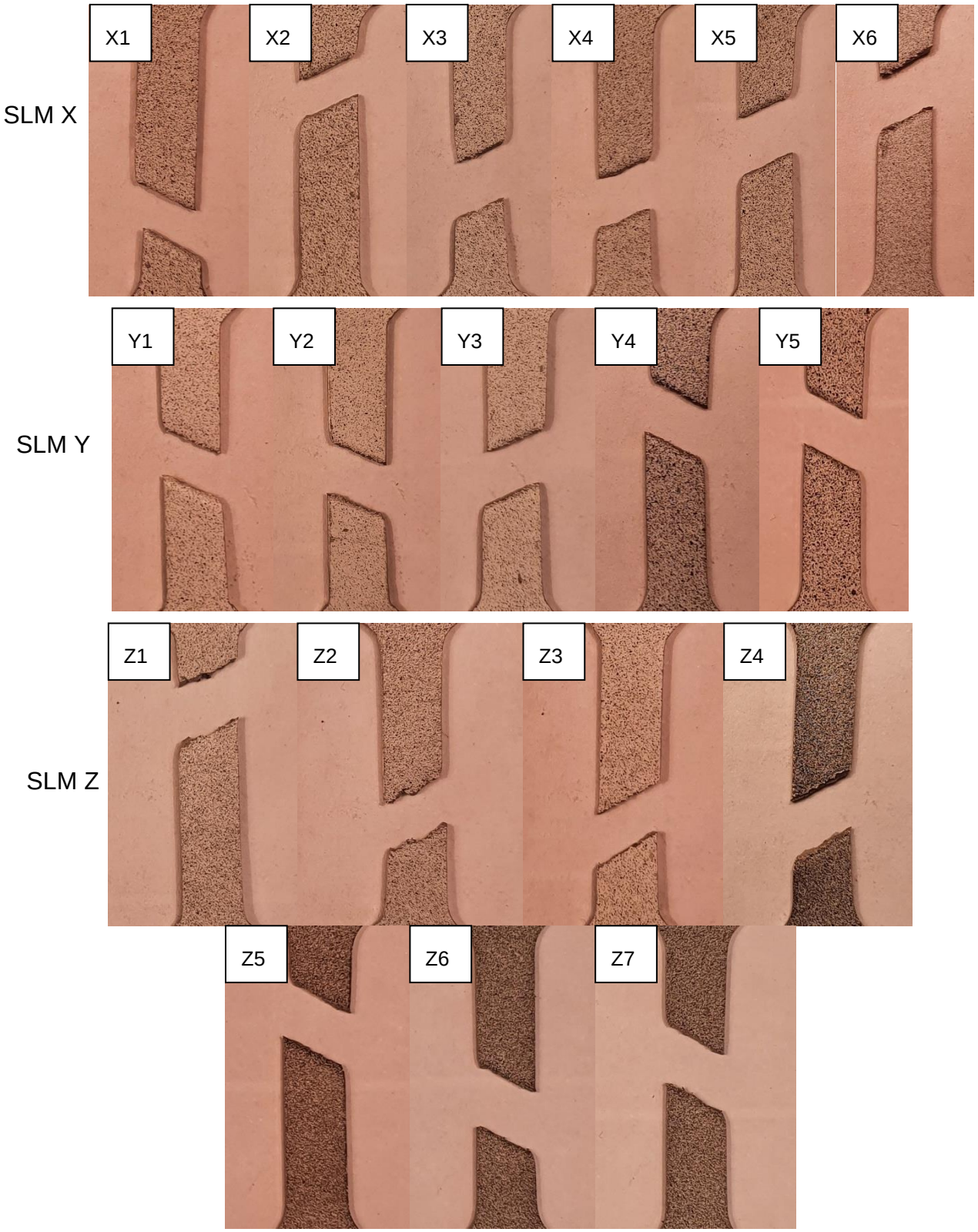
SLM X
X1
X2
X3
X4
X5
X6
SLM Y
Y1
Y2
Y3
Y4
Y5
SLM Z
Z1
Z2
Z3
Z4
Z5
Z6
Z7

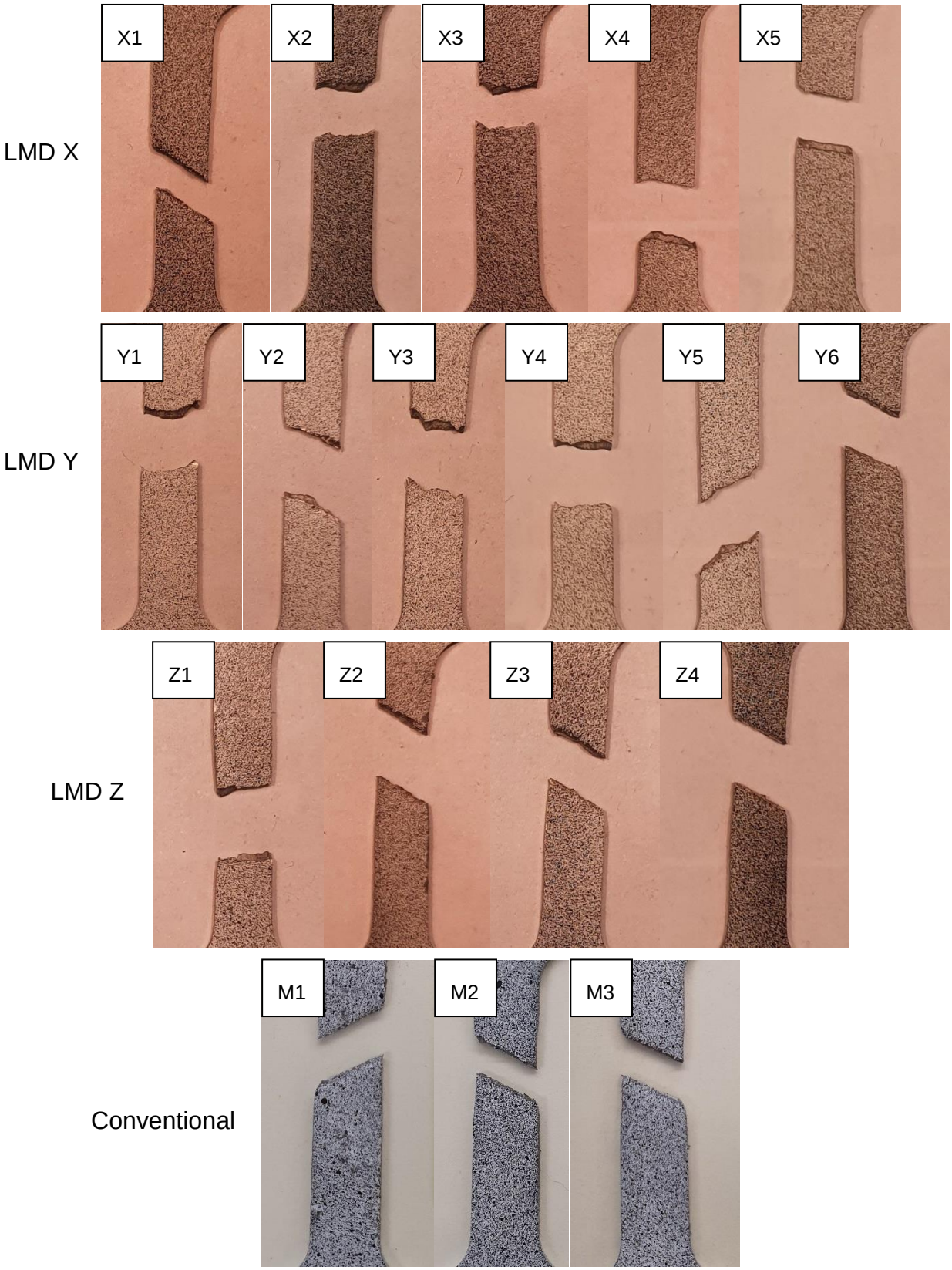
LMD X
X1
X2
X3
X4
X5
LMD Y
Y1
Y2
Y3
Y4
Y5
Y6
LMD Z
Z1
Z2
Z3
Z4
Conventional
M1
M2
M3

# ATATCHMENT nr. 7

# Technical drawing of the tensile specimen

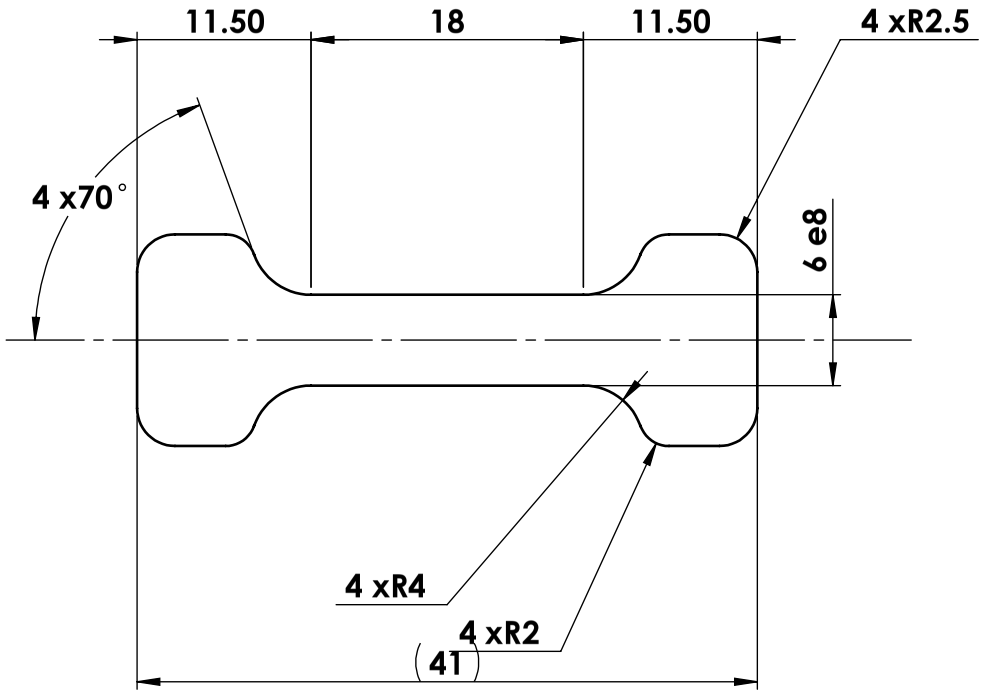


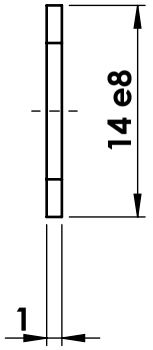


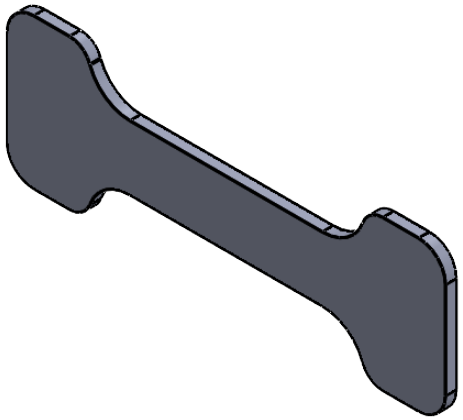

**30 specimens for static and dynamic:**
**Built direction**
**10 X-diretion**
**10 Y-direction (Printing direction be longitudinal )**
**10 Z-direction**

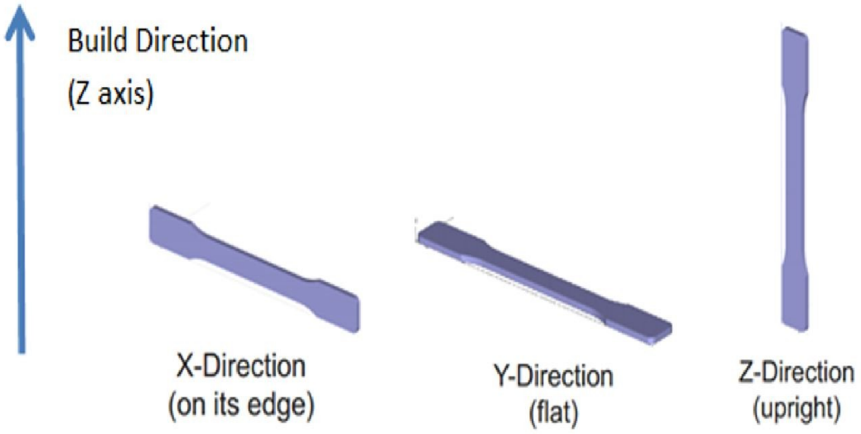


| | | | | | |
|---|---|---|---|---|---|
| inegi | | TÍTULO: SLM Dynamic Specimen | | | |
| MATERIAL: Stainless Steel | | DSNH Nº: QUA 01.11.02.21 | | | |
| PESO: ± XXX g | ESCALA:2:1 | | A4 | mm | FOLHA 1 DE 1 |

# ATTACHMENT nr. 8

# Manufacturing process of combined specimens

# PEÇA: 0707Q75A0BBH_

OPERADOR :

| Peça: | X60 | Y30 | Z27 |
|---|---|---|---|

FOLHA DE PROGRAMAS - 28/abr/2022

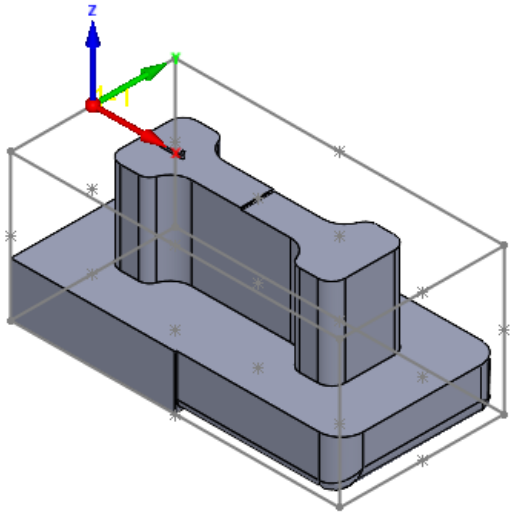


**CENTRAMENTO DA 1ª POSIÇÃO**

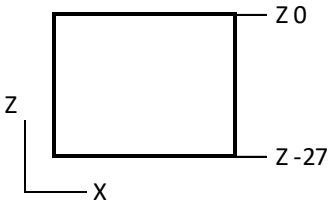


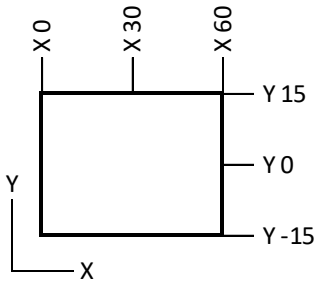


| Cotas Máx. (Stock) | X: 60 | Y: 30 | Z: 27 | 1_IBARMIA-H530i |
|---|---|---|---|---|
| R:\Processos2022\0707_QTL\0707Q75A - AM\PROGRAMAÇÃO CNC\MAQUINAÇÃO\0707Q75A0BBH_\0707Q75A0BBH_.SLDPRT | | | | PROGRAMADO POR: Ana Andrade |
| Limites maquinação | Xmax:66 Xmin:-6 \| Ymax:21.843Ymin:-21.2 | | | Tempo Total: **0:05:24** |

TABELA DE FERRAMENTAS

| | | | | | | | |
|---|---|---|---|---|---|---|---|
| T2 | TD 12MD INOX | Ø=12 | | Ltotal=90 Lutil=55 | EmptyHolder - 20.000 | TEMPO: | 0:01:01 |
| T3 | TD 8MD INOX | Ø=8 | | Ltotal=90 Lutil=55 | EmptyHolder - 20.000 | TEMPO: | 0:01:49 |
| T11 | HITACHI_2020M_LIGAR AR | Ø=20 | RC=2 | Ltotal=125 Lutil=10 | BT40 MAXIN 20x85 | TEMPO: | 0:02:33 |

LISTA DE OPERAÇÕES

Legenda: ap - incremento em Z | ae - incremento lateral | SL - Stock Lateral | SF - Stock Fundo | Z T - Z Topo | Z F - Z Fundo

| T | Nome da operação | ZTopo \| Zfundo | Spindle \| Feed | Diam | RC | TEMPO |
|---|---|---|---|---|---|---|
| T2 | TD 12MD INOX | Z Minimo de operação: 0 | S4000 F900 | Ø=12 | | *0:01:01* |
| T11 | HITACHI_2020M_LIGAR AR | Z Minimo de operação: -17 | S2864 F9999 | Ø=20 | RC=2 | *0:02:33* |
| T3 | TD 8MD INOX | Z Minimo de operação: -17 | S5000 F900 | Ø=8 | | *0:01:49* |

**Inserir compensação do diâmetro na tabela dos offsets da máquina em todas a fresas.**

**Em todas as maquinações de ferramentas, para o bloco sair à cota temos que fazer o zero no lado de baixo do bloco (lado já maquinado), subir a cota pedida no desenho e voltar a fazer o zero maquina.**

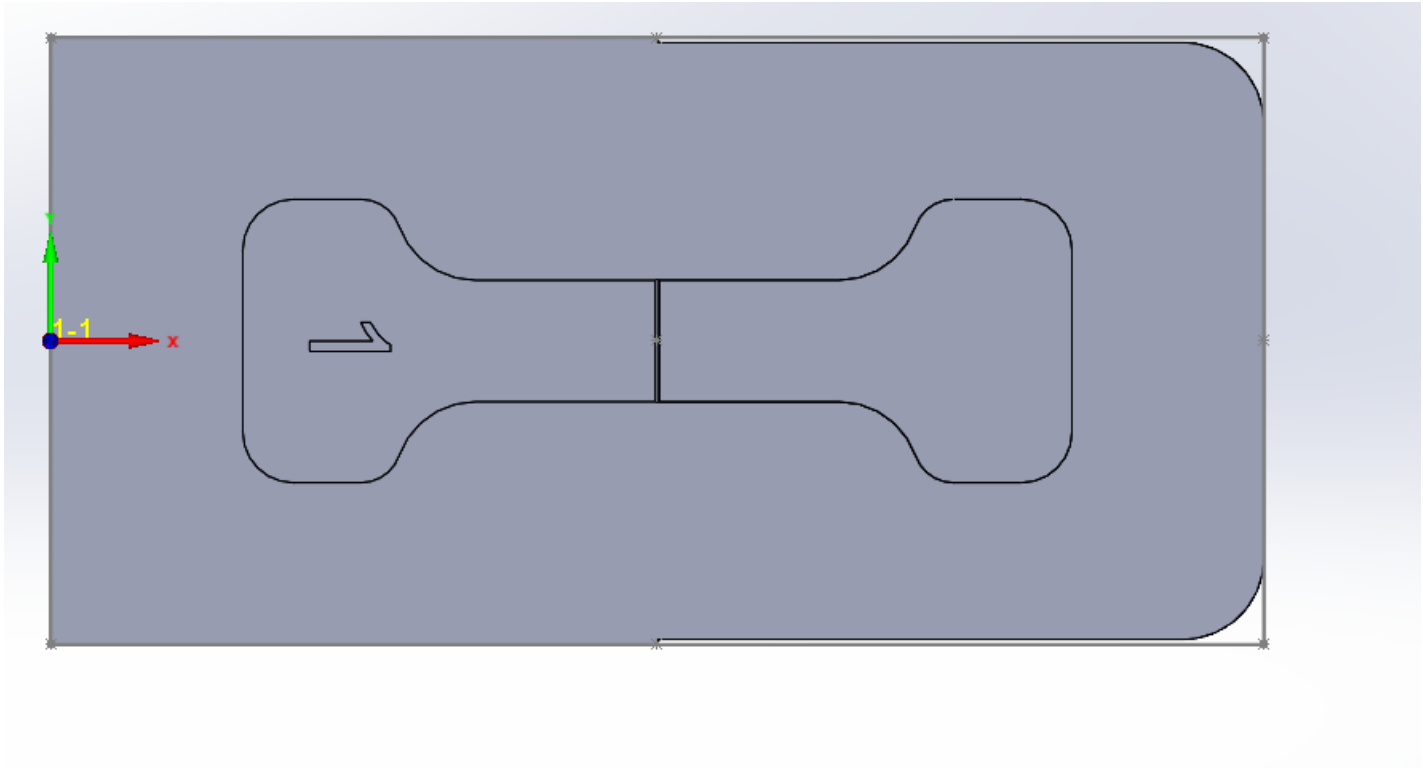


**X→ LADO ESQUERDO do bloco (C300)**

**Y→ ao centro do bloco**

**Z→na parte de cima do bloco**